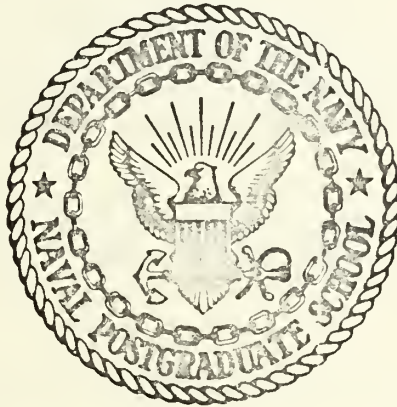


MEASURED AND PREDICTED PRESSURE DROPS
IN
TWO-PHASE AIR WATER FLOWS

By

John Meredith Bonds

United States Naval Postgraduate School



THESIS

MEASURED AND PREDICTED PRESSURE DROPS
IN
TWO-PHASE AIR WATER FLOWS

by

John Meredith Bonds

September 1970

This document has been approved for public release and sale; its distribution is unlimited.

1137363

Measured and Predicted Pressure Drops
in
Two-Phase Air Water Flows

by

John Meredith Bonds
Lieutenant (junior grade), United States Navy
B.S.A.E., University of Michigan, 1968

Submitted in partial fulfillment of the
requirements for the degree of

MASTER OF SCIENCE IN AERONAUTICS

from the

NAVAL POSTGRADUATE SCHOOL
September 1970

ABSTRACT

Two-phase, air-water flow is studied in a horizontal pipe. Water injection methods are compared to determine an efficient means of attaining fully developed homogeneous flow. Wall shear forces are measured directly through flexures attached to a "floating" test section. The pressure drops are compared to those predicted by the Lockhart-Martinelli and Chenoweth-Martin correlation schemes. A computer program is presented for data reduction. For the flow rates investigated it is concluded that the Lockhart-Martinelli correlation gives better results than does the Chenoweth-Martin scheme providing one knows the existing flow pattern. A new method is suggested for predicting the transition between the Annular and Mist flow regimes.

TABLE OF CONTENTS

I.	INTRODUCTION TO TWO-PHASE FLOW -----	11
A.	BACKGROUND -----	11
B.	THEORETICAL TWO-PHASE FLOW MODELS -----	11
1.	Homogeneous Flow Model -----	12
2.	Momentum Exchange Model -----	13
3.	Separated Phase Model -----	15
C.	EMPIRICAL FLOW MODELS -----	16
1.	Lockhart-Martinelli Correlation -----	16
2.	Chenoweth-Martin Correlation -----	20
D.	TRANSITION -----	24
II.	THE TWO-PHASE FLOW TEST APPARATUS -----	27
A.	EQUIPMENT AND DESIGN -----	27
B.	CALIBRATION OF THE RIG -----	30
1.	Pipe Coefficient Calibration -----	30
2.	Labyrinth Air Leakage Calibration -----	31
3.	Flexure Calibration -----	31
4.	Equivalent Pipe Roughness Factor -----	32
C.	DATA REDUCTION -----	33
III.	INJECTION STUDIES -----	34
A.	INTRODUCTION AND DESCRIPTION OF INJECTORS -----	34
1.	Case I -----	35
2.	Case II -----	35
3.	Case III -----	35
4.	Case IV -----	36
B.	CONCLUSIONS -----	37

IV.	CORRELATION RESULTS -----	39
A.	DISCUSSION -----	39
B.	CONCLUSIONS AND RECOMMENDATIONS -----	42
FIGURES	-----	43
APPENDIX I	Data Reduction Program Nomenclature and Sample Output -----	88
LIST OF REFERENCES	-----	110
INITIAL DISTRIBUTION LIST	-----	111
FORM DD 1473	-----	113

LIST OF FIGURES

1. Types of Flow Patterns in Horizontal Two-Phase Flow -----	43
2. Two-Phase Flow Correlation of Lockhart-Martinelli -----	44
3. Correlation of Chenoweth and Martin for Turbulent Two-Phase Pressure Drop in Horizontal Pipes -----	45
4. Two-Phase Air-Water Pressure Drop in Vertical Pipes -----	46
5. Flow Pattern Transition Effects -----	47
6. Chien-Ibele Transition Criteria -----	48
7. Two-Phase Flow Test Rig Prior to Modification -----	49
8. Two-Phase Flow Rig Schematic -----	50
9. Air and Water Supply with Pressure Regulators -----	51
10. Main Air Orifice -----	52
11. Flow Orifice Details -----	53
12. Air-Water Mixing Duct -----	54
13. Labyrinth Seal -----	55
14. Detailed Views of Labyrinth Seal -----	56
15. Test Section Supports -----	57
16. Flexures -----	58
17. Pipe Coefficient Calibration Curves -----	59
18. Labyrinth Air Leakage Curves -----	60
19. Strain Gage Readout Equipment -----	61
20. Strain Gage Wiring Schematic -----	61
21. Flexure Calibration Set-Up -----	62
22. Flexure Calibration Curves -----	63
23. Friction Factor Calibration -----	64
24. Mixing Duct and Injector Geometry -----	65
25. Case I Injection Pattern -----	66

26.	Case I Flow Pattern at Exit of Straight Pipe -----	66
27.	Case II Injection Pattern -----	67
28.	Case II Flow Pattern at Exit of Straight Pipe -----	67
29.	Case III Injection Pattern -----	68
30.	Case III Flow Pattern at Exit of Straight Pipe -----	68
31.	Case IV Injection Pattern -----	69
32.	Case IV Flow Pattern at Exit of Straight Pipe -----	69
33.	Case IV Flow Pattern at Exit of Test Section -----	70
34.	Percentage Mist for the Four Nozzle Types -----	71
35.	Case IV Nozzle Water Separation -----	72
36.	Measured Pressure Drop - Red Flexure -----	73
37.	Measured Pressure Drop - Black Flexure -----	74
38.	Lockhart-Martinelli Predicted Pressure Drop -----	75
39.	Chenoweth-Martin Predicted Pressure Drop -----	76
40.	Predicted and Measured Pressure Drop for Air Constant at .35 lbm/sec -----	77
41.	Predicted and Measured Pressure Drop for Air Constant at .40 lbm/sec -----	78
42.	Predicted and Measured Pressure Drop for Air Constant at .43 lbm/sec -----	79
43.	Predicted and Measured Pressure Drop for Air Constant at .50 lbm/sec -----	80
44.	Predicted and Measured Pressure Drop for Air Constant at .55 lbm/sec -----	81
45.	Predicted and Measured Pressure Drop for Air Constant at .60 lbm/sec -----	82
46.	Effect of Changing the Transition Criteria from Re = 2000 to Re = 3000 -----	83
47.	Flow Transition Indicated by the Change in Slope of ($\Delta P/\Delta L$) _{TP} -----	84
48.	Transitions of the Pressure Gradient -----	85

49. Percentage Mist Indicating Transition -----	86
50. Pressure Drop as a Function of Percentage Mist -----	87

TABLE OF SYMBOLS

SYMBOL	MEANING	
A	Chien-Ibele transition number	
D	diameter	(ft)
d	orifice diameter	(inches)
f	friction factor	
F_a	thermal expansion factor	
G	mass flux	(lbm/ft ²)
g_o	unit conversion factor	$\left[32.17 \left(\frac{\text{lbm-ft}}{\text{lbf-sec}^2} \right) \right]$
g	local acceleration of gravity	(ft-sec ²)
h_{fg}	heat of vaporization	(Btu/lbm)
h_w	differential pressure of manometer in inches of water @ 68°F	(inches)
K	friction loss coefficient for valves and fittings	
L	length	(ft)
\dot{m}	mass flow rate	(lbm/sec)
P	pressure	(lbf/ft ²)
ΔP	pressure drop	(lbf/in ²) or (lbf/ft ²)
\dot{q}	heat transfer rate	(Btu/sec)
Re	Reynolds number	
V	velocity	(ft/sec)
\bar{V}_{fg}	specific volume change	(ft ³ /lbm)
W_{swr}	separated water ratio	
x	flowing mass quality	
X	Lockhart-Martinelli flow modulus	
α	void fraction	

SYMBOL	MEANING	
η	specific weight of flowing fluid	(lbf/ft ³)
λ	Chenoweth-Martin correlation parameter	
μ	fluid viscosity	(lbm/ft-sec)
Ω	Chenoweth-Martin predicted two-phase to fictitious all liquid pressured drop ratio	
Φ	Lockhart-Martinelli correlation parameter	
ρ	density	(lbm/ft ³)
τ_w	wall shear stress	(lbf/ft ²)

SUBSCRIPT	MEANING
L	liquid
g	gas

SUPERSCRIPT	MEANING
'	Lockhart-Martinelli fictitious
*	Chenoweth-Martin fictitious

I. INTRODUCTION TO TWO-PHASE FLOW

A. BACKGROUND

The prediction of pressure drops in fluid flow is simple and straightforward when the fluid is of single component. However the addition of a second component (two-phase flow) or many (multi-phase flow) complicates things considerably. The interaction of flow components, such as slip between fluids, phase changes, heat exchanges, and turbulence all make the problem nearly unmanageable from the theoretical point of view. Empirical methods have been devised with varying degrees of success and used in limited applications. Two of the more popular and successful schemes are the Lockhart-Martinelli and the Chenoweth-Martin correlations.

Two-Phase flow has many classifications according to the type of fluid components, their state - solid, liquid, or gas - and the flow orientation. For example, this study is of air and water flow that is assumed to be isothermal, steady, and fully developed in a horizontal pipe. The flow may exist in many different forms according to the volume and velocity of the fluids. Figure 1 depicts some of the different types of two-phase, gas-liquid flows. Figure 1A is a high volume liquid flow with a low gas flow rate, while Fig. 1F is the opposite extreme with high gas flow and low liquid flow rates. Combinations of the various regimes are possible and constitute the transition regions so often encountered in the experimental work.

B. THEORETICAL TWO-PHASE FLOW MODELS

Various flow models have been proposed to attempt a theoretical prediction of two-phase flow behavior. Some of these are: the

Homogeneous Flow model, the Momentum Exchange model, and the Separated Phase model.

1. Homogeneous Flow Model

This model assumes one dimensional steady flow of a homogeneous, two-phase, gas-liquid mixture in a constant area duct at thermodynamic equilibrium with no relative velocity between the phases. The conservation of mass, the conservation of linear momentum and the energy equations are developed and lead to the expression of pressure drop per unit length shown below

$$(dP/dx) = (dP/dx)_{acc.} + (dP/dx)_{fric.} + (dP/dx)_{grav.} \quad (1)$$

Here, $(dP/dx)_{acc.}$ is the acceleration or deceleration of flow due to large changes of volume. This occurs during gas-liquid phase changes when flow pressure level is below the thermodynamic critical pressure for the substance involved and is given by

$$(dP/dx)_{acc.} = - \frac{16}{g_o} \frac{\dot{m}_T \dot{q} \bar{V}_{fg}}{(\pi D^2)^2 L h_{fg}} \quad (2)$$

with, \dot{m}_T = total mass flow rate (lbm/sec)
 \dot{q} = heat transfer rate (BTU/sec)
 \bar{V}_{fg} = specific volume changes during vaporization (ft³/lbm)
 h_{fg} = heat of vaporization (BTU/lbm)
 D = diameter of duct (ft)
 L = length of duct (ft)
 g_o = unit conversion factor (32.17 lbm-ft/lbf-sec²)

The remaining terms in Equation 1 are:

$(dP/dx)_{grav.}$ due to the acceleration or deceleration of gravity and is zero for horizontal flows.

$(dP/dx)_{\text{fric.}}$ the pressure drop due to wall friction,
no other viscous forces are considered by
this model and is given by

$$(dP/dx)_{\text{fric.}} = \frac{-4 \tau_w}{D} \quad (3)$$

where τ_w is the wall shear stress.

To determine the pressure drop, some formulation for τ_w must be found and it is the subject of various models. Reference 1 contains the details of these developments.

2. Momentum Exchange Model

This model assumes that each phase satisfies the momentum equation separately and that the static pressures for each phase are equal to one another at any arbitrary cross section. A constant area, cylindrical control volume is defined for each phase and the flow is considered steady and one dimensional within each phase. The Momentum model accounts for the momentum exchange between phases due to vaporization and the total shear forces, dF_{sl} and dF_{sg} , acting on the liquid and gas phases respectively.

The pressure drop is again due to three factors; friction, momentum change, and the "hydrostatic heat changes". That is,

$$(dP/dx) = (dP/dx)_{\text{fric.}} + (dP/dx)_{\text{m.c.}} + (dP/dx)_{\text{h.h.c.}} \quad (4)$$

$$\text{where, } (dP/dx)_{\text{m.c.}} = \frac{-4}{g_o \pi D} \frac{d}{dx} (V_g \dot{m}_g + V_L \dot{m}_L) \quad (5)$$

with, \dot{m}_g = gas flow rate (lbm/sec)

\dot{m}_L = liquid flow rate (lbm/sec)

V_L = liquid velocity (ft/sec)

V_g = gas velocity (ft/sec)

$$g_o = \text{unit conversion factor} \quad (32.17 \text{ lbm-ft/lbf-sec}^2)$$

$$\text{and} \quad (dP/dx)_{h.h.c.} = \frac{1}{g_o} \left[\rho_g \left(\frac{D_g}{D} \right)^2 + \rho_L \left(\frac{D_L}{D} \right)^2 \right] g \cos \theta \quad (6)$$

$$\text{with,} \quad D_g = \text{diameter of gas core} \quad (\text{ft.})$$

$$D_L = \text{diameter of liquid annulus} \quad (\text{ft.})$$

$$\rho_g = \text{density of the gas} \quad (\text{lbm/ft}^3)$$

$$\rho_L = \text{density of the liquid} \quad (\text{lbm/ft}^3)$$

$$\theta = \text{flow orientation} \quad (0 \text{ for horizontal flow})$$

$$\text{and,} \quad (dP/dx)_{\text{fric.}} = \frac{-4}{g_o \pi D^2} \left(\frac{dF_s}{dx} \right) \quad (7)$$

To obtain a solution for the pressure drop assume that Equation 3 holds and that

$$\tau_w = \rho_L f'_L \frac{V_L^2}{2g_o} \quad (8)$$

where f'_L is the friction factor for the liquid phase and V_L is the average water flow velocity given by,

$$V_L = \frac{4 \dot{m}_L}{\pi \rho_L D_L^2} = \frac{G (1-x)}{\rho_L (1-\alpha)} \quad (9)$$

$$\text{with,} \quad x = \text{flowing mass quality} \quad (\dot{m}_g / \dot{m}_{\text{total}})$$

$$\alpha = \text{void fraction} \quad \left(\frac{\text{volume gas}}{\text{total vol.}} \right)$$

$$G = \text{mass flux} \quad (\text{lbm/ft}^2)$$

Substituting Eqns. 9 and 8 into Eqn. 3, the two phase pressure drop becomes

$$\left(\frac{dP}{dx} \right)_{\text{TP}} = \frac{2 f'_L G^2 (1-x)^2}{g_o D \rho_L^2 (1-\alpha)^2} \quad (10)$$

The remaining problem is to determine the correct value for f'_L since the gas phase will have some influence on the liquid flow and since

f_L' will not be a function of the liquid Reynolds number alone. Reference 1 details the solution.

3. Separated Phase Model

This model is often called a flow pattern model because the analytical models are derived for three distinct patterns of flow: annular, stratified, and slug. An annular flow model [Levy 1952] is particularly applicable in this study and is discussed below. There are, however, many different annular flow models, as well as stratified and slug models which differ in sophistication and application.

Levy assumed: steady, horizontal, annular, fully developed, two-phase, two component flow in a horizontal pipe with no gravity effects, no interfacial shear stress and no changes in either phase velocity, and that there are no momentum or gravity changes. Again the momentum equation reduces Eqn. 3. Levy obtained an expression for the velocity distribution in the concentric liquid annulus as well as the gas core for both laminar and turbulent flows.

Using the velocity profiles to obtain the wall shear stress and after much manipulation [Ref. 1] the following expressions are obtained for fully turbulent flows.

$$X_{tt} = \left(\frac{\dot{m}_L}{\dot{m}_g} \right)^{7/4} \frac{\rho_g}{\rho_L} \left(\frac{\mu_L}{\mu_g} \right)^{1/4} \quad (11)$$

where, μ = fluid viscosity (lbm/ft-sec)

$$\text{and, } \Phi_{Ltt} = \left(\frac{7}{120} \right)^{7/4} \frac{1}{(1-\alpha^2) \left[.125 - \frac{1}{15}(1-\alpha^2) \right]} \quad (12)$$

where, $X = (dP/dx)_L / (dP/dx)_g$ (liquid to gas pressure drop ratio)

$\Phi_L = (dP/dx)_{TP} / (dP/dx)_L$ (two-phase to liquid pressure drop ratio)

which are the familiar Lockhart-Martinelli parameters and will be discussed in more detail below.

Reference 1 discusses the various modeling techniques and the limited success of each, because no one model is applicable to the entire range of two-phase flow. For example the Homogeneous Flow model would be expected to give good results for flows where one component completely dominated the other, as in Mist flow or Bubble flow, whereas the same analysis would probably give poor results for Slug flow.

C. EMPIRICAL FLOW MODELS

It is difficult to obtain solutions from analytical models when dealing with turbulent two-phase flows, and empirical methods are used to resolve this difficulty. There are nearly as many empirical correlations for two-phase pressure loss prediction as there are experiments on the subject. Two of the more successful are discussed in the following sections and are used in this thesis. In general each correlation scheme is only good for the range of data collected. The Chenoweth-Martin correlation was obtained from fully turbulent flows, while the Lockhart-Martinelli prediction is based on low pressure flows in small diameter pipes. Dukler, Wicks, and Cleveland [Ref. 2] noted that the Chenoweth-Martin correlation is more applicable to large diameter pipes and slug flow than is the Martinelli scheme.

1. Lockhart-Martinelli Correlation

In 1949 R. W. Lockhart and R. C. Martinelli [Ref. 3] proposed a correlation for predicting two-phase pressure drops for horizontal pipe flow based on two-component gas-liquid data. The correlation depends upon the turbulence level of each flow component, thus four

distinct types of flow are possible depending upon whether the liquid or gas phases are laminar or turbulent. The four flow categories are: viscous-viscous, viscous-turbulent, turbulent-viscous, or turbulent-turbulent, where viscous refers to laminar flow. The data available for the correlation were grouped according to the four categories and correlated as a function of the Lockhart-Martinelli parameters, X and Φ . Lockhart and Martinelli assumed transition from laminar to turbulent flow to occur in the range of Reynolds numbers between 1000 and 2000. They point out that the criterion of Reynolds number equal to 2000 for turbulence is a conservative one and could be improved upon. [Ref. 3]

A special assumption made by Lockhart and Martinelli is that the static pressure drop for the liquid phase was equal to the static pressure drop for the gas phase regardless of the flow pattern, as long as an appreciable radial static pressure difference did not exist. Further they assumed that the volume occupied by the gas plus the volume occupied by the liquid was equal to the total pipe volume, which eliminates stratified flows from consideration.

The two-phase pressure drop can be predicted based on a fictitious all-liquid pressure drop or based on a fictitious all-gas pressure drop; either approach will yield the same result. This is accomplished by separating two phase flow into its two component flows and treating the pressure drop as a unique function of either component.

The term "fictitious" is used to describe the resulting parameters of each flow component. To determine the fictitious all gas pressure drop a fictitious Reynolds number is used. That is,

$$Re'_g = 4 \frac{\dot{m}_g}{\pi D \mu_g} \quad (13)$$

where, \dot{m}_g = gas mass flow rate (lbm/sec)
 μ_g = gas viscosity (lbm/sec-ft)
 D = inside diameter of pipe (ft)

similarly,

$$Re'_L = \frac{4 \dot{m}_L}{\pi D \mu_L} \quad (14)$$

This fictitious Reynolds number is used to determine the fictitious friction factor from the Moody diagram. This fictitious gas, or liquid, friction factor is used to determine the fictitious all gas, or liquid, pressure drop.

$$\Delta P'_g = \frac{1}{g_o} \rho_g f'_g \frac{L}{D} \frac{V_g'^2}{2} \quad (15)$$

where, $\Delta P'_g$ = fictitious all gas pressure drop (lbf/ft²)
 ρ_g = gas density (lbm/ft³)
 L = length of pipe section (ft)
 f'_g = fictitious gas friction factor
 V'_g = fictitious gas velocity (ft/sec)

similarly,

$$\Delta P'_L = \frac{1}{g_o} \rho_L f'_L \frac{L}{D} \frac{V_L'^2}{2} \quad (16)$$

The fictitious fluid velocities can be determined from continuity assuming that the component of flow occupies the entire pipe.

The Lockhart-Martinelli correlation expresses the two-phase pressure drop in terms of a parameter Φ times the fictitious pressure drop. That is, based on liquid flow,

$$(\Delta P)_{TP} = \phi_L^2 \Delta P_L' \quad (17)$$

or gas flow

$$(\Delta P)_{TP} = \phi_g^2 \Delta P_g' \quad (18)$$

The parameter ϕ was found to be a function of another dimensionless parameter, χ , which in turn can be expressed in terms of the ratio of liquid and gas mass flow rates, the ratio of densities of the flow components, the viscosity ratio, and the tube diameter. To simplify things Lockhart and Martinelli introduced a new parameter, X , similar to χ , but in a more generalized form. Or simply,

$$X^2 = \Delta P_L' / \Delta P_g' \quad (19)$$

Figure 2 is the Lockhart-Martinelli correlation of X and ϕ for each of the four flow cases mentioned. Eight curves are possible, four each for each flow component.

To predict a two-phase pressure drop the mass flow rates of each component must be known along with the fluid properties such as density and viscosity. For example, a two-phase pressure drop based on the liquid flow may be made in the following manner: First the fictitious liquid Reynolds number is calculated from equation (14). Next the fluid velocity can be calculated from the definition of the Reynolds number. That is,

$$v_L' = \frac{R_L'}{D} \frac{\mu_L}{\rho_L} \quad (20)$$

The fictitious friction factor, f_L' , is determined from a Moody plot and the fictitious liquid pressure drop is calculated from equation

(16). Similarly, the fictitious gas pressure drop is determined and the two-phase flow modulus X is calculated by taking the square root of equation (19). Figure 2 is entered with the X value and the appropriate curve is chosen depending on the flow turbulence. For example, if the gas flow and liquid flow Reynolds numbers were both greater than 2000 the ϕ_{Ltt} curves would be used.

The liquid correlation parameter based on turbulent flow, ϕ_{Ltt} , or the gas correlation parameter, ϕ_{gtt} , is the output from Figure 2. The resulting two-phase pressure drop prediction is obtained by substituting ϕ_{Ltt} into Equation (17) or ϕ_{gtt} into Equation (18).

More recent studies on air water flows by Carl Gazley and O. P. Bergelin [Ref. 3] indicate that the scatter of data around the predicted values is within +20% and -30%. Also noted was that a better correlation is realized if separate plots are made for each constant water rate for various air flows. This implies that the parameter ϕ_g is not a function of X alone but depends upon the liquid flow rate.

2. Chenoweth-Martin Correlation

In 1955 J. Chenoweth and M. Martin [Ref. 4] developed an "improved" correlation scheme for two-phase flow pressure drop prediction in horizontal pipes valid for pressures up to 100 psia and pipe sizes up to three inches in diameter. The correlation differs from the previous one in that it can be used to predict single-phase as well as two-phase pressure drops, and that this formulation is only valid for fully turbulent flows.

This correlation used a friction factor based on a fictitious Reynolds number that is derived from the total mass flow in the pipe. For example the fictitious gas Reynolds number is given by,

$$\text{Re}_g^* = 4 (\dot{m}_g + \dot{m}_L) / \pi D \mu_g \quad (21)$$

where the superscript "*" is used to differentiate between the Lockhart-Martinelli fictitious formulation. Similarly,

$$\text{Re}_L^* = 4 (\dot{m}_g + \dot{m}_L) / \pi D \mu_L \quad (22)$$

Using the same approach as did Lockhart and Martinelli the fictitious friction factor can be determined. To calculate the fictitious gas, or liquid pressure drop the fictitious gas, or liquid, velocity is calculated based on total mass flow. That is,

$$V_g^* = \frac{\dot{m}_L + \dot{m}_g}{\rho_g A} = \frac{\text{Re}_g^*}{D} \frac{\mu_g}{\rho_g} \quad (23)$$

and

$$V_L^* = \frac{\dot{m}_L + \dot{m}_g}{\rho_L A} = \frac{\text{Re}_L^*}{D} \frac{\mu_L}{\rho_L} \quad (24)$$

where A = cross sectional area of the total flow. The fictitious pressure drops are then given by,

$$\Delta P_g^* = \rho_g f_g^* \frac{L}{D} V_g^{*2} \quad (25)$$

and

$$\Delta P_L^* = \rho_L f_L^* \frac{L}{D} V_L^{*2} \quad (26)$$

The Chenoweth-Martin correlation is given in terms of the amount of liquid flow in the total flow and of a correlation parameter based on the ratio of the all liquid to all gas pressure drops. The measure of the amount of liquid flow in the two-phase flow is the liquid volume fraction and is given by

$$\text{LVF} = \frac{\text{Volume Flow Rate of Liquid}}{\text{Total Flow Rate}} = \frac{1}{1 - \frac{\dot{m}_g \rho_L}{\dot{m}_L \rho_g}} \quad (27)$$

The correlation parameter is given by

$$\lambda = \frac{\text{EQN. (26)}}{\text{EQN. (25)}} = \frac{f_L^* \rho_g}{f_g^* \rho_L} \quad (28)$$

if no losses are experienced in valves and fittings.

A more exact expression can be used accounting for the losses by adding a constant factor. That is, let

$$\Psi_L^* = f_L^* \frac{L}{D} + \sum K_L \quad (29)$$

and

$$\Psi_g^* = f_g^* \frac{L}{D} + \sum K_g \quad (30)$$

then

$$\lambda = \frac{\rho_g \Psi_L^*}{\rho_L \Psi_g^*} \quad (31)$$

which is the expression in Figure 3. The Chenoweth and Martin two-phase pressure drop prediction is given in terms of the ratio of the two-phase pressure drop to the fictitious all liquid pressure drop, i.e.,

$$\Omega = \frac{\Delta P_{TP}}{\Delta P_L^*} \quad (32)$$

To use the Chenoweth-Martin correlation to predict the two-phase pressure drop the same approach is used as in Lockhart-Martinelli except only the fictitious liquid pressure drop is needed. For example, a fictitious gas Reynolds number is calculated from equation (21) and the liquid Reynolds number from equation (22). The fictitious friction factors are again determined from a Moody plot using the fictitious Reynolds numbers.

The correlation parameter is determined from equation (28) neglecting the losses in fittings and valves. The LVF is calculated from equation (27) and Figure 3 is used to determine Ω .

The fictitious all liquid pressure drop is calculated from equation (26) and is multiplied by Ω to arrive at the predicted two-phase pressure drop.

No single analytical expression could be found for Figure 3 because of the logarithmic scales on both axis. However a subroutine was devised using a fifth order polynomial expression for the five curves based on an artificial linear scale. A conversion from logarithmic to linear scale is made upon entry, another subroutine (Splinn) is used to extrapolate for the correct value of λ and the output linear scale (Ω) is again converted to logarithmic scale. This is the subroutine CHNWITH given in Appendix I. It is estimated that there is an average error of about two percent in the subroutine which is considered accurate enough in view of the errors that can be made by a hand calculation.

Studies made by Reid, et al, [Ref. 5] and Dukler, Wicks and Cleveland [Ref. 2] indicate that for larger diameter pipes the Chenoweth-Martin correlation gives consistently better results, while the Lockhart-Martinelli scheme predictions differed by as much as 250% from the former's prediction. The data used in the study by Reid and associates was for four and six inch diameter pipes with fully turbulent flow.

Chenoweth and Martin based their correlation on data collected with pipe sizes up to three inches in diameter and flow pressures up to

100 psia. The Chenoweth correlation has been reported accurate to within $\pm 25\%$ for pipe sizes ranging from one and one-half to three inches in diameter.

D. TRANSITION

Figure 4 shows that the slope of the pressure gradient changes at a specific point in two-phase flow indicating the phenomenon of transition. Chien and Ibele [Ref. 6] have shown that the change is related to the change in flow pattern. For example the transition from Annular flow to Annular-Mist flow is accompanied by a corresponding change in the pressure gradient. It has been reasoned that since Annular flow has low-speed, high-viscosity water in contact with the pipe wall and Annular-Mist flows have high-speed, low-viscosity air in contact, this difference in fluid properties can give radically different wall shear forces.

Figure 5 shows the development from pure Mist to fully Annular flow. Figure 5D has a portion of the friction factor curve with the fictitious liquid friction factor noted and with the air flow at a high, constant Reynolds number. The pressure drop for the two-phase flow would follow the same pattern as shown in Figure 5E, that is, the flow would be dominated by the air portion for low water rates (Fig. 5A), but as the liquid flow increases (Fig. 5B), the liquid friction factor is superimposed upon the air flow. At the high water rates (Fig. 5C), the liquid is primarily responsible for the pressure drop.

Chien and Ibele have conducted an extensive study of two-phase pressure drop and fluid film thickness in vertical pipe flow as related to the transition from Annular to Annular-Mist flow. Using the Lockhart-

Martinelli notation, Figure 4 is taken from Reference 6 and shows the two-phase pressure drop plotted against the fictitious gas Reynolds number for various water flow rates. Chien and Ibele mention the transition phenomenon in the following:

"The friction pressure gradient along the test section increases with both gas and liquid flow rates...however for each liquid flow rate there is a transition gas Reynolds number at which the pressure gradient has a change. A careful study of these flow rates together with observations of the flow pattern indicated that the changes in the pressure gradient was associated with a change in the flow pattern."

In addition to this real transition there will occur a numerical transition when predicting the pressure drop with the Martinelli scheme. Numerical transition refers to the change from the laminar curve to the turbulent curve used in the correlation, which results in a discontinuity in the Lockhart-Martinelli pressure gradients. The transition criterion is somewhat arbitrary and could be modified to give better correlations when the flow regime is known accurately. Lockhart and Martinelli readily admit that the weakness of their correlation is in the transition criteria. Since Chenoweth and Martin treat only fully turbulent flows they are not afflicted with this problem but suffer the exclusion of laminar flows from their correlation.

The Ibele study correlated the pressure drop and the observed transition of the flow to derive an expression for predicting the transition. The correlation arrived at is only appropriate for low flow velocities in horizontal pipes, but the technique used by Chien and Ibele is discussed here to indicate the significance of the problem and how it might be solved.

An oscilloscope and film probes were used to measure the flow properties. Figure 6, taken from Reference 6, shows fictitious gas Reynolds number plotted against fictitious liquid Reynolds number for transition points indicated by the film probes and pressure gradient changes. The flow was observed through a transparent portion of the test section and the transition from Annular-Mist flow was confirmed. The transition can be calculated to occur when the product of the liquid and gas fictitious Reynolds numbers reach a critical value. Their transition Equation is

$$A = Re'_g (Re'_L)^{0.301} \quad (33)$$

When A is less than 1.199×10^6 , Annular flow exists, and when A is greater than 1.199×10^6 , Annular-Mist flow exists.

Horizontal flow differs from vertical flow in that there is no gravity term in the momentum equation and that the annular flow is not symmetrical to the pipe axis. This particular flow geometry usually prevents the formation of pure Annular flow and some form of Annular-Mist flow occurs because gravity causes the liquid flow to concentrate along the pipe bottom. Consequently the transition criteria described above will have limited applications in this study, specifically, to low water rates since vertical and horizontal pipe flows are similar in this case.

II. THE TWO-PHASE FLOW TEST APPARATUS

The test rig used to study the two-phase flow is shown in Figure 7 prior to modification for the current study. Figure 8 is a flow schematic of the rig showing the top and side views. Pressure regulators for the air and the water modulate the flow into the system at point A in Figure 8. Each flow is measured by thin plate orifices using both flange taps as well as $D-\frac{1}{2}D$ taps to provide a cross check on the data and then the flows are mixed together at B in Figure 8. The two-phase flow is allowed to become fully developed by a run of 20 feet of straight pipe after which the flow is turned down into the test section at C. The two phase flow exhausts to atmosphere where the separated water flow is measured to determine the percentage mist.

Figure 9 shows the flow inputs to the rig and the pressure regulators. Two air supplies and one water supply are used in this present study.

The water enters the system through a section of one inch diameter stainless steel tubing which contains a metering orifice. An identical metering section is used for measuring low air flows. The orifice pressures are measured by water-filled mercury manometers that have bleed valves to allow entrapped air to escape. The water flow temperature is measured after the metering orifice by an Iron-Constantan thermocouple. The water flow metering section consists of 20 feet of tubing parallel to and located four feet above the bottom of the test rig. After metering, the water flow turns up three more feet to enter the mixing duct. A T-fitting with two valves, joins the metering

section to the injection section. One valve can be used to regulate the water flow to the injector and the other is used to measure the true water flow rate which is used to calibrate the water orifice. (See section B-1) An identical system is used to supply low air flows to the rig except water filled manometers are used instead of water filled mercury manometers.

The main air supply comes from a plenum which is fed by a reciprocating compressor capable of supplying 700 SCFM at 150 psig. The air enters the system through a 2 inch diameter steel pipe after the flow is regulated by a pressure regulator that can be set to deliver pressures as low as 25 psig. The same type of flow metering orifice is used as in water flow, and mercury manometers are used to measure the orifice pressures. Figure 10 shows the main air orifice and Figure 11 shows the details of the orifice design. The same type of thermocouple is used to measure the air flow temperature after the orifice. The main air flow is parallel to the water flow but on the bottom of the test rig. The metered air flow enters the mixing duct from below and at an angle of forty-five degrees from the vertical. The details of the injection schemes used to mix the air and water flows are the subject of Section III of this thesis and will not be detailed here. Figure 12 shows the configuration of the mixing duct with the 1" diameter water supply line entering axially and the 2" diameter air supply entering at 45° from below. The two-phase flow mixes in the subsequent 20 feet of 3" diameter pipe. The flow is dropped down and turned by a four foot long "U" bend in the pipe. Ten more feet of pipe is used to allow the flow to develop after the bend.

The "floating" test section consists of a labyrinth seal, Figure 13, and a horizontal, three inch diameter, ten foot long pipe. The labyrinth seal details are shown in Figure 14 and has a pressure tap located at the top and a water drain at the bottom. The pressure tap provides for the measurement of the test-section inlet static pressure using an inclined water manometer. This pressure was used in correcting the flexure readings for labyrinth seal pressure force as well as in the air leakage measurement; furthermore, the two correlation schemes mentioned earlier use the pressure to calculate the predicted pressure drops.

The test section shown in Figure 15 is supported two feet from either end by four stainless steel, one-eighth inch diameter rods that are attached to the frame of the rig through bearings to allow axial mobility of the test section. Figure 16 shows the two cantilever beam flexures that are mounted to the frame and contact the test section through knife edges mounted at its mid-point. These flexures resist the forward motion of the pipe that results from the wall shear forces exerted by the flow. Each beam flexure has four strain gages mounted and wired to form a Wheatstone bridge circuit. Through calibration the strain gage bridge output can be related to the loads on the flexures. Again, the use of two flexures provide a cross check on the data. The two-phase flow exhausts to the atmosphere where a trough collects the separated portion of the flow while the mist portion is allowed to dissipate.

The apparatus has the hardware for adding water flow through a three inch pipe fed by a centrifugal water pump capable of water flow rates up to 500 gpm at 80 psig. However, to implement this capability would

have required the addition of a water collection tank and return piping for the water. Ultimate studies will concern separating the pressure drop due to the wall shear from the pressure drop resulting from the mixing process immediately after injection.

B. CALIBRATION OF THE RIG

Before two-phase flow tests could be conducted the following preliminary work was done: (1) determination of the small diameter pipe coefficient, (2) labyrinth air leakage calibration, (3) flexure calibration, and (4) determination of the relative pipe roughness factor.

1. Pipe Coefficient Calibration

The pipe coefficient, K , is a unique function of the orifice diameter ratio and the flow Reynolds number for a particular pressure tap connection. K was determined for various Reynolds numbers by measuring the actual water flow rate and solving the mass flow rate equation for K . Letting the velocity of approach factor be included in K , the formulation is, in American units,

$$K = \dot{m} / 359 (d^2) F_a (h_w \eta)^{\frac{1}{2}} \quad (33)$$

where, \dot{m} = mass flow rate (lbm/sec)
 d = diameter of orifice (inches)
 F_a = thermal expansion factor (ratio)
 h_w = differential pressure in water at 68°F (inches)
 η = specific weight of the flowing fluid (lbf/ft³)

The water was collected at the dump valve in a bucket and weighed to determine the mass flow rate. The data was collected separately for

each pressure connection type, Figure 17 shows the pipe coefficient as a function of the flow Reynolds number. The curves were added to the computer program and are used in water and secondary air mass flow calculations.

2. Labyrinth Air Leakage Calibration

Because higher pressure exists in the test section with respect to the atmosphere there is a small amount of flow leakage through the seal. This loss is a function of the test section pressure and can be calibrated for various test section pressures. Water leakage posed no problem because it could be measured directly but the air leakage had to be based on a dry calibration determined by sealing off the test section exit and metering small air flows into the system. The amount of air measured by the orifice was the amount that leaked through the labyrinth, assuming no other leaks in the system. The system pressure integrity was checked before and after each calibration run. Data was collected separately for both the D- $\frac{1}{2}$ D taps and the Flange taps. Figure 18 shows the data for both taps plotted as labyrinth differential pressure ratio against mass flow rate. A least squares regression was used to generate the equation describing the relation. Only one curve is shown in Figure 18 for the sake of clarity in drawing, however the computer program calculates the mass flow leakage separately for each pressure tap connection.

3. Flexure Calibration

The original design of the rig was to measure large pressure drops resulting from the use of the large water supply, consequently the flexures were designed for loads approaching fifty pounds. However the early, low pressure studies never exceeded loads of six pounds which

obviated the use of the Daytronic Strain Gage Indicator used by Watson [Ref. 7]. To overcome this difficulty without rebuilding the flexures a direct readout from the strain gages was obtained using a millivoltmeter with a six volt d.c. input to the bridges. This setup is shown in Figure 19 and the wiring schematic in Figure 20B. The power source was switched between the flexures, depending on which one was being measured, thus eliminating cross feed of signals due to a common power source. Resolution of the system without signal amplification was about a tenth of a pound which was considered adequate for this study.

Calibration of the flexures, to obtain the relationship between load and voltage reading, was performed prior to and after each run. Figure 21 shows the system of weights and pulley used in the calibration. Figure 22 is a typical calibration curve for the two flexures. The flexures were color coded red and black. The colors corresponded to the color of the wire leads from each flexure and made identification easier.

4. Equivalent Pipe Roughness Factor

The computation of predicted pressure drop requires an accurate knowledge of the friction factor as a function of pipe Reynolds number. Standard pipe friction factor curves (Moody plot) are used but pipe roughness must be known to choose the appropriate curve. This was accomplished by measuring pressure drops for pure air flows, computing the friction factors and plotting them as a function of the Reynolds number. Figure 23 shows a portion of the friction factor graph for three pipe roughness factors of; .0002, .0004, and .0006, together with the experimental values. Again a least squares regression was used to fit the data and the dashed curve represents the curve fit. A pipe

roughness factor of .0004 was subsequently used for the turbulent flow calculations while for laminar flow the friction factor is,

$$f = 64 / \text{Re}_D \quad (35)$$

No attempt was made to smooth the transition between the curves and a transition criterion of $\text{Re} = 2000$ was used.

C. DATA REDUCTION

A computer program is used for data reduction and prediction of the two-phase pressure drop according to Lockhart-Martinelli and Chenoweth-Martin. The program calculates the mass flow rates for each pressure tap and corrects the air flow for the labyrinth leakage rate. Percentage mist is also calculated (see Section III A).

The Lockhart-Martinelli curves and the Chenoweth-Martin curves, figures 2 and 3, are programed in the computer routine for the calculation of predicted pressure drop. The flexure readings are corrected for the labyrinth pressure force and are converted to pressure drop readings compatible in format to the predicted pressure drop. Appendix I contains the entire computer program with a sample case to illustrate the output format.

III. INJECTION STUDIES

A. INTRODUCTION AND DESCRIPTION OF INJECTORS

Early studies of two-phase flow were to be conducted in the pure Mist flow regime; however, it soon became apparent that more than half the flow would remain as a separate component regardless of the water and air flow rates. This was originally thought to be a result of poor water injection techniques. Studies were conducted on four different methods of water injection in an attempt to determine the most efficient means of achieving pure Mist flow. A further reason for the fluid separation was thought to result from the sharp bend in the piping that was required to turn the flow into the test section. A major redesign of the rig would have been required to eliminate the bend and the studies were expanded to investigate the effect that the pipe geometry had on the flow separation.

The study consisted of a photographic analysis of flow patterns at injection and then at the exit from the twenty foot long, straight section of pipe prior to the turning section. In addition to the photographs the amount of separated water was collected and measured to get a quantitative means for comparison of the photographs. The separated water was expressed as the ratio of water rate collected over total water flux entering the section

$$\text{Separated water ratio} = W_{\text{SWR}} = \frac{\dot{m}_{\text{sep}}}{\dot{m}_{\text{total water}}} \quad (36)$$

The percentage mist is

$$\text{Percentage mist} = 100 (1 - W_{\text{SWR}}) \quad (37)$$

Limited space prevented the measure of separated water at injection but some feeling for the efficiency of injection is obtained from the photographs. Figures 24A through 24D show the 30 inch long, 3 inch diameter mixing duct and the geometries of the four injection methods that were used.

1. Case I

Figure 24A shows the simplest injection scheme tested. Water was allowed to flow from the water flange 1" diameter opening across the air entrance. Atomization of the water occurs because of the large difference in relative flow velocities at that point. At low water rates, when the fluid is unable to carry across the plane of the air injection, the atomization is not as complete and the injection efficiency degrades.

Figure 25 shows the injection pattern for a fixed air to water flow ratio. Figure 26 is the flow pattern after twenty feet of straight 3 inch diameter piping. The mist portion of the flow appears nearly solid white, while the separated portion can be seen as a streaked region below the mist.

2. Case II

This method of injection is similar to Case I except that water was introduced into the air beyond the point of air injection using a standard $\frac{1}{4}$ " pipe. This method eliminated the degradation of the mixing due to low water rates that occurs in the Case I scheme. Figure 27 shows the injection pattern and 18 shows the pattern of flow at exit.

3. Case III

A standard bathroom shower nozzle was used to inject the water in this case. The nozzle face is two inches in diameter with a spray

plate to spread the flow radially, the nozzle base threads on to the standard $\frac{1}{4}$ " pipe used in Case II and the air is forced through a converging duct created by the nozzle body and the pipe wall (approximately $\frac{1}{2}$ inch radial clearance), thereby causing the air flow to accelerate. This resulted in maintaining the liquid portion of the flow in the core of the pipe surrounded by the air flow. This appeared to be the most efficient means of injection (Fig. 29), however, the maximum water flow rate was restricted by the nozzle capacity and to achieve comparable air to water ratios, as in the other cases, the air velocity had to be reduced. Figure 30 is the pattern of flow at exit and is nearly the same as the previous two cases.

4. Case IV

The shower nozzle of Case III is replaced by a nozzle designed to inject the water into the pipe wall area in addition to the core of the pipe. Figure 24D details the geometry of the injector. The cylindrical body of the nozzle is 2 inches long and one inch in diameter with four quarter inch diameter rods mounted normal to the injector axis. Each rod has an eighth inch diameter hole through which the water is ejected perpendicular to the pipe wall. Also, water is injected through a quarter inch orifice along the central axis of the pipe. The lack of mixing can be seen in Figure 31 at injection, this was considered the worst method of water injection when trying to achieve pure Mist flow. But the flow pattern at exit, Figure 32, is nearly the same as the others. Further, the pipe bend was connected and the flow pattern after the bend, 8 more feet of pipe and the 10 foot test section is shown in Figure 33.

B. CONCLUSIONS

Figure 34 is a plot of percentage Mist against air to water ratios for a range of air and water rates in the 20 foot straight pipe section. Air was held constant whenever possible at approximately 0.62 lbm/sec and all four injection cases are shown on the same plot for comparison.

The low data point for the Case III nozzle is probably due to a change in the air flow rate. The maximum water flow rate was limited to 0.22 lbm/sec using this nozzle whereas the other nozzles could attain flow rates of 0.36 lbm/sec. To get data points for the air to water ratio of 1.5 the air flow had to be reduced from 0.62 lbm/sec to 0.33 lbm/sec. This suggests that the amount of mist in the flow is dependent upon the gas velocity. The Case IV nozzle was used in a further study of the dependence of the percentage mist on the gas velocity as well as the pipe bend and longer piping. Figure 35 is a plot using the Case IV nozzle of a run with constant water flow and variable air flow as well as the usual constant air flow. The Case IV plot from Figure 34 is carried over for comparison. Very little loss was experienced with the addition of the pipe bend and test section which leads to the conclusion that flow equilibrium is reached by the end of the 20 foot mixing section. Although some water separation probably occurs as a result of the pipe bend, most of this water is again entrained in the 10 feet prior to the test section. The differences in gas velocity appears to be the only reason for the slight loss between the two constant air flow curves. The constant water plot indicates that there is some critical gas velocity below which there is an inability to sustain water droplets. Chapter 12 of Reference 9 has a good discussion of this effect.

As expected, the Case III nozzle was the most efficient means of water injection but it was not used in the pressure drop studies due to its limited water capacity. The Case IV nozzle was considered the best overall giving high water rates at nearly constant Mist percentages and was used in the correlation studies.

IV. CORRELATION RESULTS

A. DISCUSSION

Sixty-seven runs were made at varying air and water flow rates using the Case IV nozzle. A set of runs consists of eight water flow rates ranging from 0.1 lbm/sec to 0.43 lbm/sec for one constant air flow rate. Six constant air flows were used ranging from 0.35 lbm/sec to 0.60 lbm/sec. The remaining nineteen runs represent random repeat runs that were used to verify the data collected.

Figure 36 shows the red flexure data plotted as a function of the Lockhart-Martinelli fictitious gas Reynolds number. Figure 37 shows the black flexure readings. The spread in the pressure drops is primarily due to the varying water flow rates. The higher pressure drops indicate the higher water flow rates, further there appears to be a larger spread in the data at higher gas flow rates, which probably indicates the flow pattern transition from Annular to Annular-Mist flow. The effect of the two different flow patterns has been previously discussed in Section I-D.

The Lockhart-Martinelli pressure drop predictions are shown in Figure 38 as a function of the fictitious gas Reynolds number. The two curves are a result of the Lockhart-Martinelli transition from viscous-turbulent flow to turbulent-turbulent flow. Figure 39 shows the Chenoweth-Martin pressure drop predictions and it also consists of two curves. Although the Martin correlation was derived for all turbulent flow it has a laminar section which is a result of the discontinuous transition from the laminar to the turbulent portion of the friction factor curve. To simplify the following discussion the

Chenoweth-Martin pressure drop prediction for fictitious water Reynolds numbers of 2000 or less will be called laminar, however this is a misnomer since the Martin prediction does not recognize laminar flow.

Both correlation schemes have a discontinuity at the water Reynolds number of 2000 which is a source of error in the predicted pressure drops. The two-phase flow does transition but rarely at the same Reynolds number that the correlations do. Figures 40 to 45 show the black flexure readings for different constant water rates as a function of the fictitious water Reynolds number. Plotting the data in this manner emphasizes the problem that transition causes. The Lockhart-Martinelli prediction is represented by the solid line and the Chenoweth-Martin is the dashed line. Two trends are apparent when comparing the curves at different constant air flows. First, the measured pressure drop appears to transition from annular flow to annular-mist flow at lower water Reynolds number for higher air flows. This effect has been noted by Chien and Ibele in Reference 6 and can be seen in Figure 4. Secondly the Lockhart-Martinelli laminar curve converges with the laminar Chenoweth-Martin curves at an air flow rate of 0.50 lbm/sec, and then diverges for higher flow rates. Both laminar curves predict too high a pressure drop for low air flows and transition well in advance of the data. However at high air flows the data soon surpasses the predicted transition (See Figure 45 at the air flow rate of 0.60 lbm/sec.). Figure 46 presents the same data as Figure 40 but with the correlation transition criteria changed to a fictitious Reynolds number of 3000. Good agreement is obtained between the predicted and actual pressure drops. However, this solution would introduce greater error

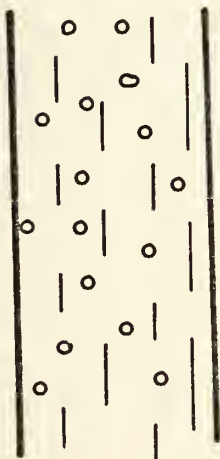
in the correlations for higher air flows which indicates the need for defining a transition criteria based on both the air and the water flow.

Following the work of Chien and Ibele a plot of the inflection points of the slope of the pressure gradient ($\Delta P/\Delta L$) for Figures 40 through 45 is used to determine a transition criterion. Figure 47 shows the data from Figure 45 with a smooth curve drawn through the points. The region within the dashed lines is the transition region of the flow where the curvature of the plot changes from a positive value to a negative value. The approximate point of change in the slope is plotted as a function of the water and air Reynolds numbers. Figure 48 is the transition criterion with the annular region to the left of the line, and the annular-mist to the right. This criterion is only a crude approximation of the work done in Reference 6, but it does give insight into the actual pressure drop transition behavior. The percentage mist should indicate the transition as does the change in slope of the pressure gradient. Figure 49 is a plot of the percentage mist versus the fictitious gas Reynolds number. The circles represent the data in the annular portion of Figure 48 and the squares denote the Annular-Mist data. It is clear that there are two distinct curves and that the percentage mist is greater for Annular-Mist flows. Figure 50 is a plot of the pressure drop using the percentage mist as the abscissa. Three sets of data are plotted for constant water rates of .16, .25, and .35 lbm/sec, both the laminar and turbulent correlations of Chenoweth-Martin and Lockhart-Martinelli are shown. The data appear to follow the Lockhart-Martinelli prediction with transition occurring in the area of 35-40% mist. The water flow rate of 0.25 lbm/sec

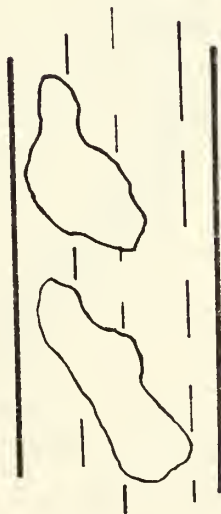
corresponds to a fictitious water Reynolds number of 1700 and a water flow rate of 0.35 lbm/sec is analogous to a fictitious water Reynolds number of 2300, which points out the weakness in the correlation schemes. That is, transition is not solely a function of the water Reynolds number nor does transition occur at a constant value of either the air or the water flow.

B. CONCLUSIONS AND RECOMMENDATIONS

It is concluded that the Lockhart-Martinelli correlation gives consistently better results than does the Chenoweth-Martin scheme for the flow rates investigated; further, some means of predicting transition must be incorporated into the Martinelli correlation. More work must be done to verify the Lockhart-Martinelli correlation for higher air and water flows and a more accurate determination of Figure 48 should be made and then incorporated into the correlation.



A. Bubble Flow



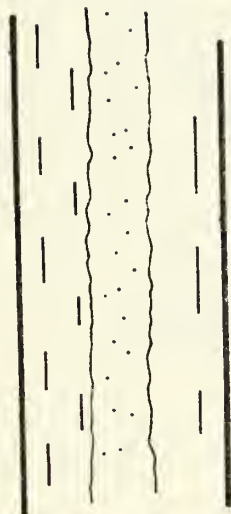
B. Plug Flow



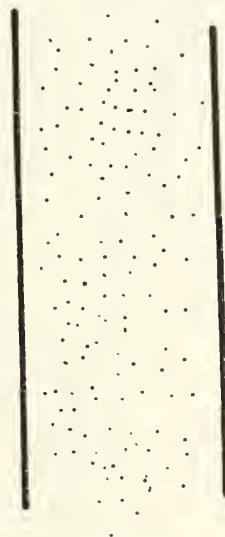
C. Stratified Flow



D. Slug Flow



E. Annular Flow



F. Mist Flow

FIGURE 1 TYPES OF TWO-PHASE, GAS-LIQUID
FLOW PATTERNS IN HORIZONTAL PIPE FLOW

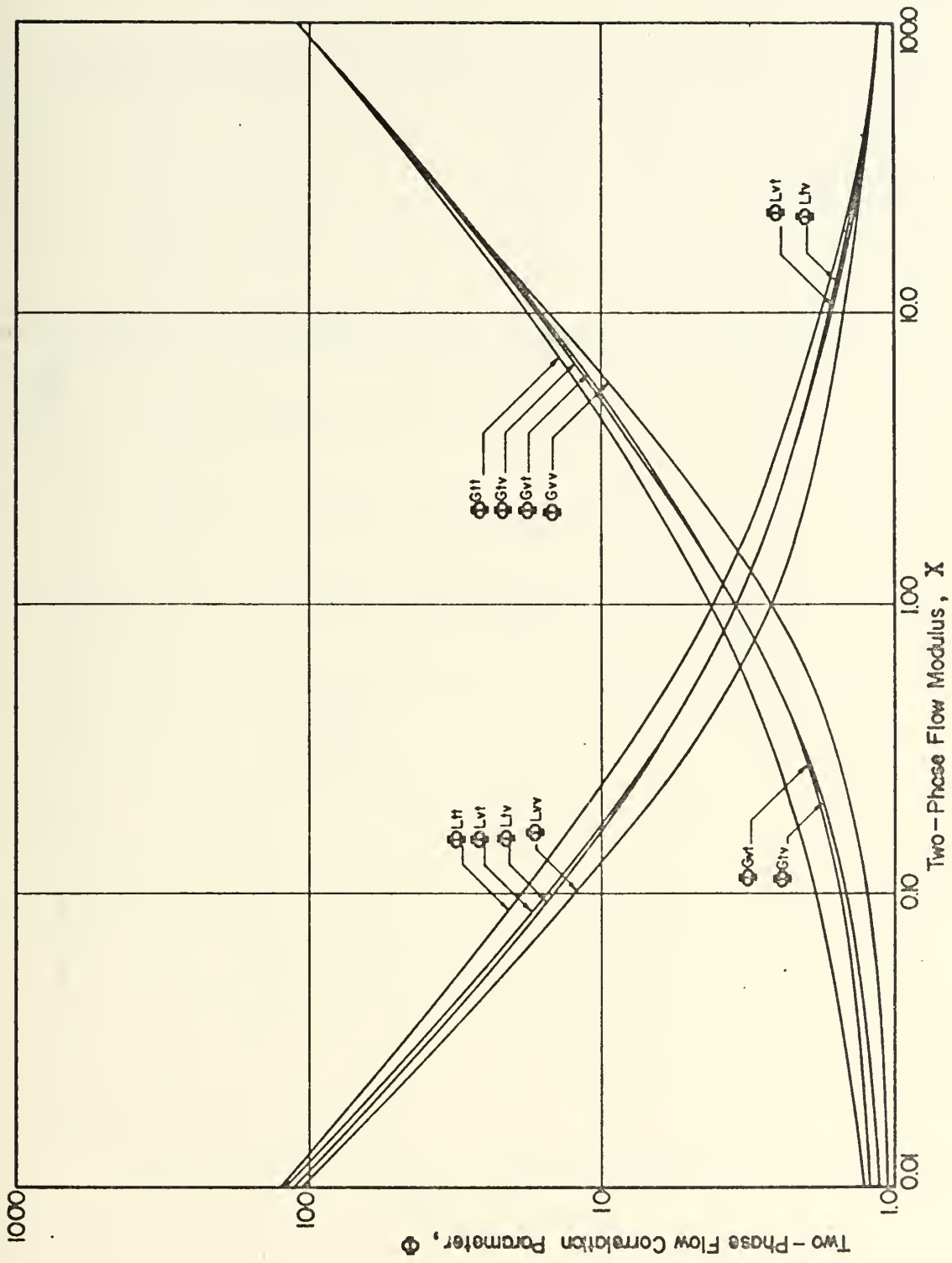


FIGURE 2. TWO PHASE FLOW CORRELATION OF LOCKHART-MARTINELLI

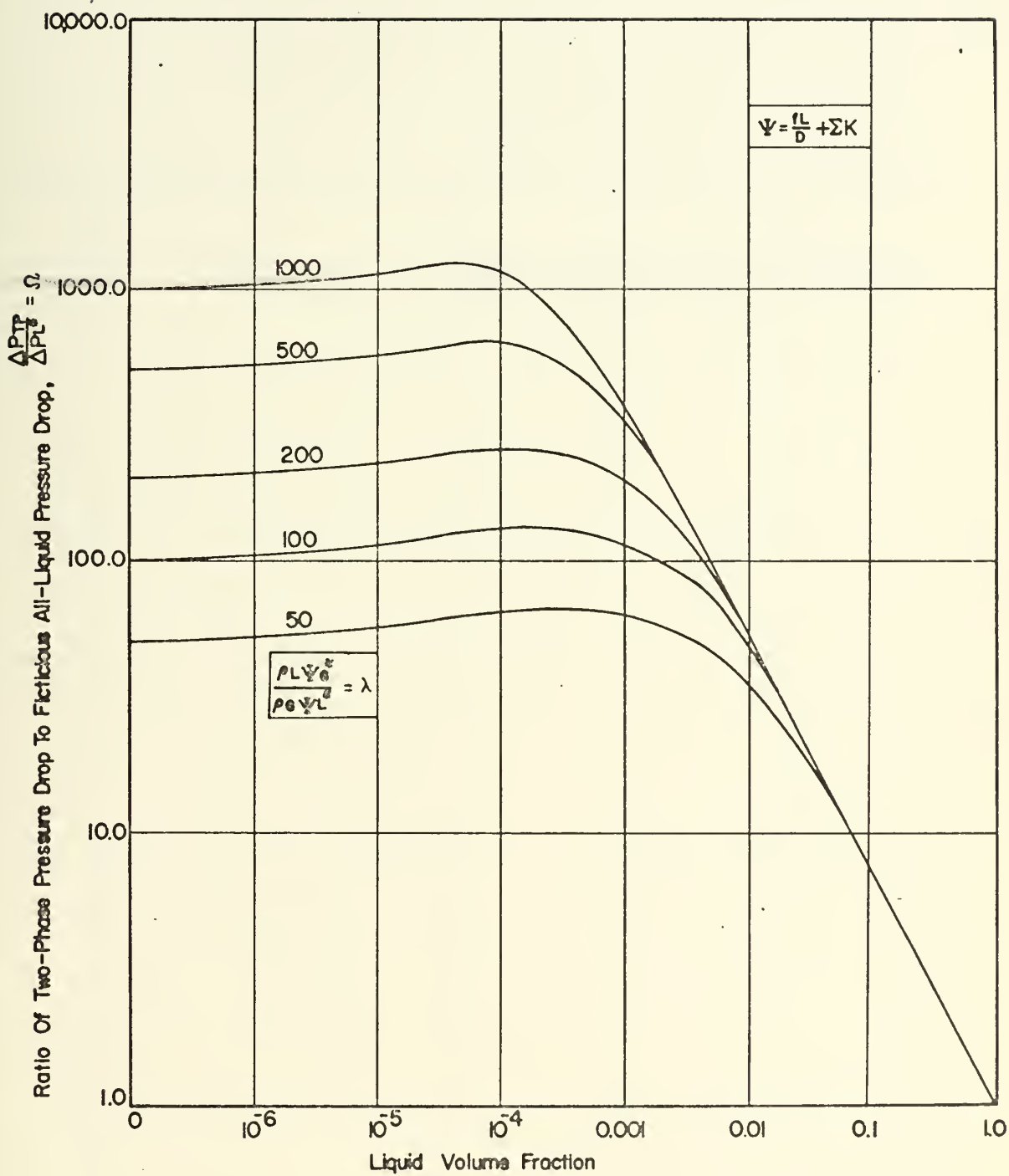


FIGURE 3. CORRELATION OF CHENOWETH AND MARTIN FOR TURBULENT TWO-PHASE PRESSURE DROP IN HORIZONTAL PIPES

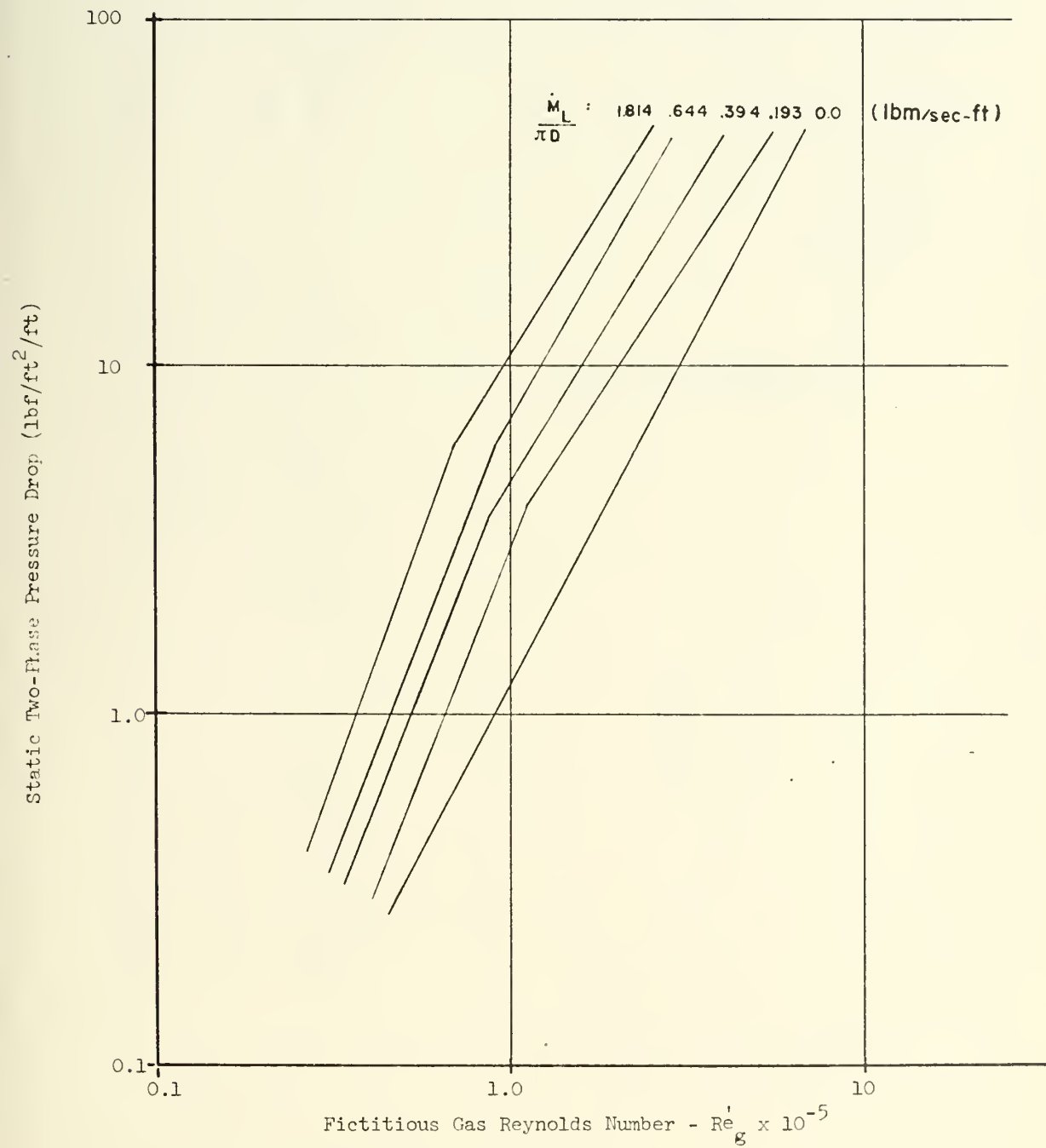
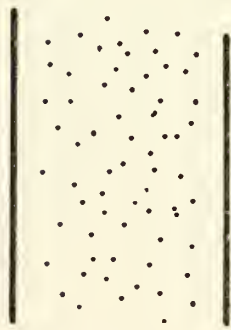


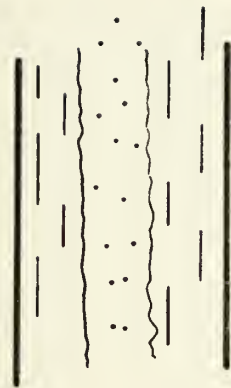
FIGURE 4 TWO PHASE AIR-WATER PRESSURE DROP
IN VERTICAL PIPES [Ref. 6]



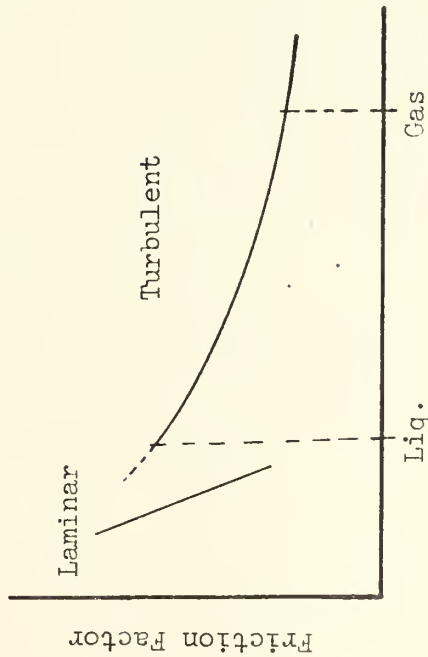
A. Mist Flow



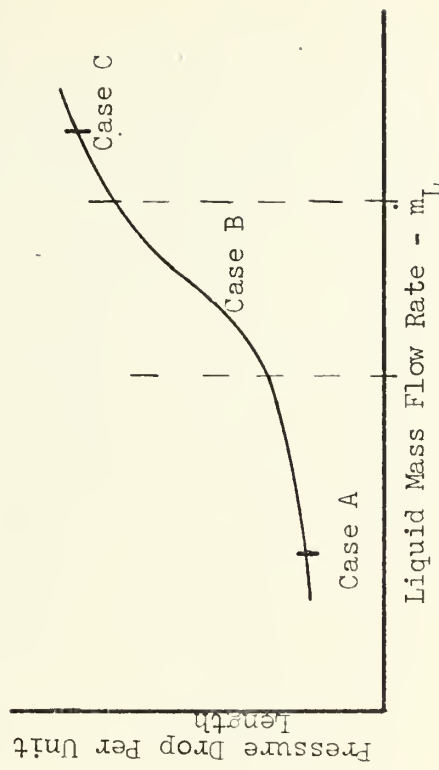
B. Annular-Mist Flow



C. Annular Flow



D. Friction Factor Curve



E. Pressure Drop vs. Water Flow Rate

FIGURE 5 FLOW PATTERN TRANSITION EFFECTS

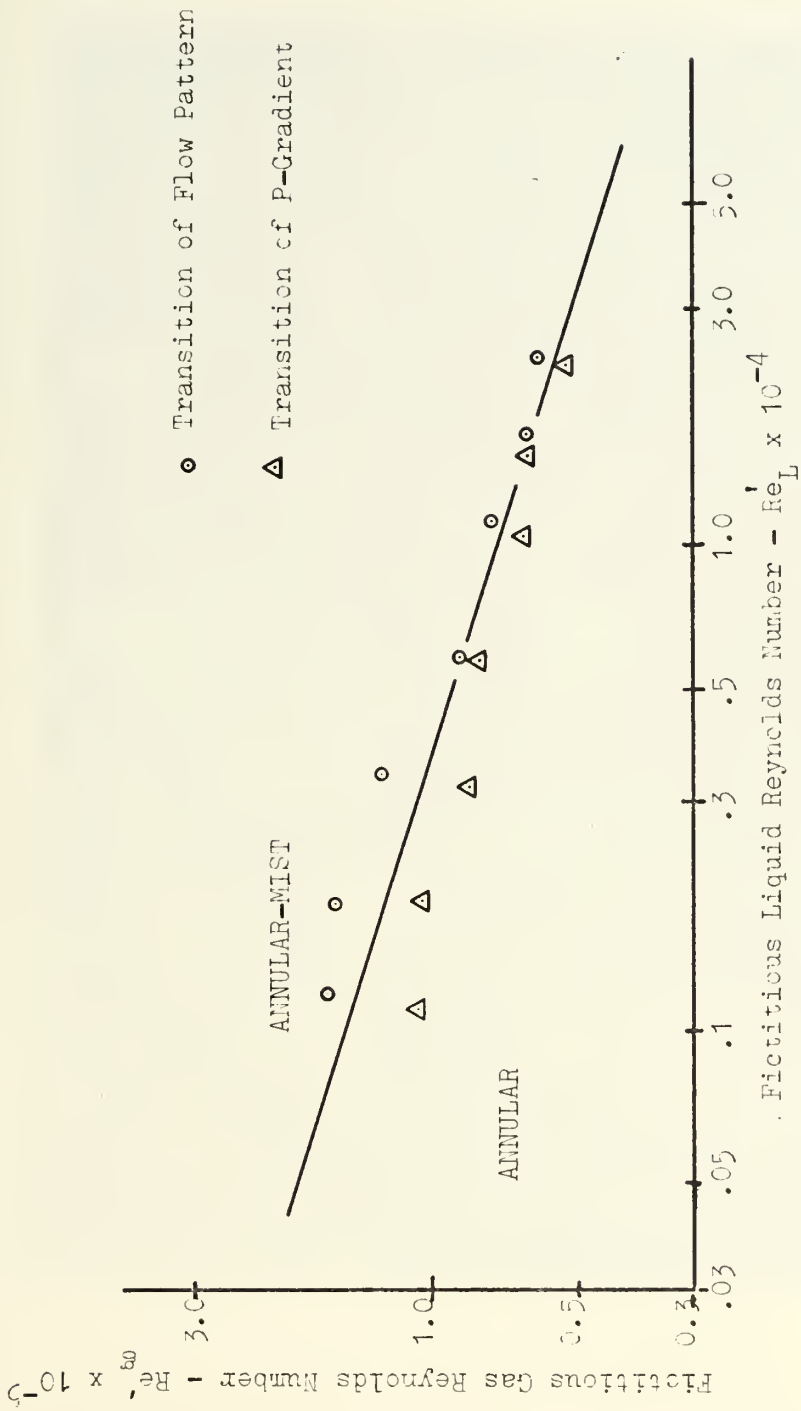


FIGURE 6 CHIEN-IBFLE TRANSITION CRITERIA [Ref. 6]



FIGURE 7
TWO-PHASE FLOW TEST RIG PRIOR TO MODIFICATION

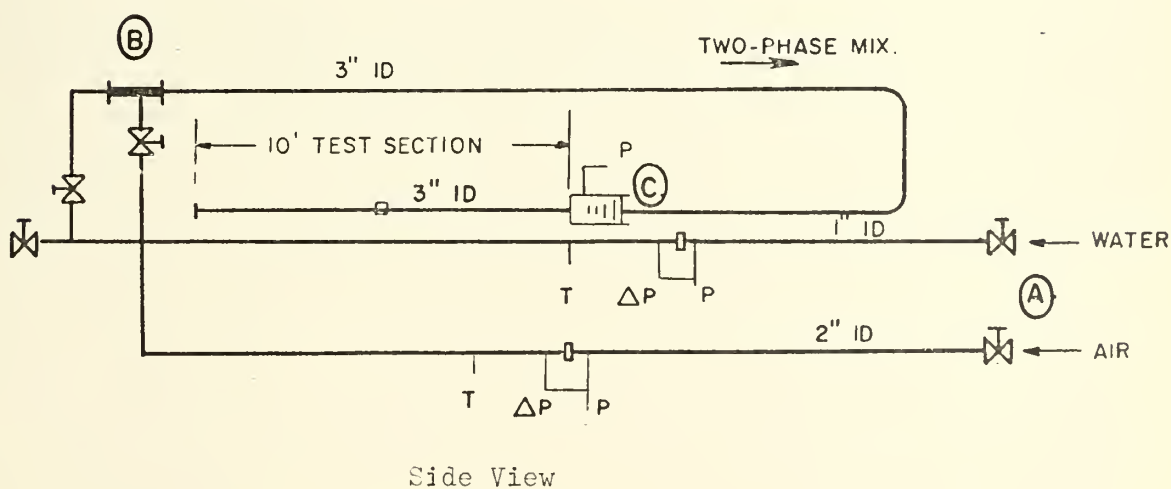
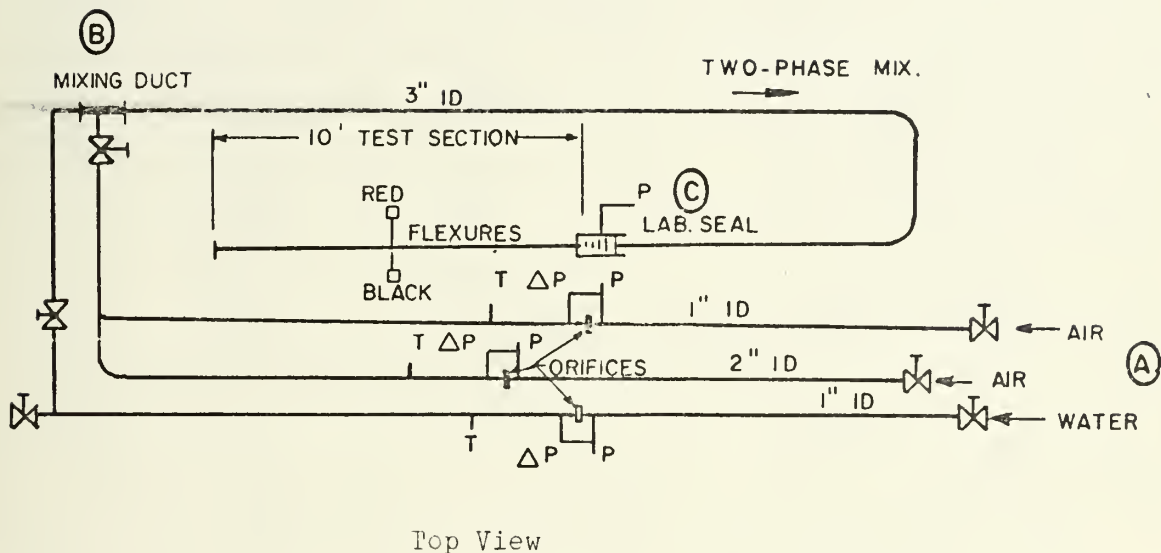


FIGURE 8 TWO PHASE FLOW RIG SCHEMATIC

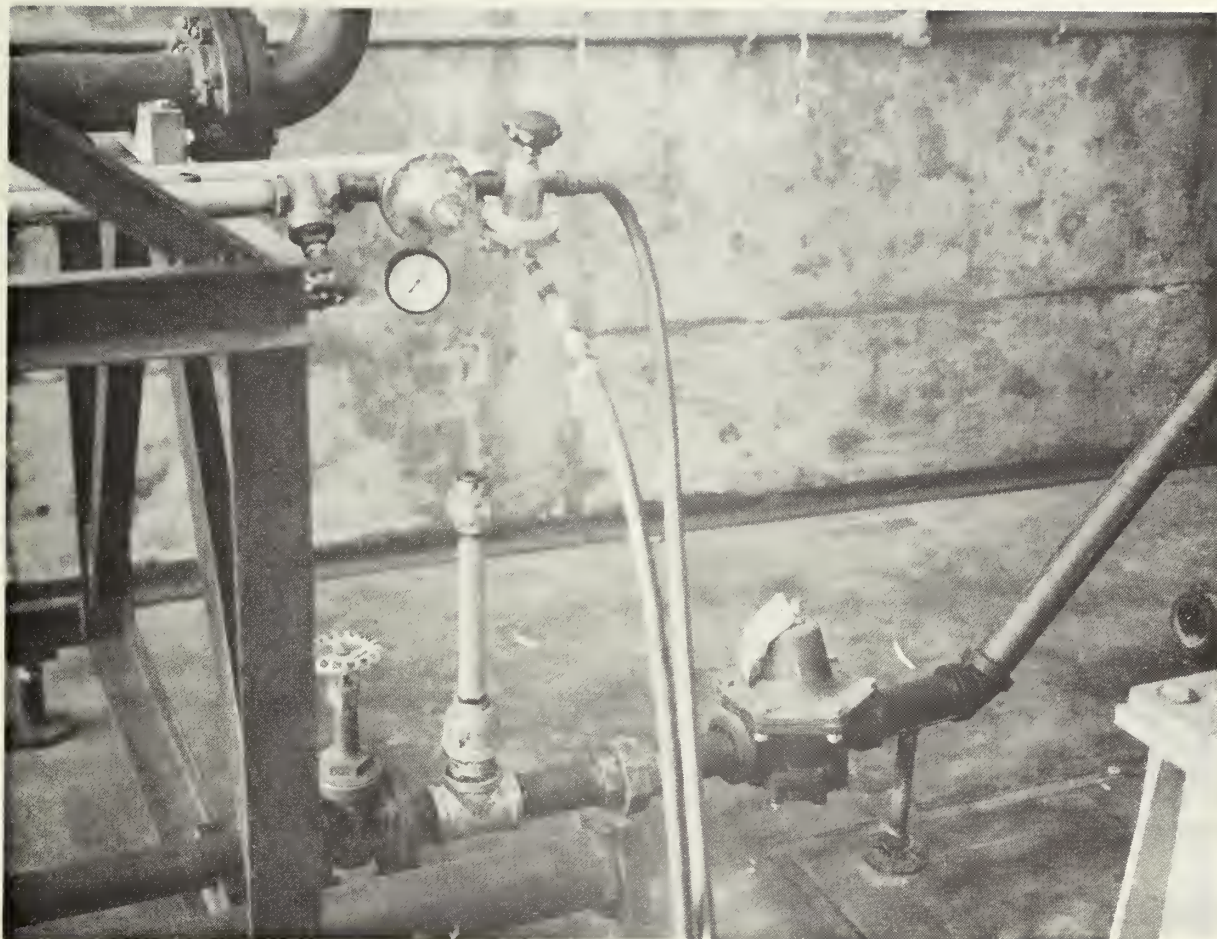


FIGURE 9

AIR AND WATER SUPPLIES WITH REGULATORS

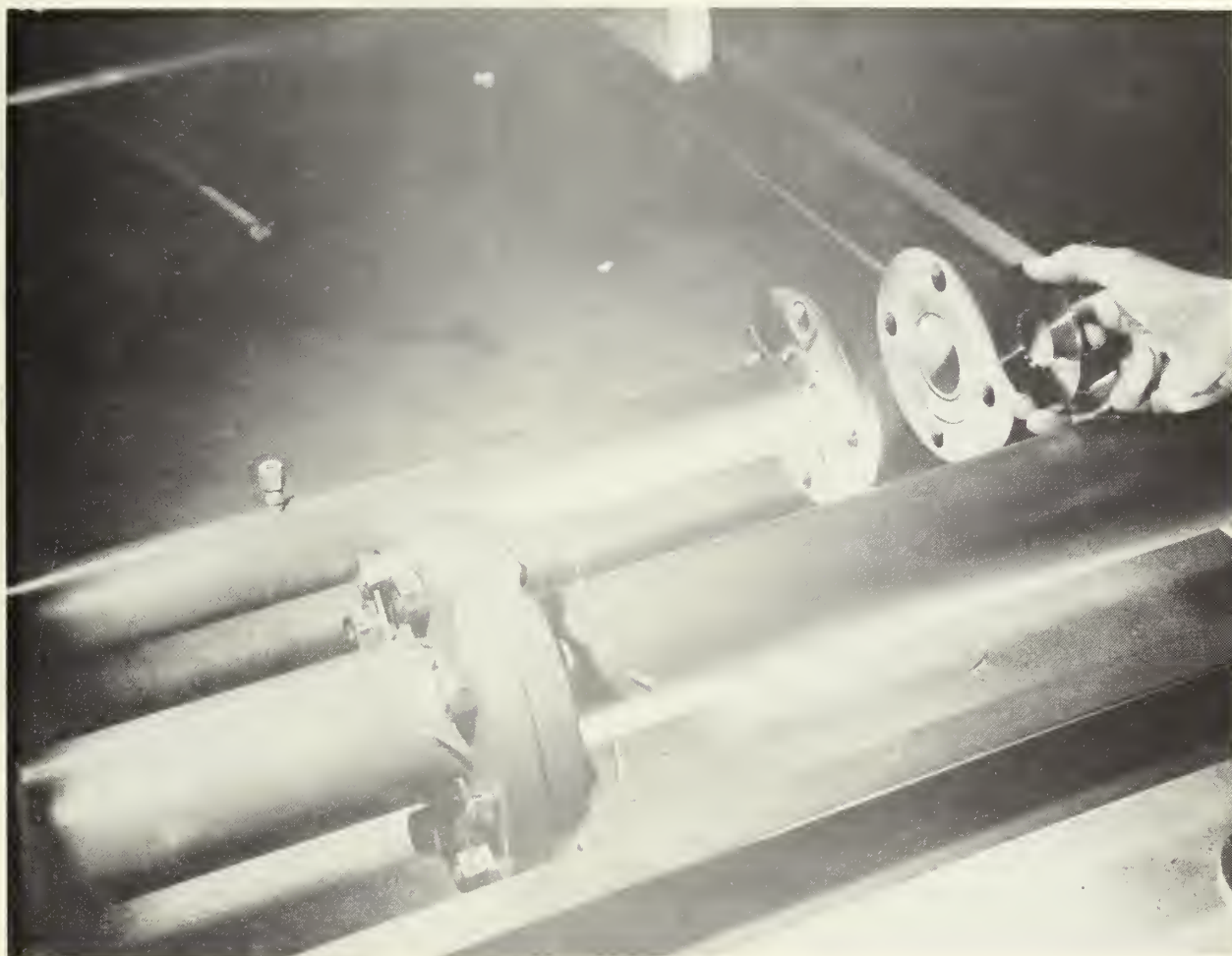


FIGURE 10 MAIN AIR ORIFICE

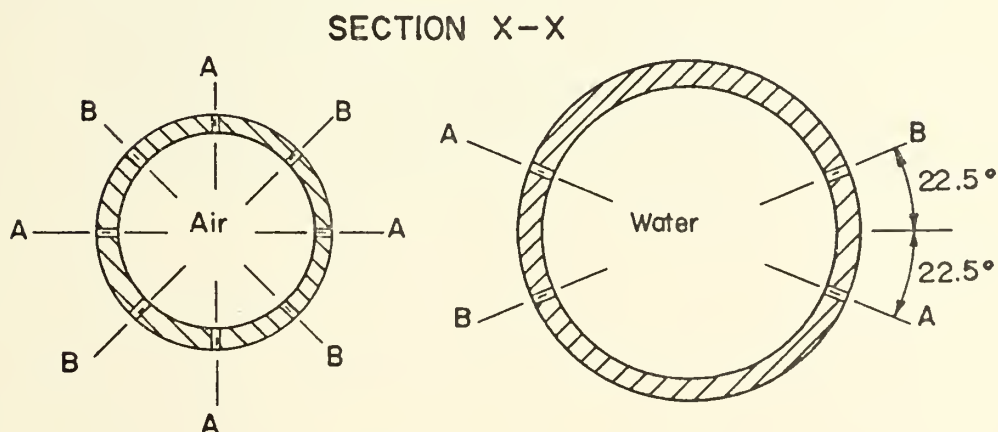
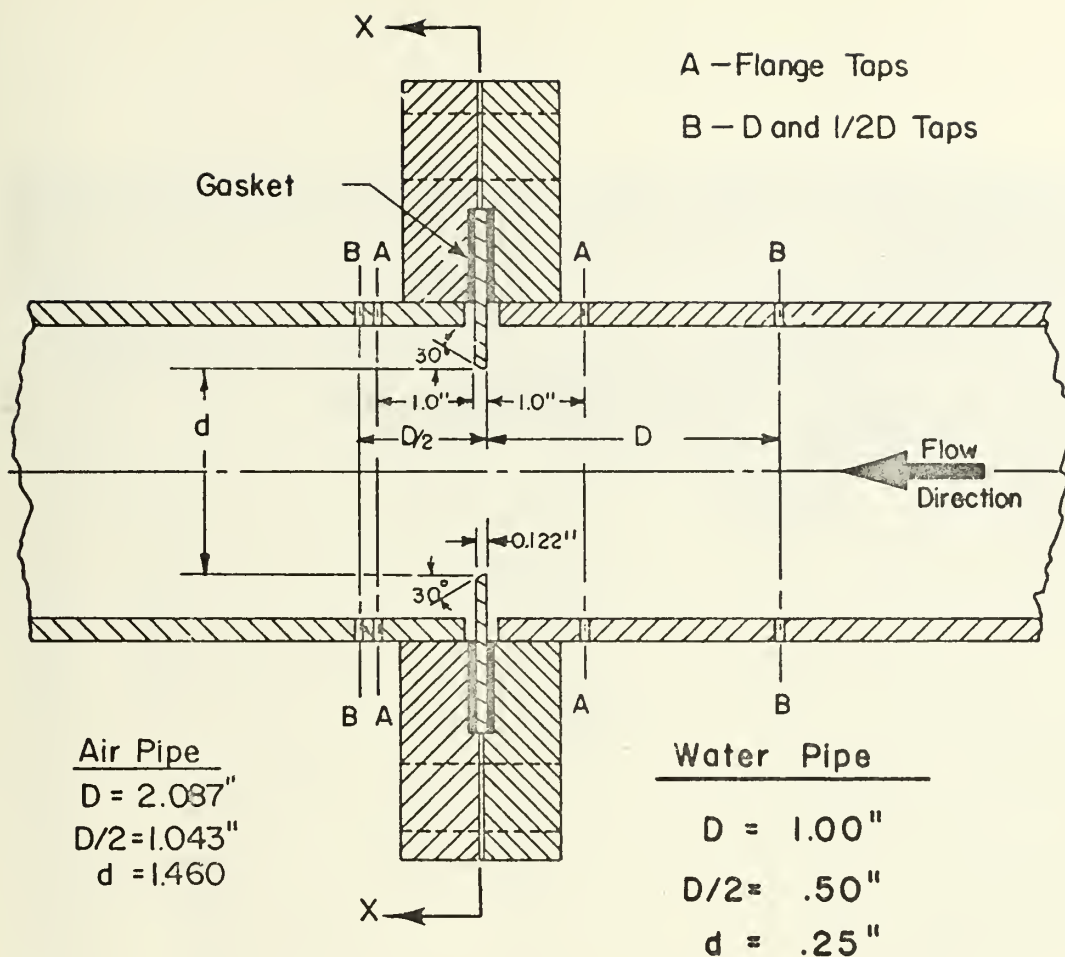


FIGURE 11

FLOW ORIFICE DETAILS



FIGURE 12
AIR WATER INJECTION DUCT



FIGURE 13
LABYRINTH SEAL

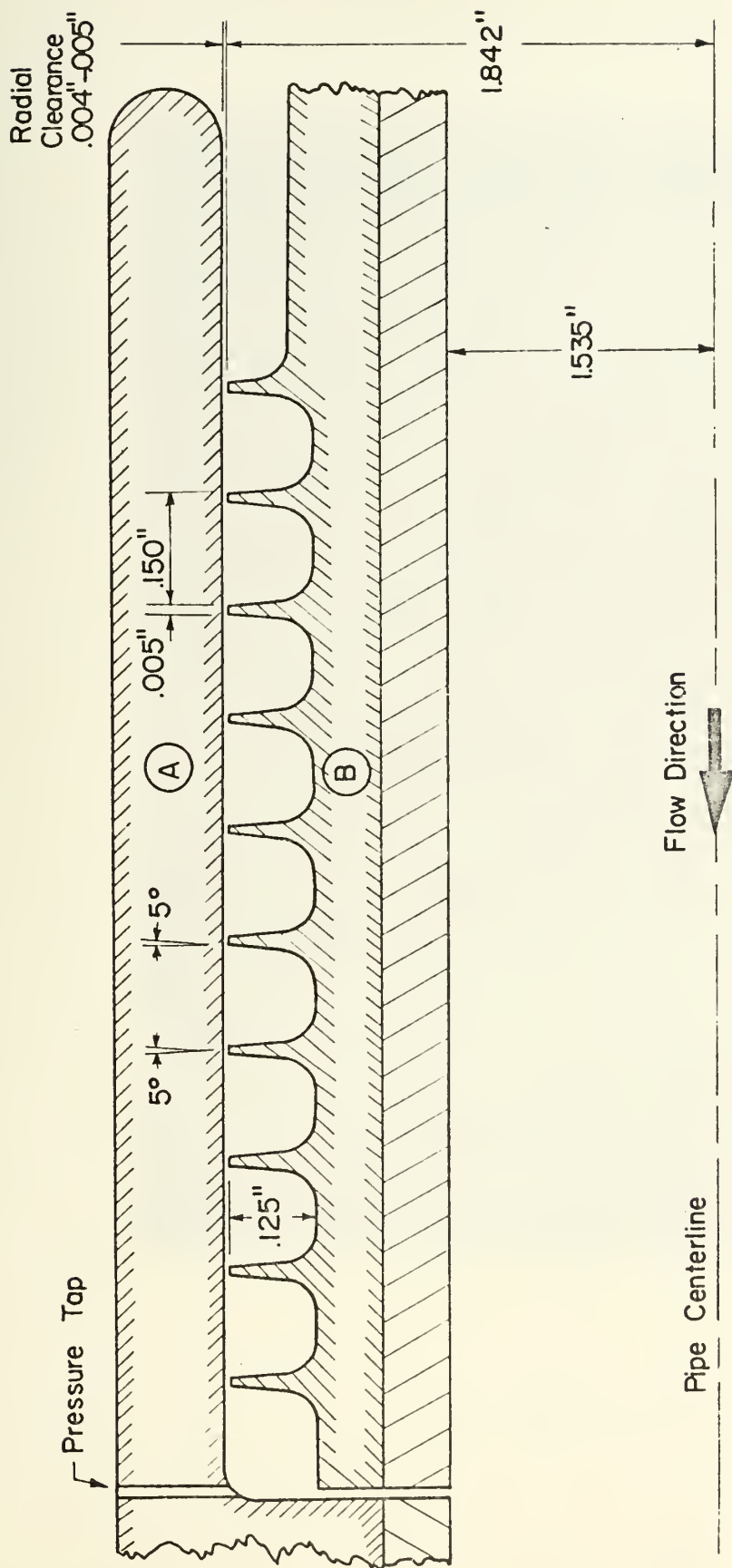


FIGURE 14.

- DETAILED VIEW OF LABYRINTH SEAL
- (A) ATTACHED TO TEST SECTION (MOVABLE)
- (B) ATTACHED TO INLET PIPE (STATIONARY)

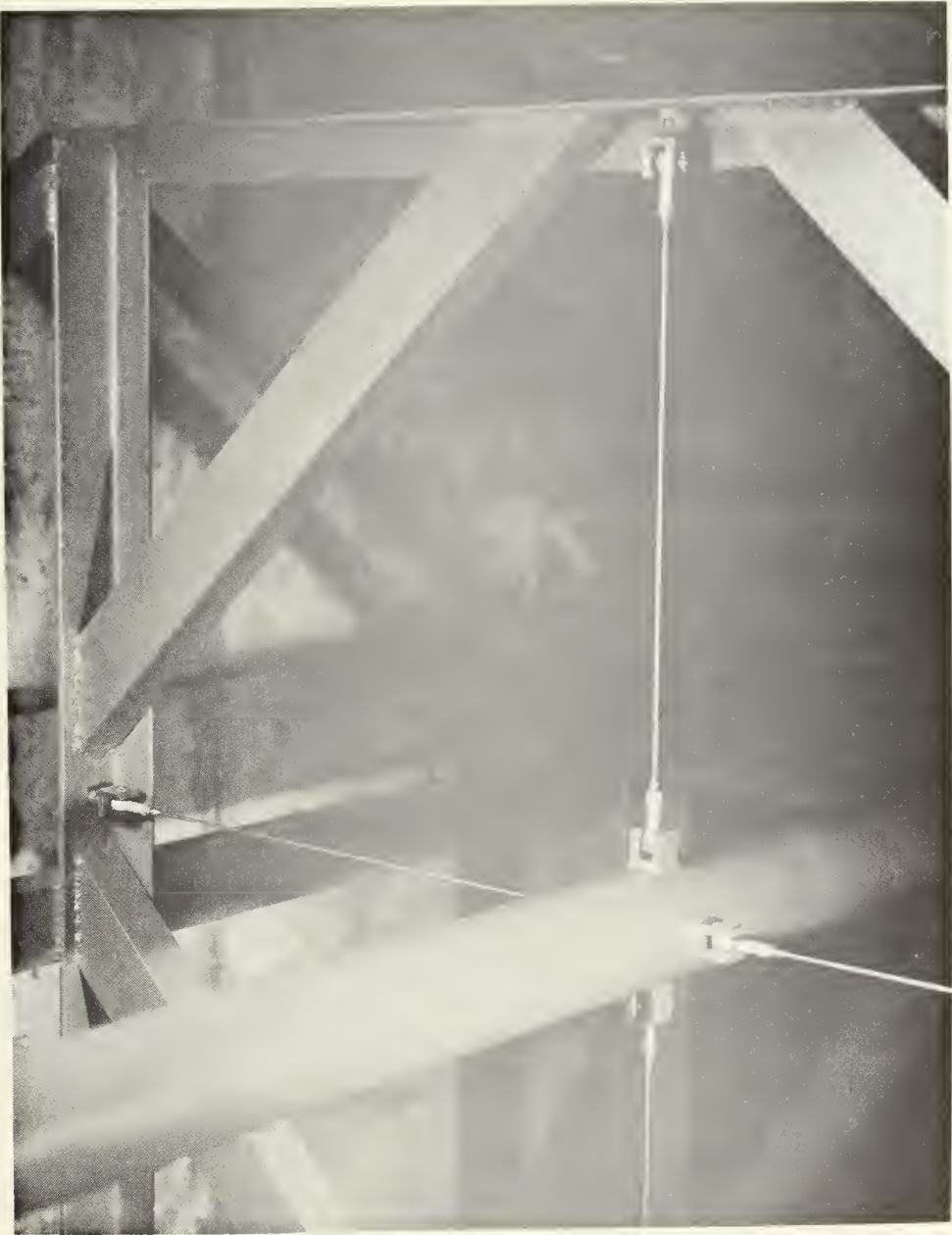


FIGURE 15
TEST SECTION SUPPORTS



FIGURE 16
FLEXURES

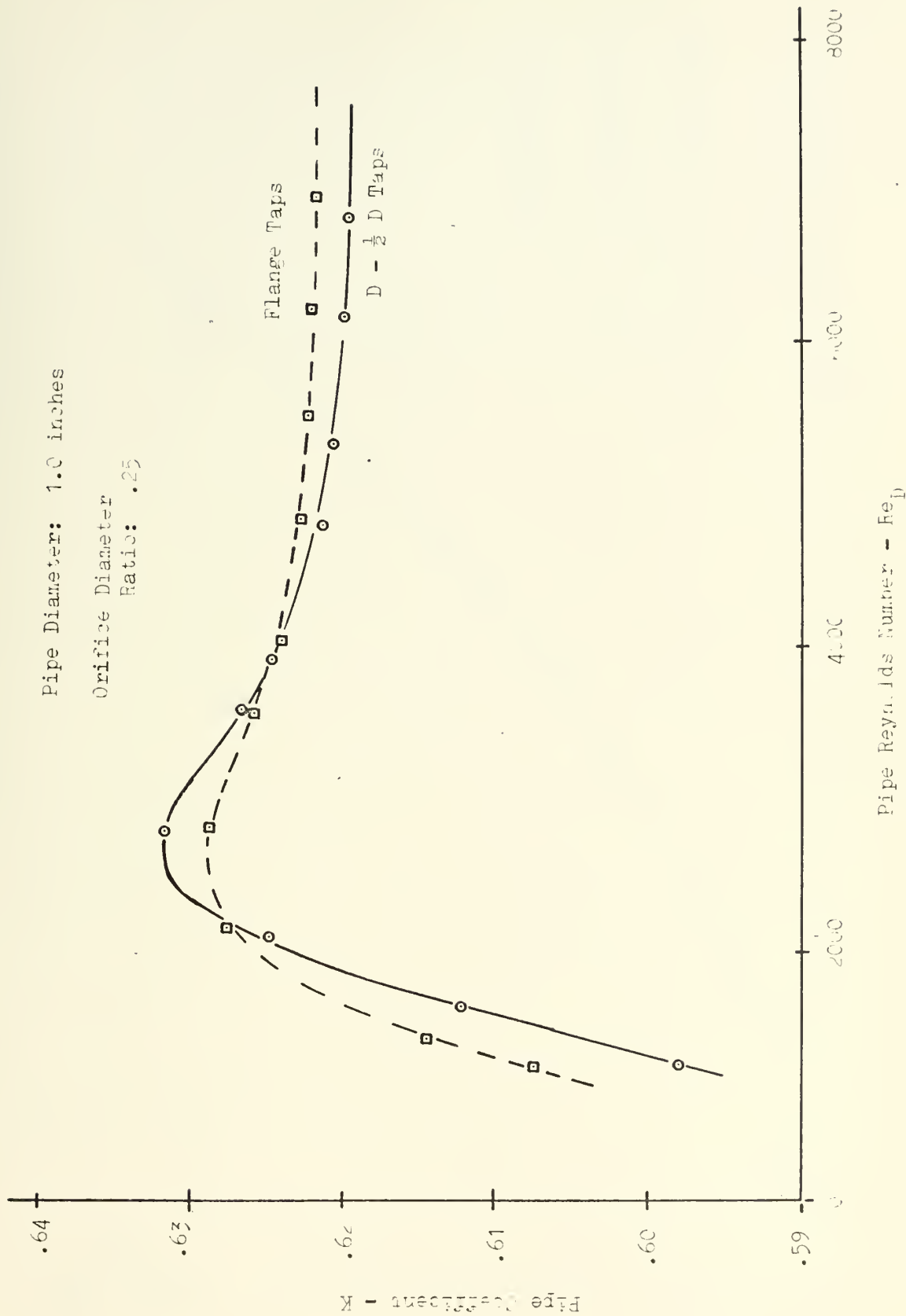


FIGURE 17 PIPE COEFFICIENT CALIBRATION FOR ONE INCH DIAMETER PIPE

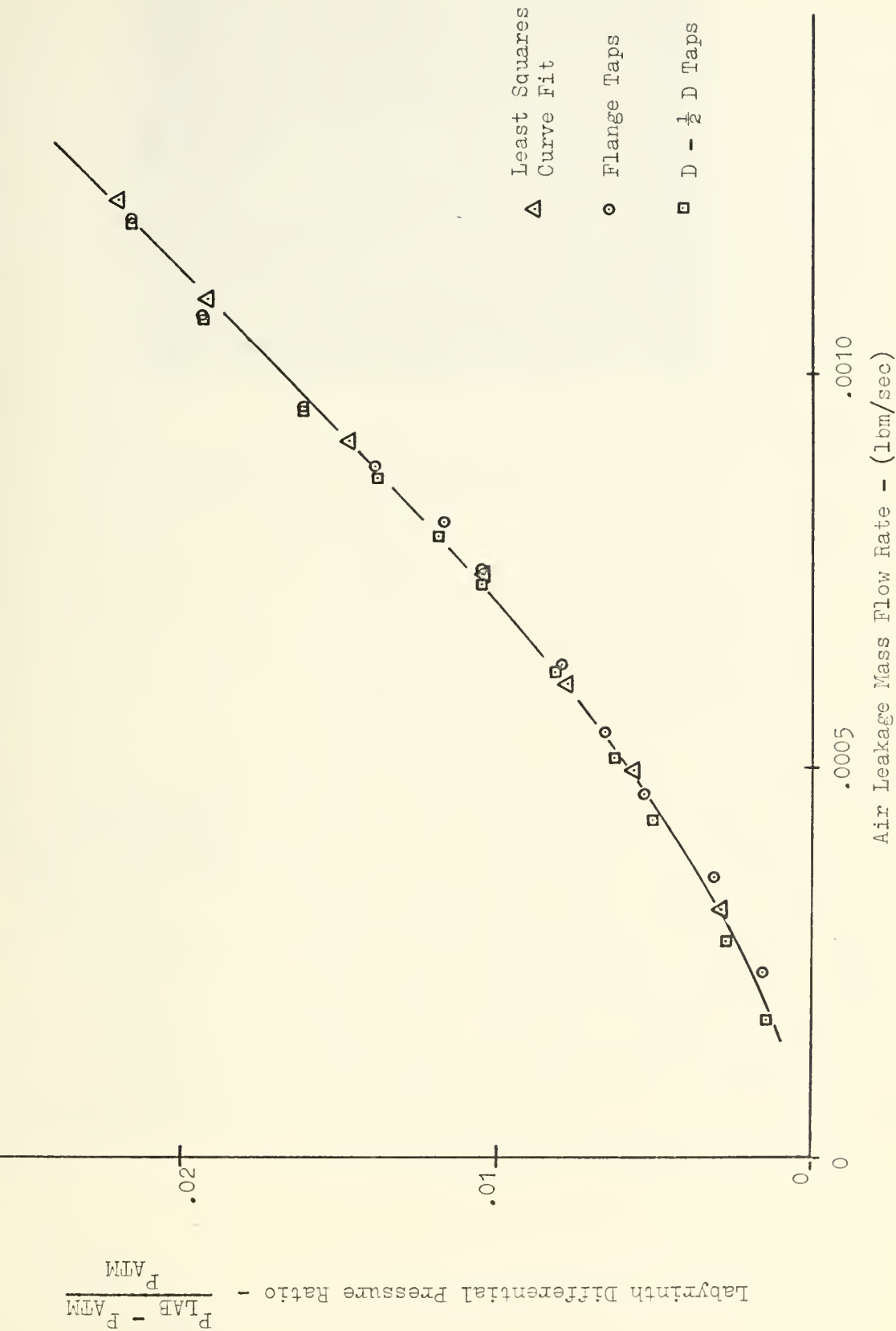


FIGURE 18 LABYRINTH AIR LEAKAGE RATE AS A FUNCTION OF LABYRINTH PRESSURE



FIGURE 19 STRAIN GAGE READOUT EQUIPMENT

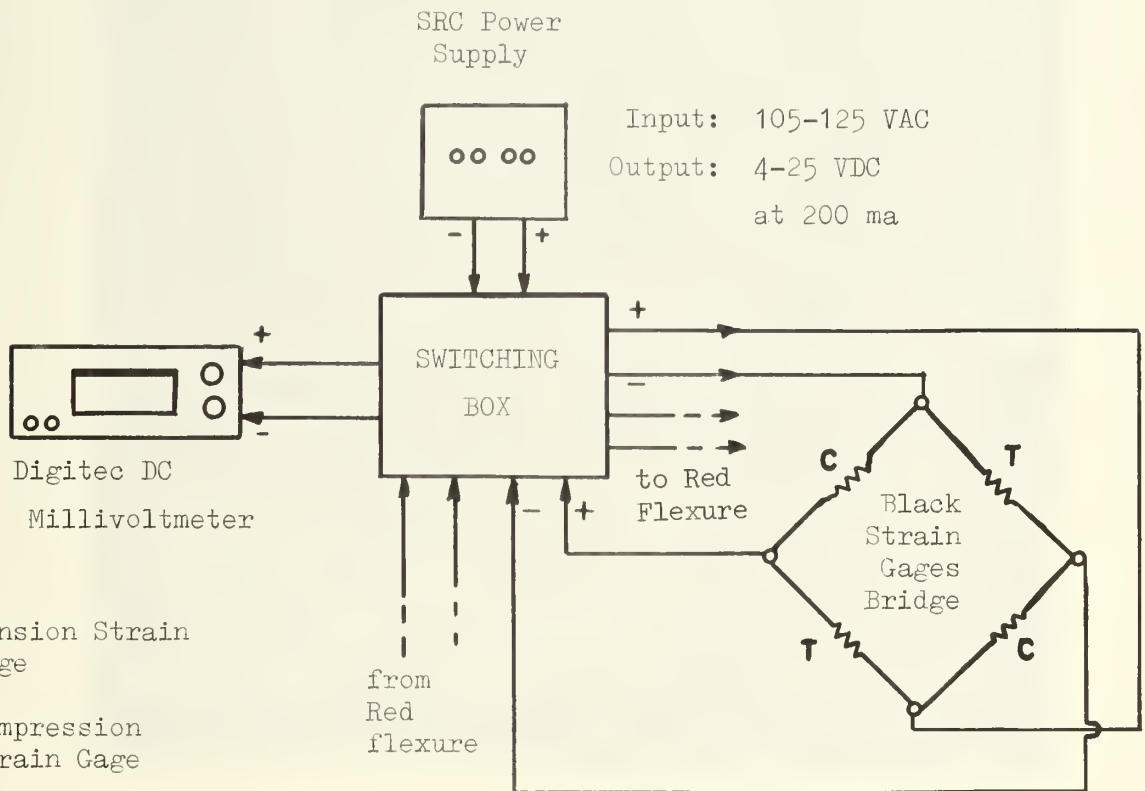


FIGURE 20 STRAIN GAGE WIRING SCHEMATIC

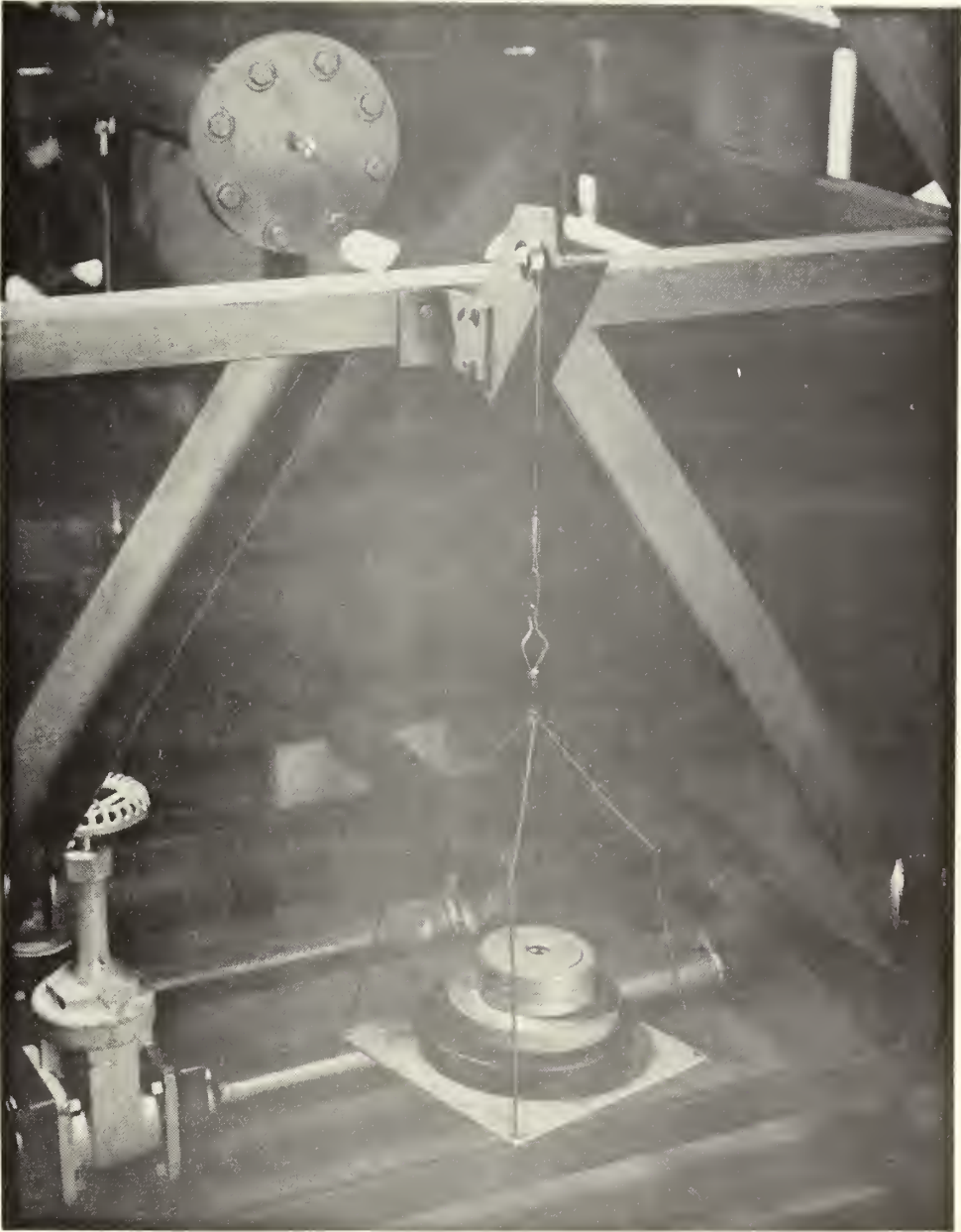


FIGURE 21
FLEXURE CALIBRATION SET-UP

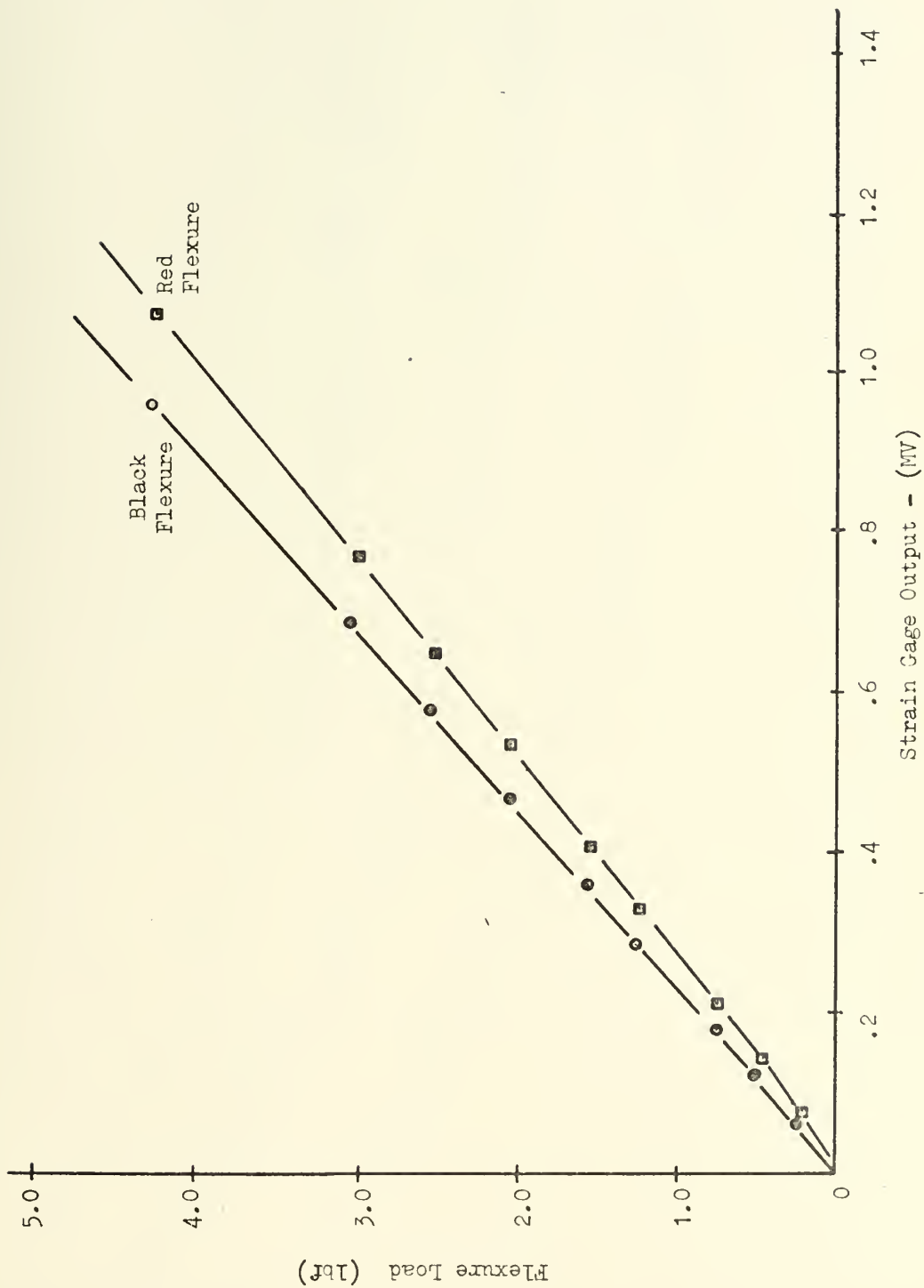


FIGURE 22 FLEXURE CALIBRATION CURVE

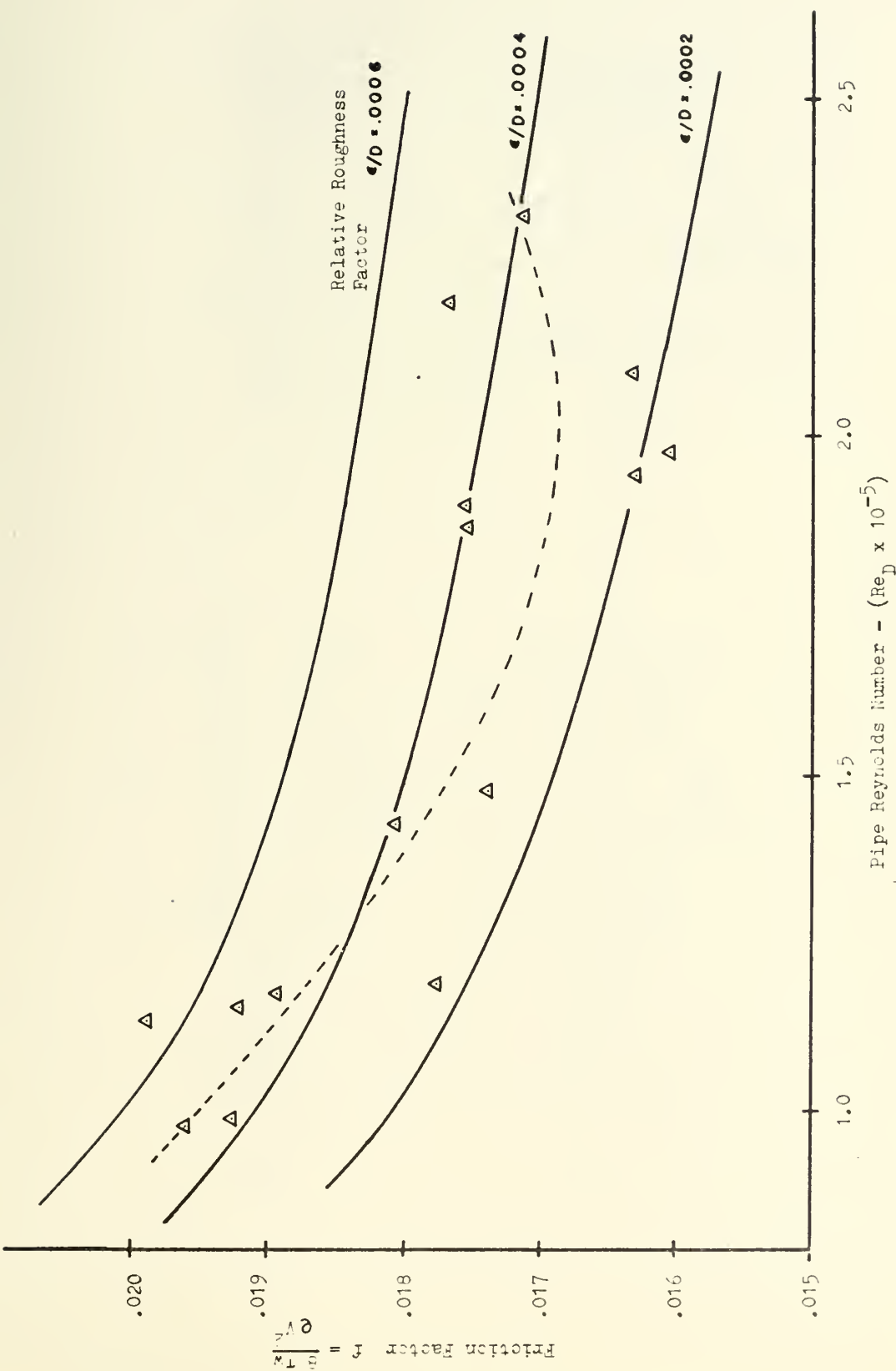


FIGURE 23 FRICTION FACTOR CALIBRATION RESULT

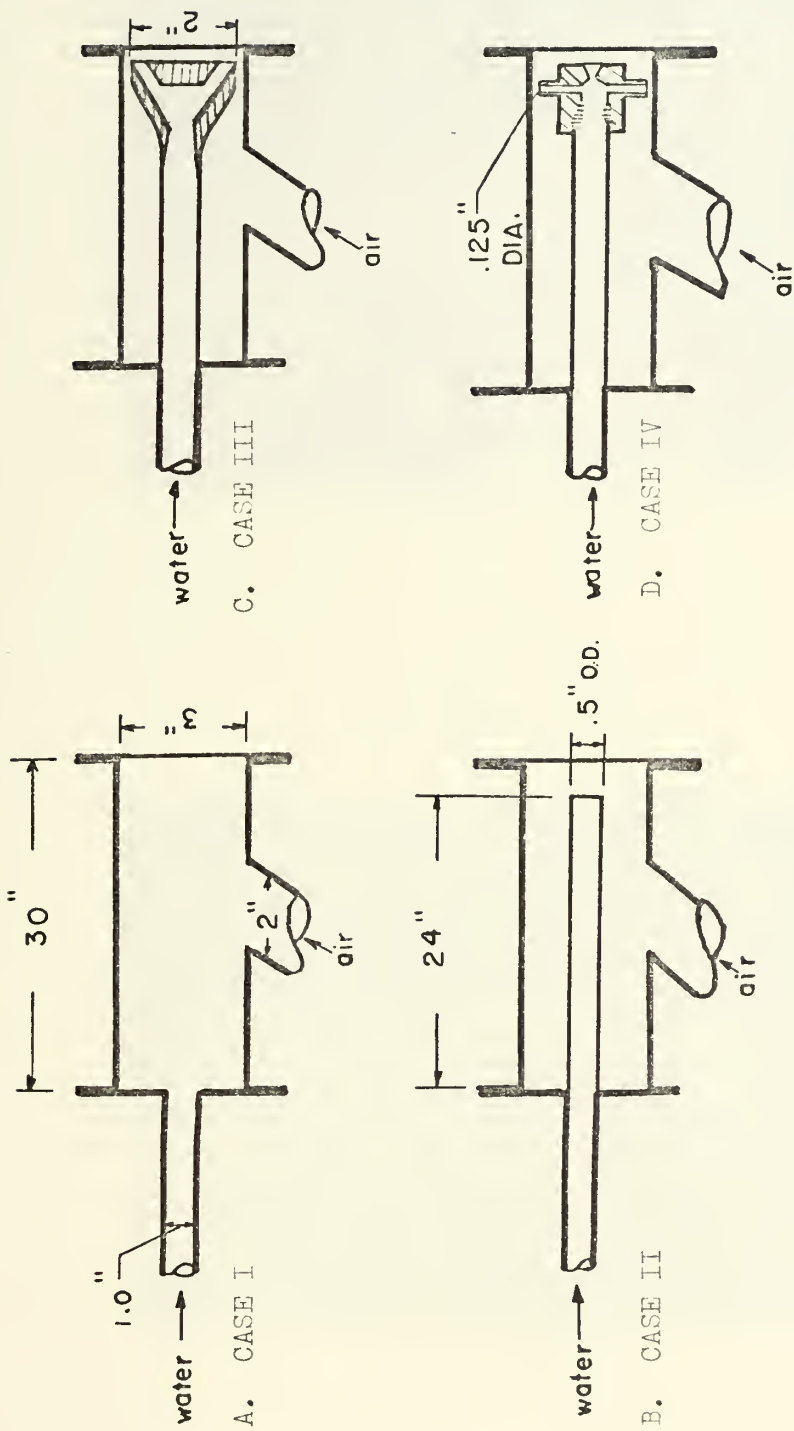


FIGURE 24
MIXING DUCT AND INJECTOR GEOMETRY



FIGURE 25
INJECTION PATTERN CASE I



FIGURE 26
FLOW PATTERN AT EXIT ST. PIPE



FIGURE 27
INJECTION PATTERN CASE II



FIGURE 28
FLOW PATTERN AT EXIT OF ST. PIPE



FIGURE 29
INJECTION PATTERN CASE III



FIGURE 30
FLOW PATTERN AT EXIT OF ST. PIPE



FIGURE 31
INJECTION PATTERN CASE 1V



FIGURE 32
FLOW PATTERN WD EXHIBIT ST. 10000



FIGURE 33
FLOW PATTERN AT TEST SECTION EXIT
INCLUDES PIPE BEND

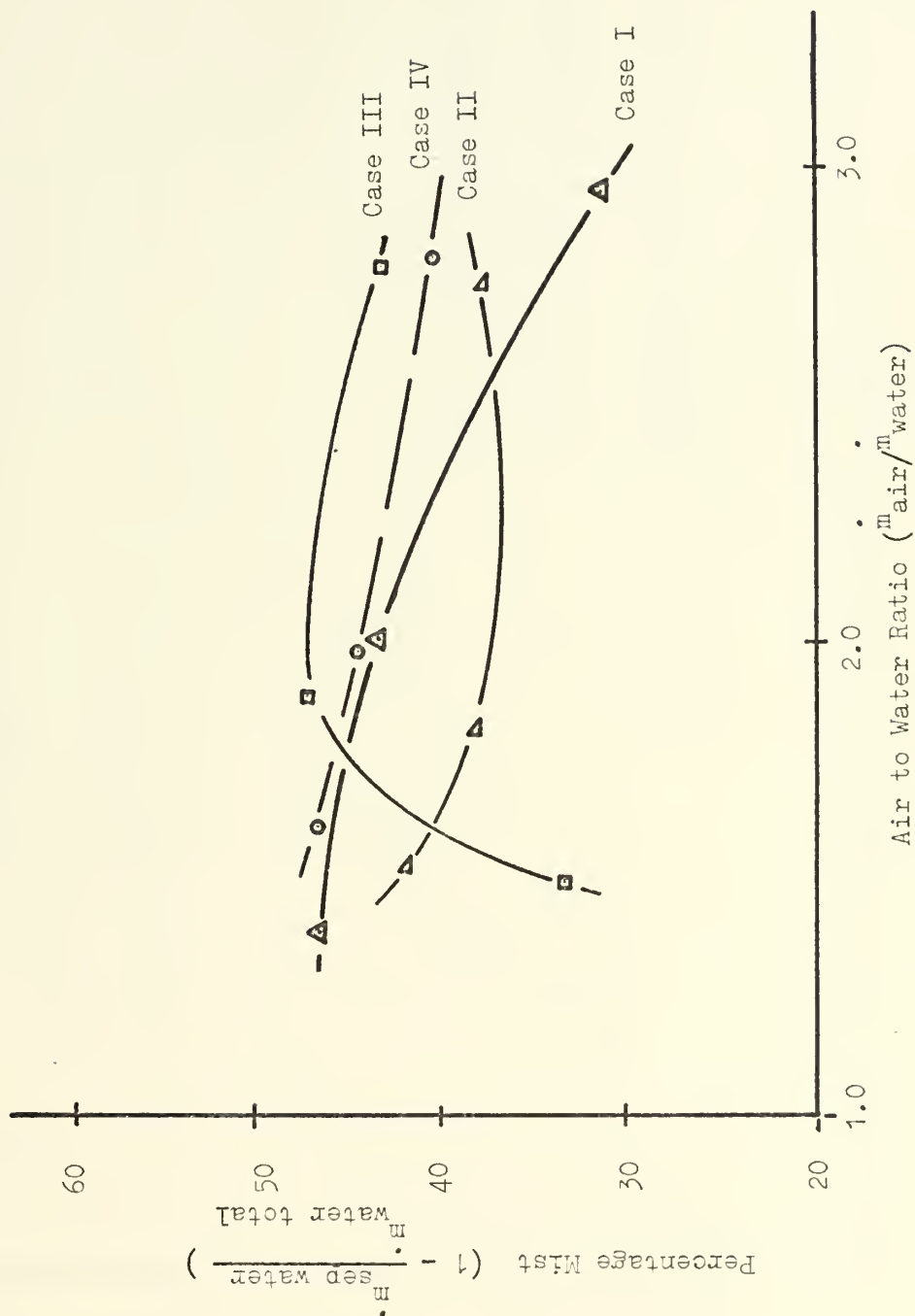


FIGURE 34 PERCENTAGE MIST FOR THE FOUR NOZZLE TYPES

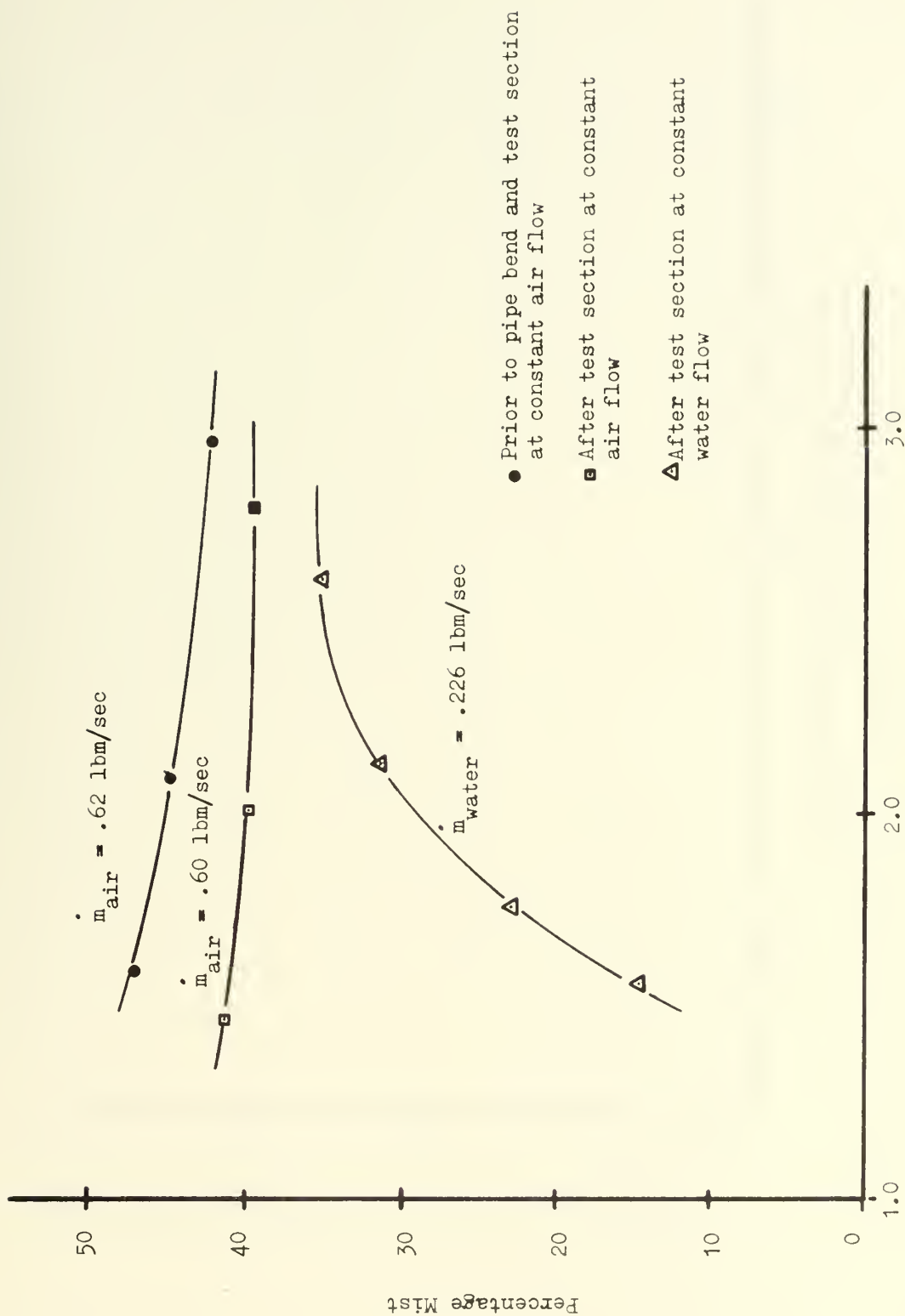


FIGURE 35 CASE IV NOZZLE WATER SEPARATION



FIGURE 36 MEASURED PRESSURE DROP-RED FLEXURE

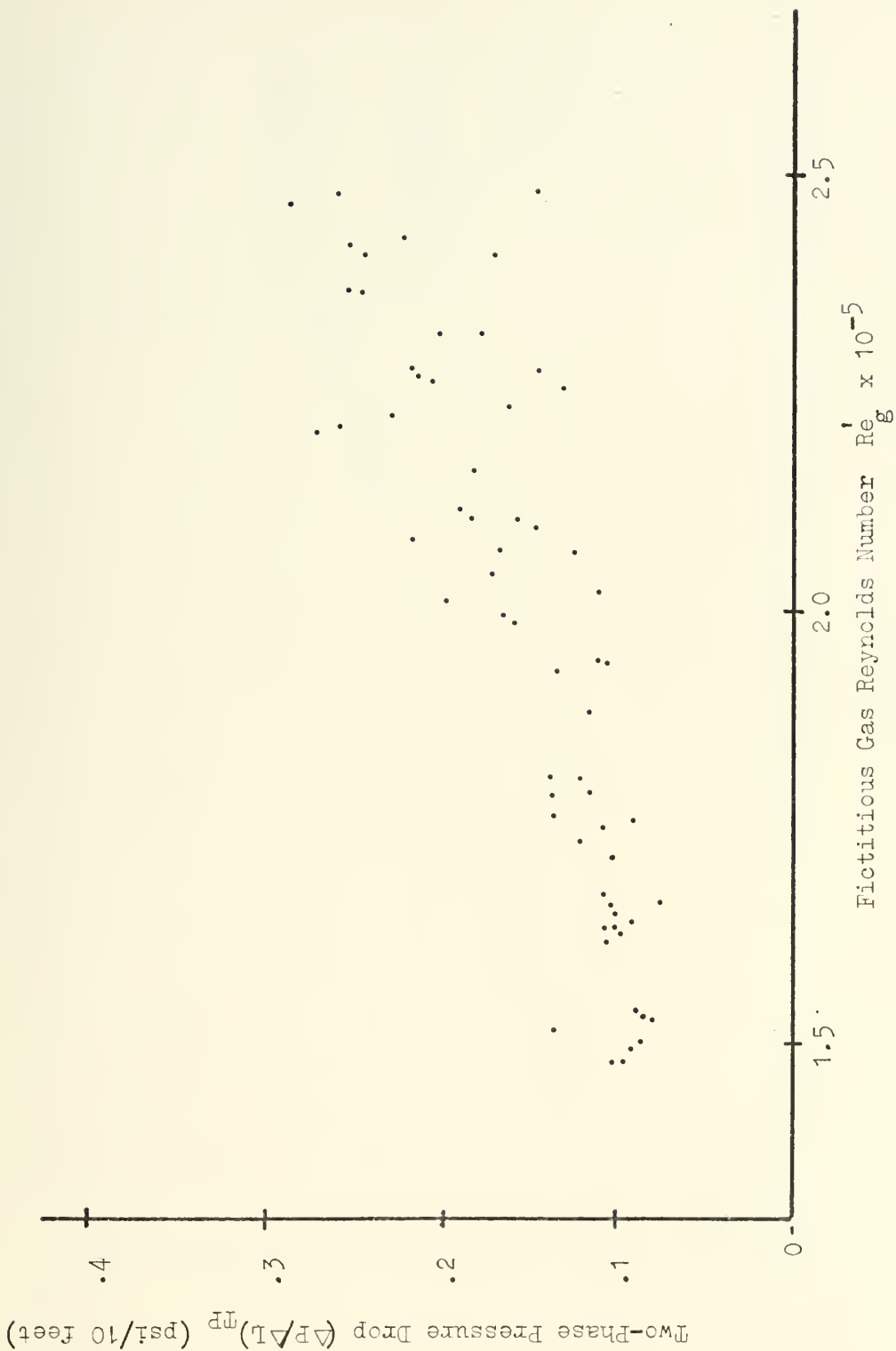


FIGURE 37 MEASURED PRESSURE DROP-BLACK FLEXURE

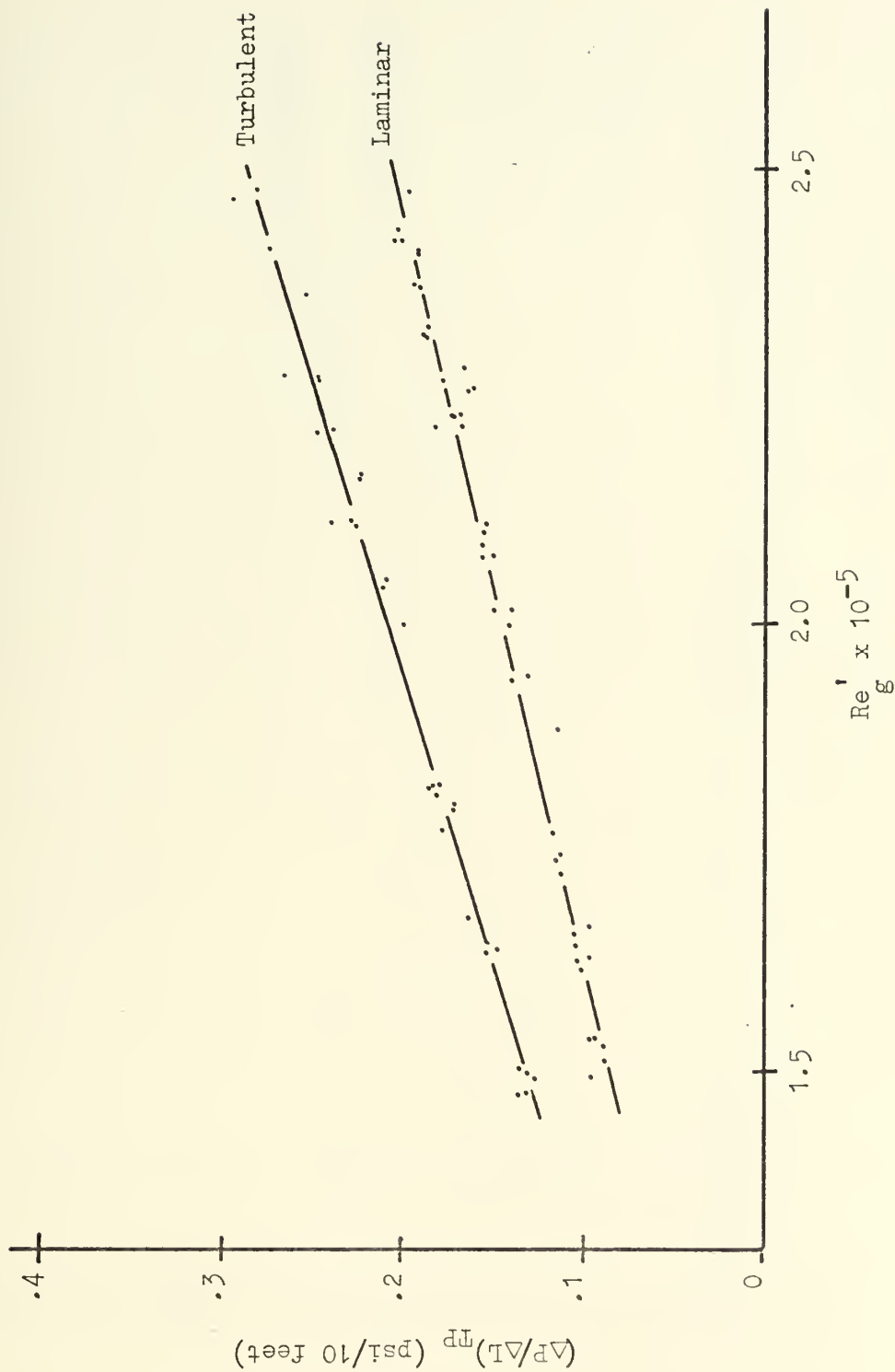


FIGURE 38 LOCKHART-MARTINELLI PREDICTED PRESSURE DROP

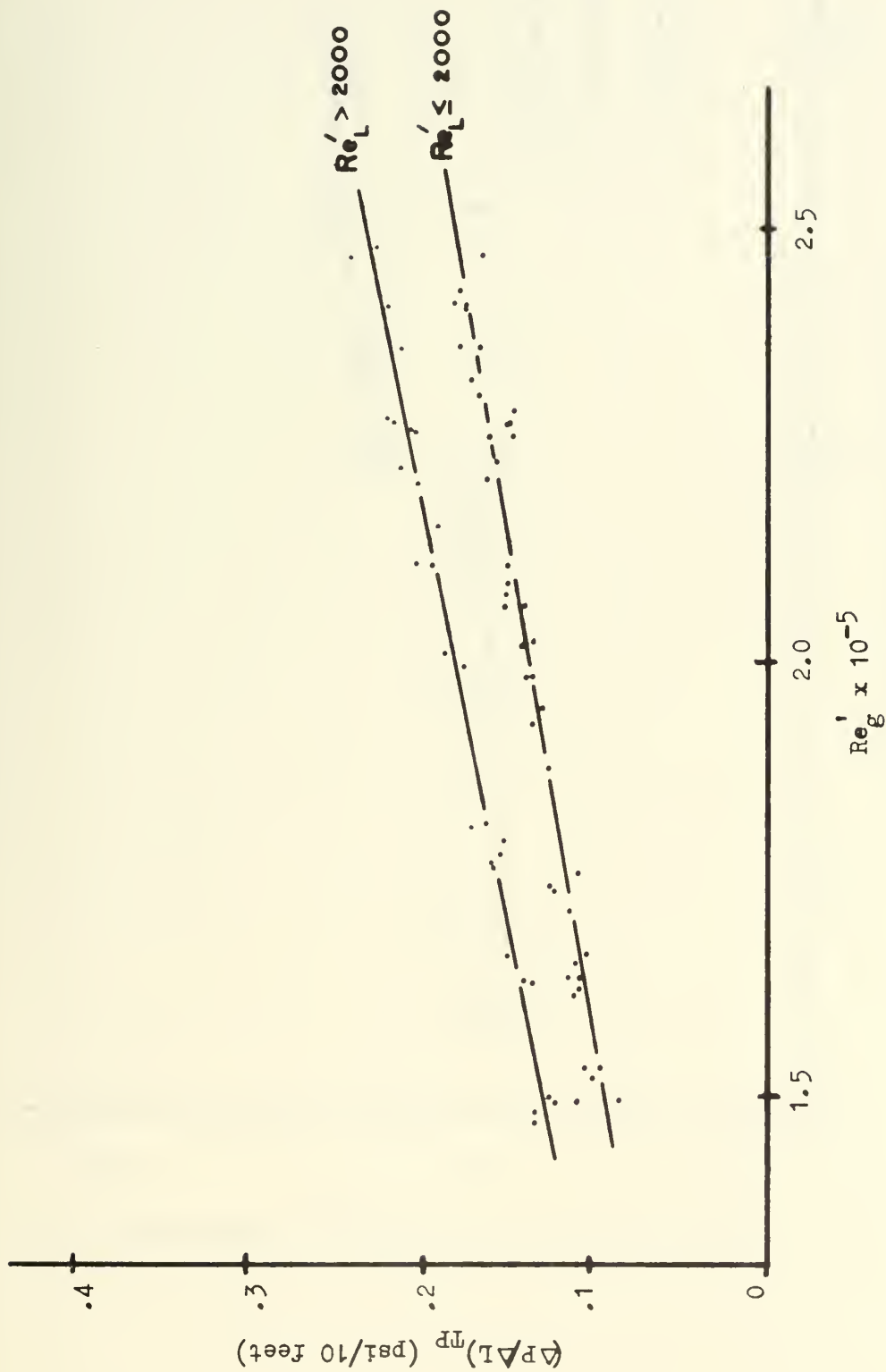


FIGURE 39 CHENOWETH-MARTIN PREDICTED PRESSURE DROP

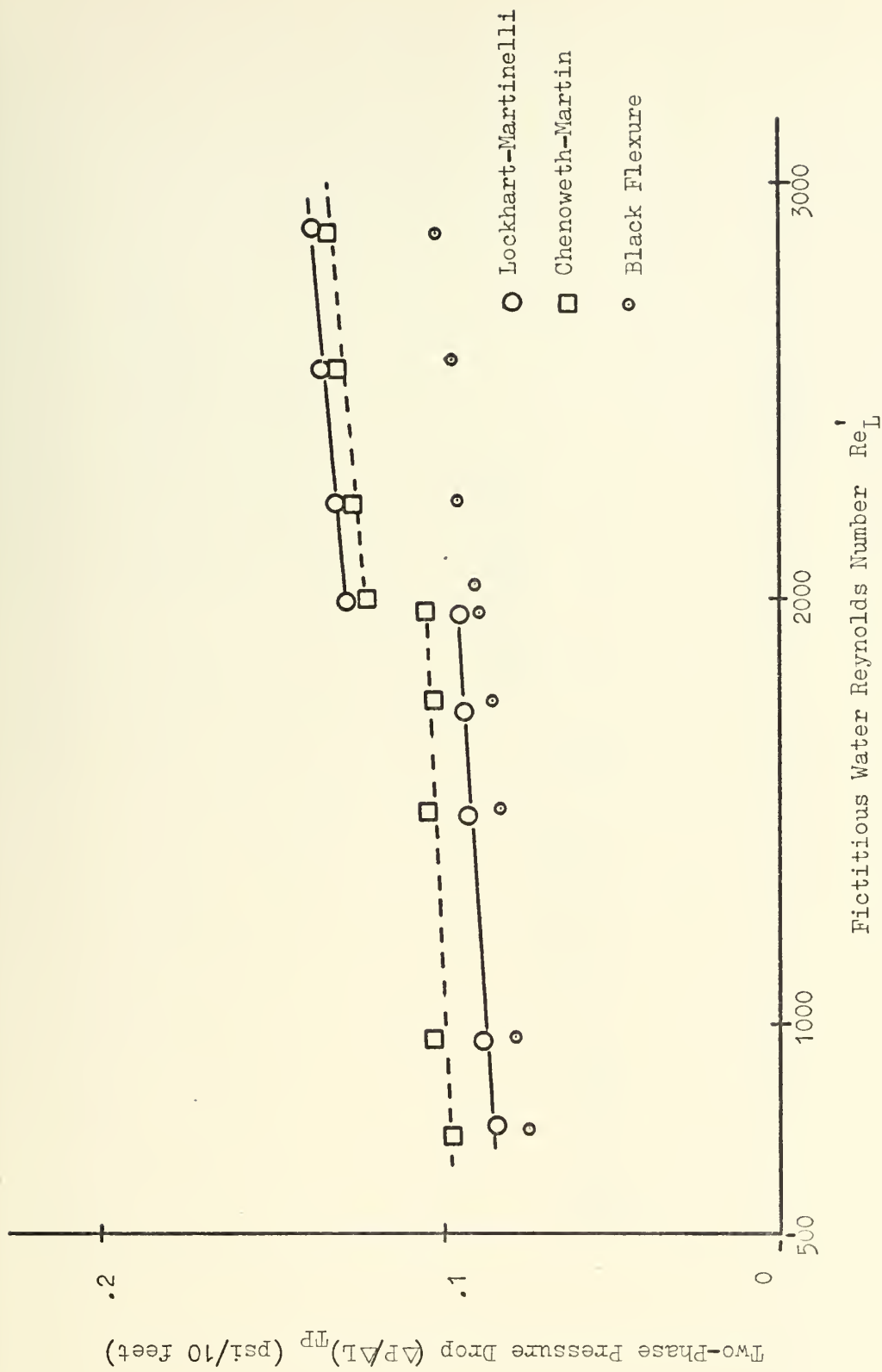


FIGURE 40 PREDICTED AND MEASURED PRESSURE DROP FOR

AIR CONSTANT AT .35 lbm/sec

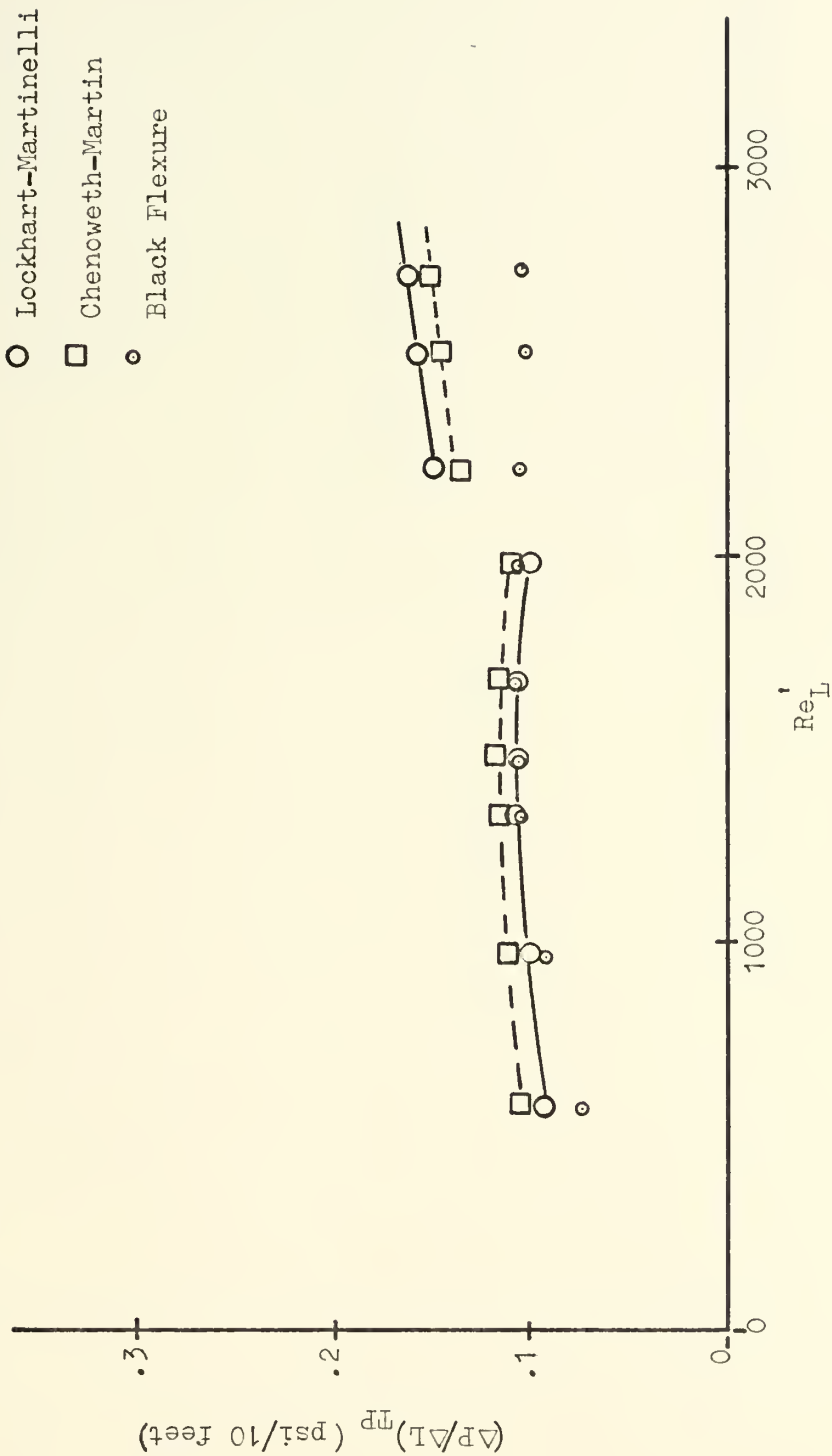


FIGURE 41 PREDICTED AND MEASURED PRESSURE DROPS FOR
AIR CONSTANT AT .40 lbm/sec

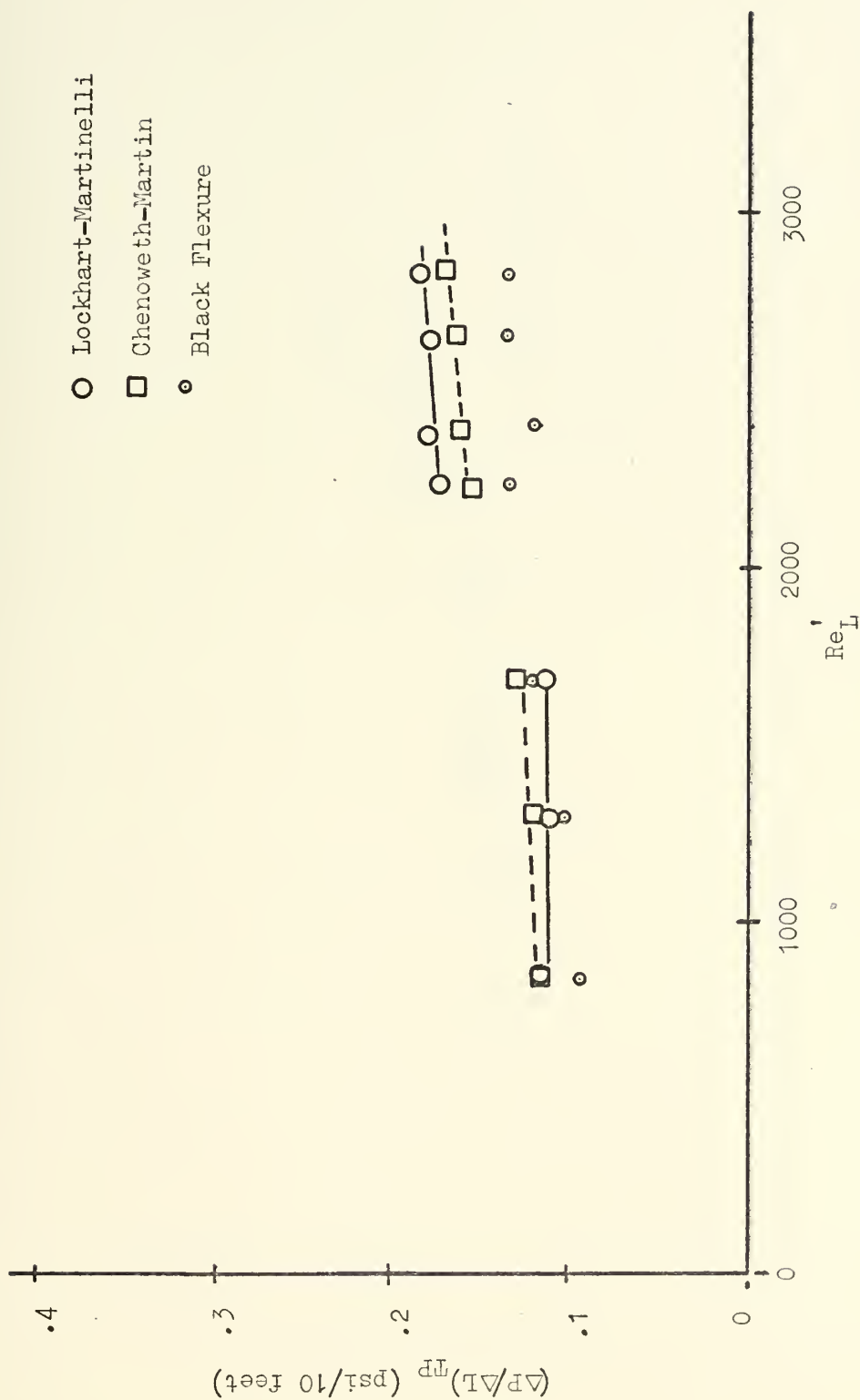


FIGURE 42 PREDICTED AND MEASURED PRESSURE DROP FOR
FOR AIR CONSTANT AT .43 lbm/sec

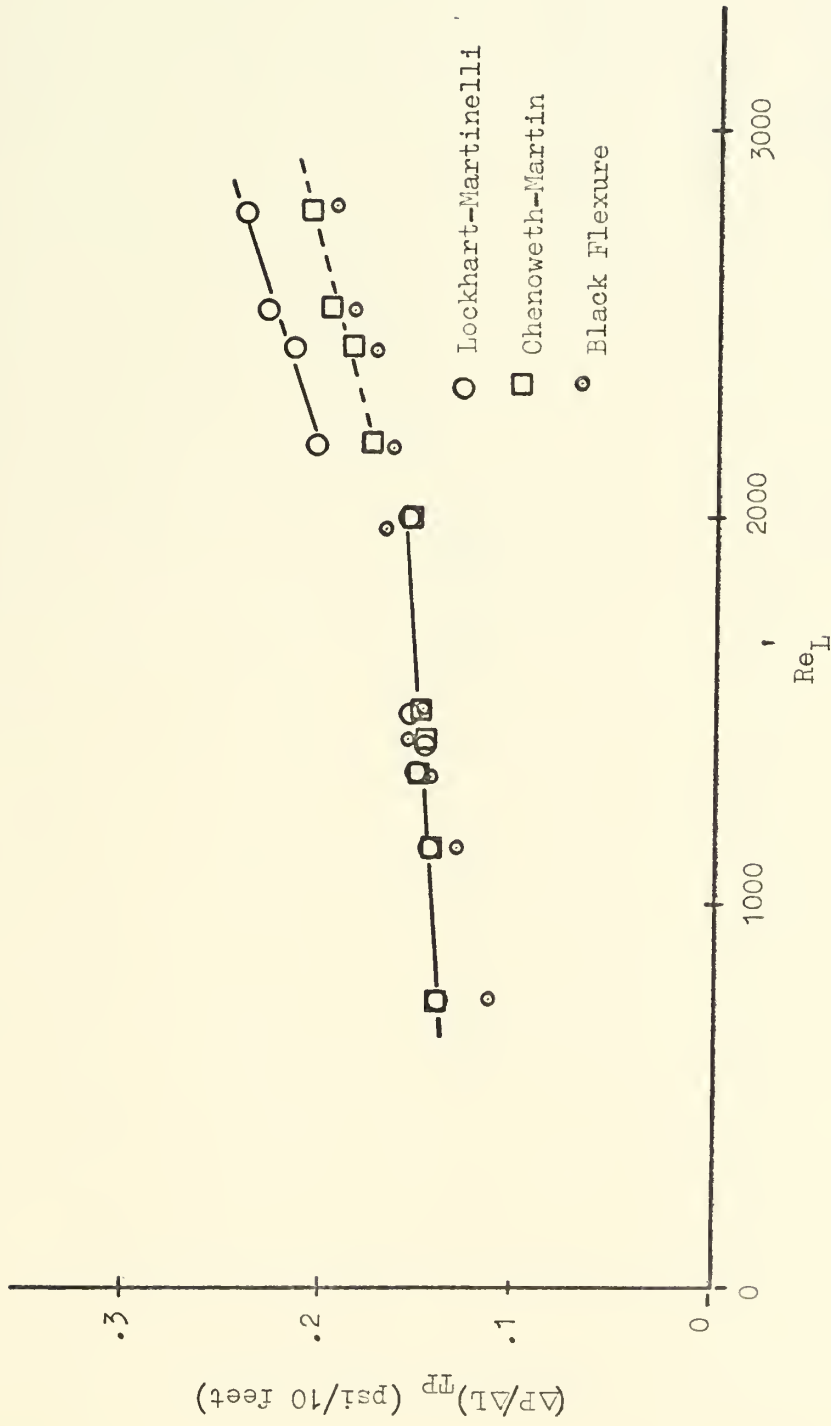


FIGURE 43 PREDICTED AND MEASURED PRESSURE DROP FOR
AIR CONSTANT AT .50 lbm/sec

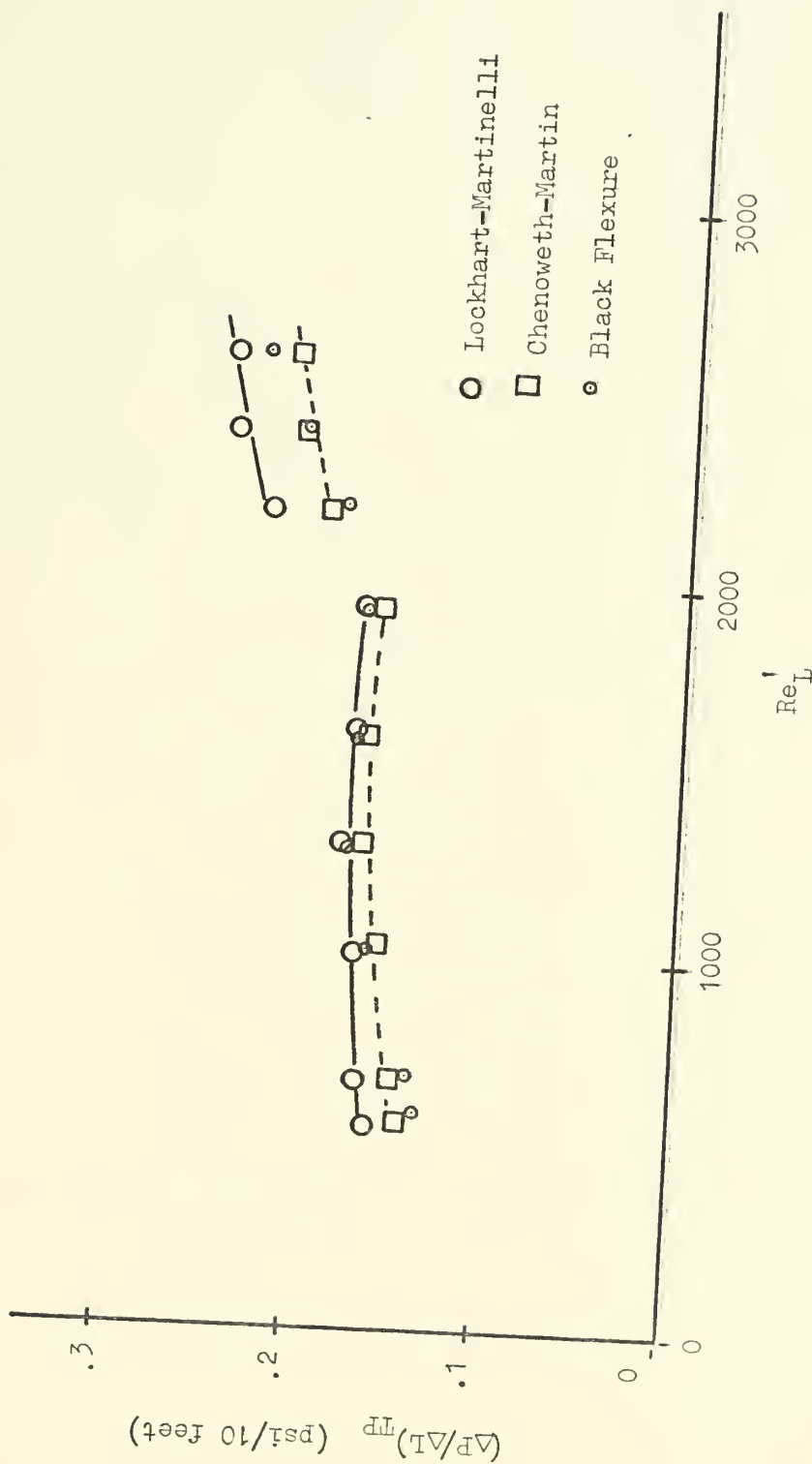


FIGURE 44 PREDICTED AND MEASURED PRESSURE DROP FOR
AIR CONSTANT AT .55 lbm/sec

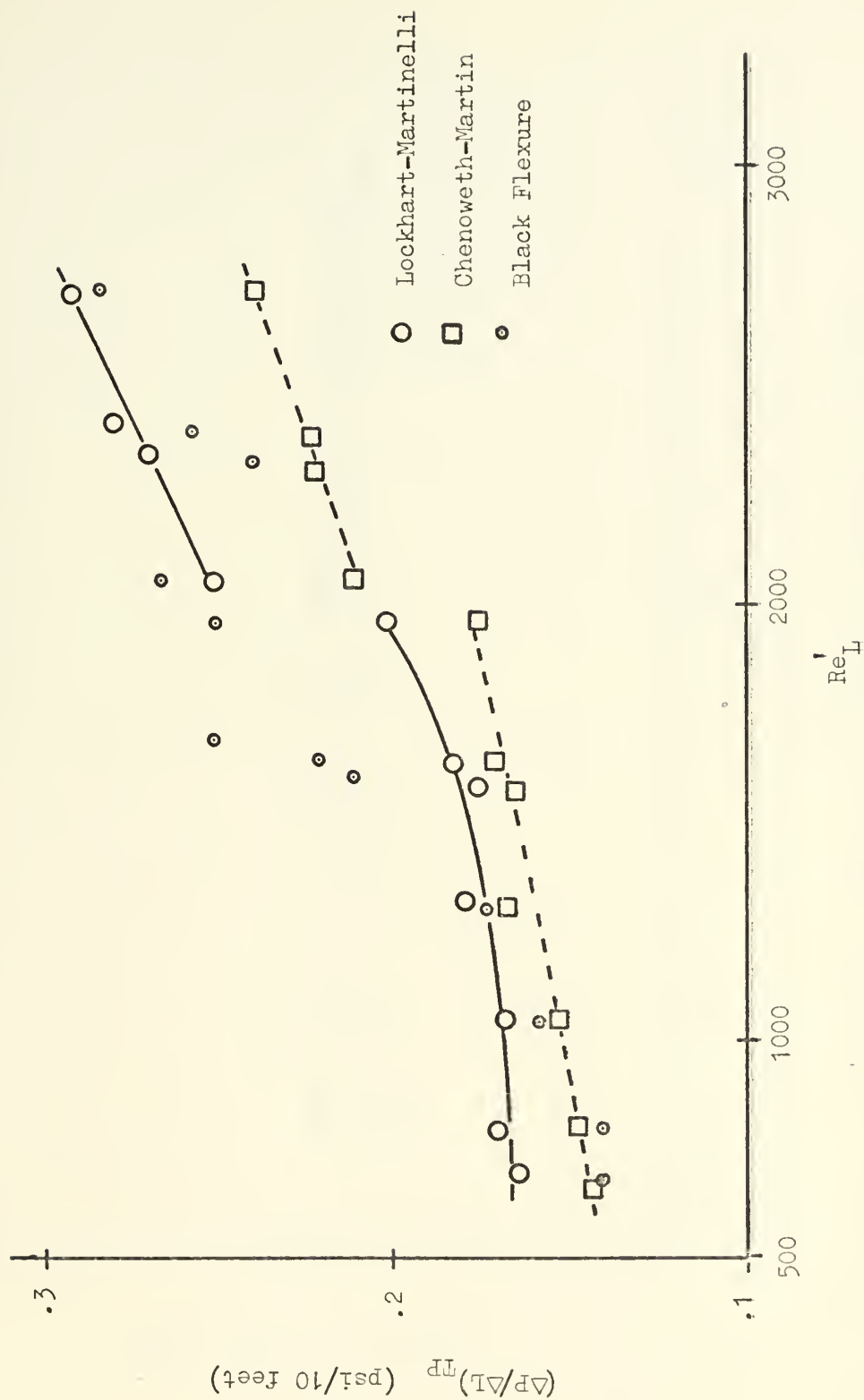


FIGURE 45 PREDICTED AND MEASURED PRESSURE DROP FOR
AIR CONSTANT AT .60 lbm/sec

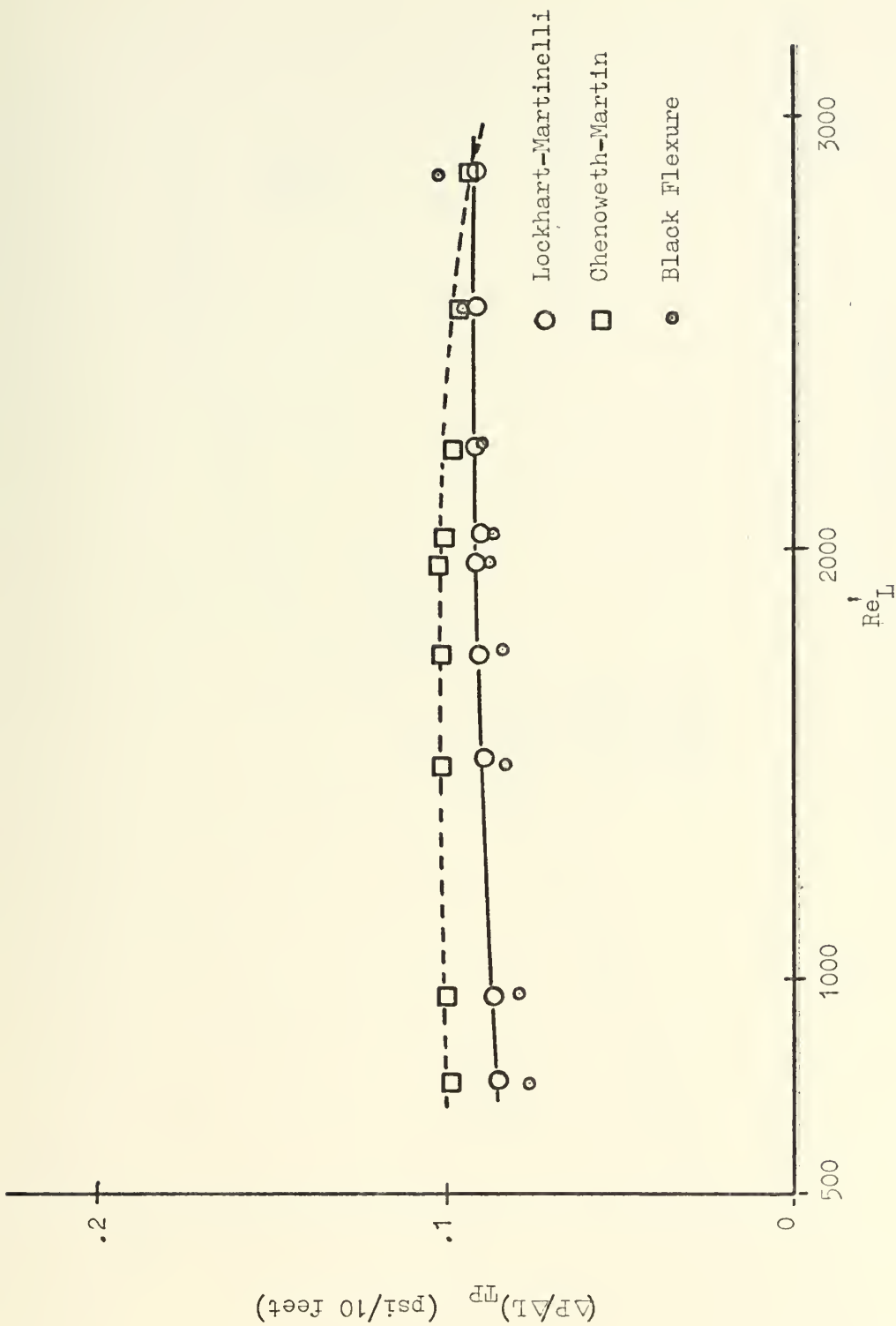


FIGURE 46 EFFECT OF CHANGING THE TRANSITION CRITERIA

FROM $Re = 2000$ to $Re = 3000$

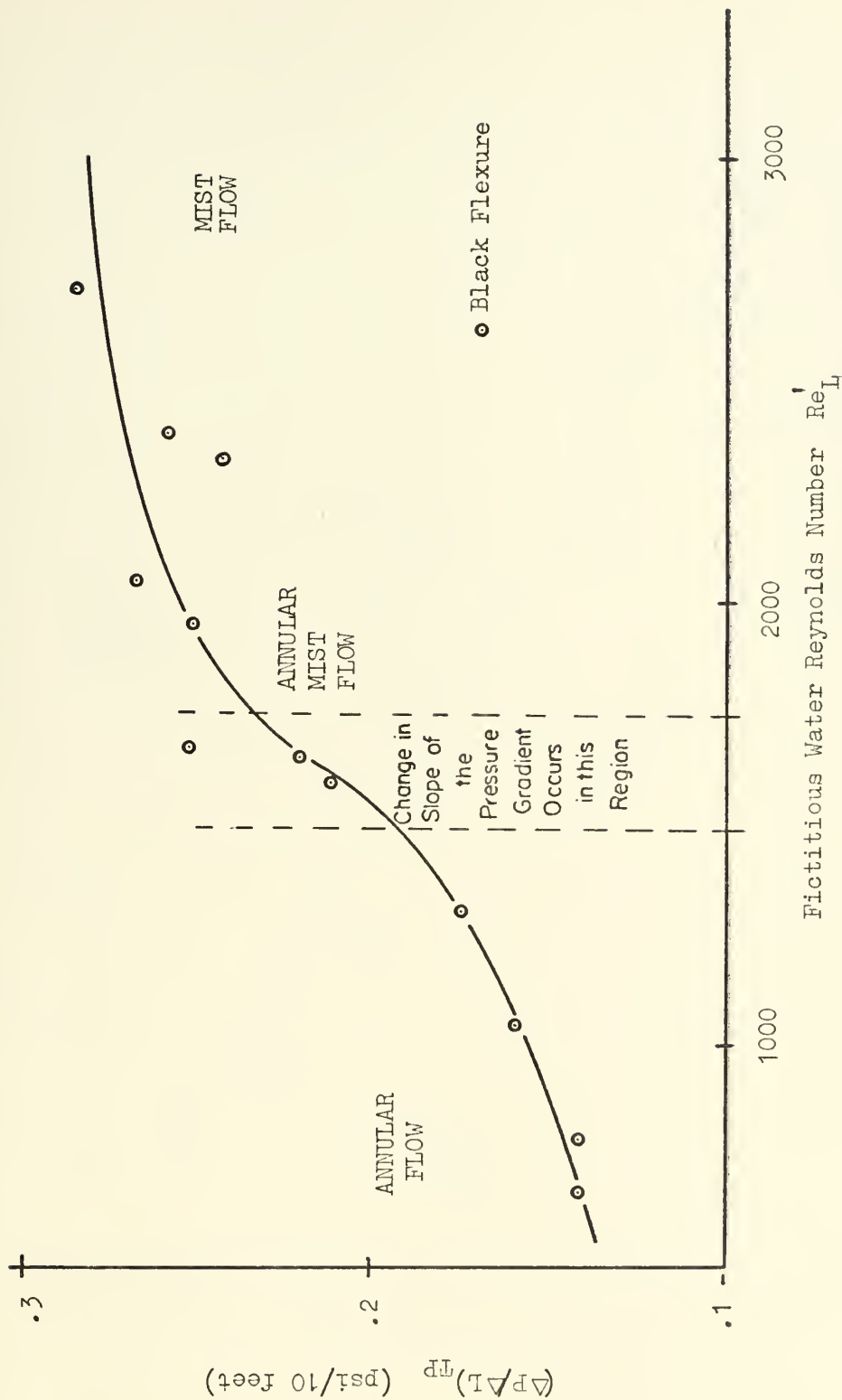


FIGURE 47 FLOW TRANSITION INDICATED BY THE CHANGE
IN THE SLOPE OF $(\Delta P / \Delta L)_{TP}$

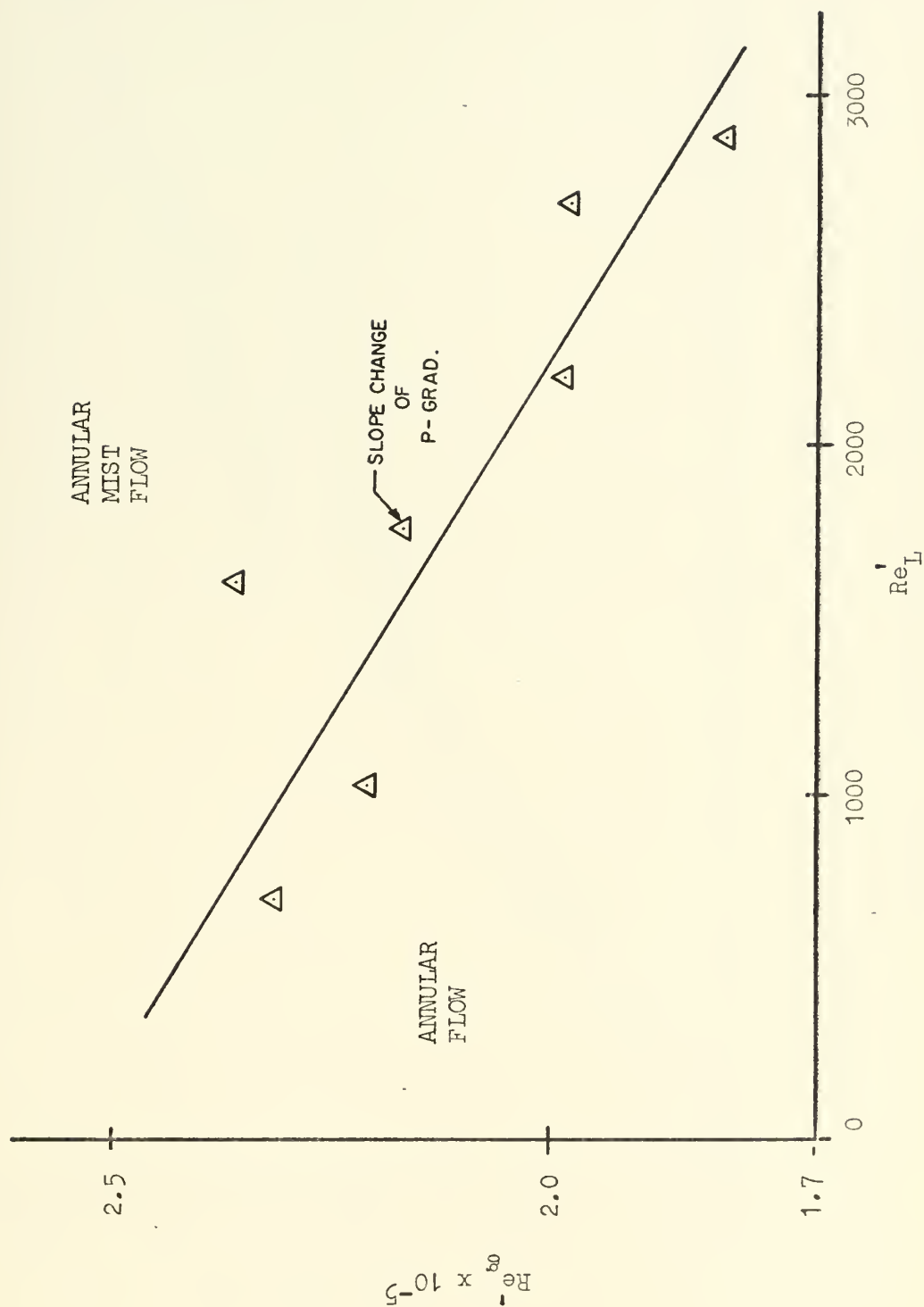


FIGURE 48 TRANSITIONS OF THE PRESSURE GRADIENT

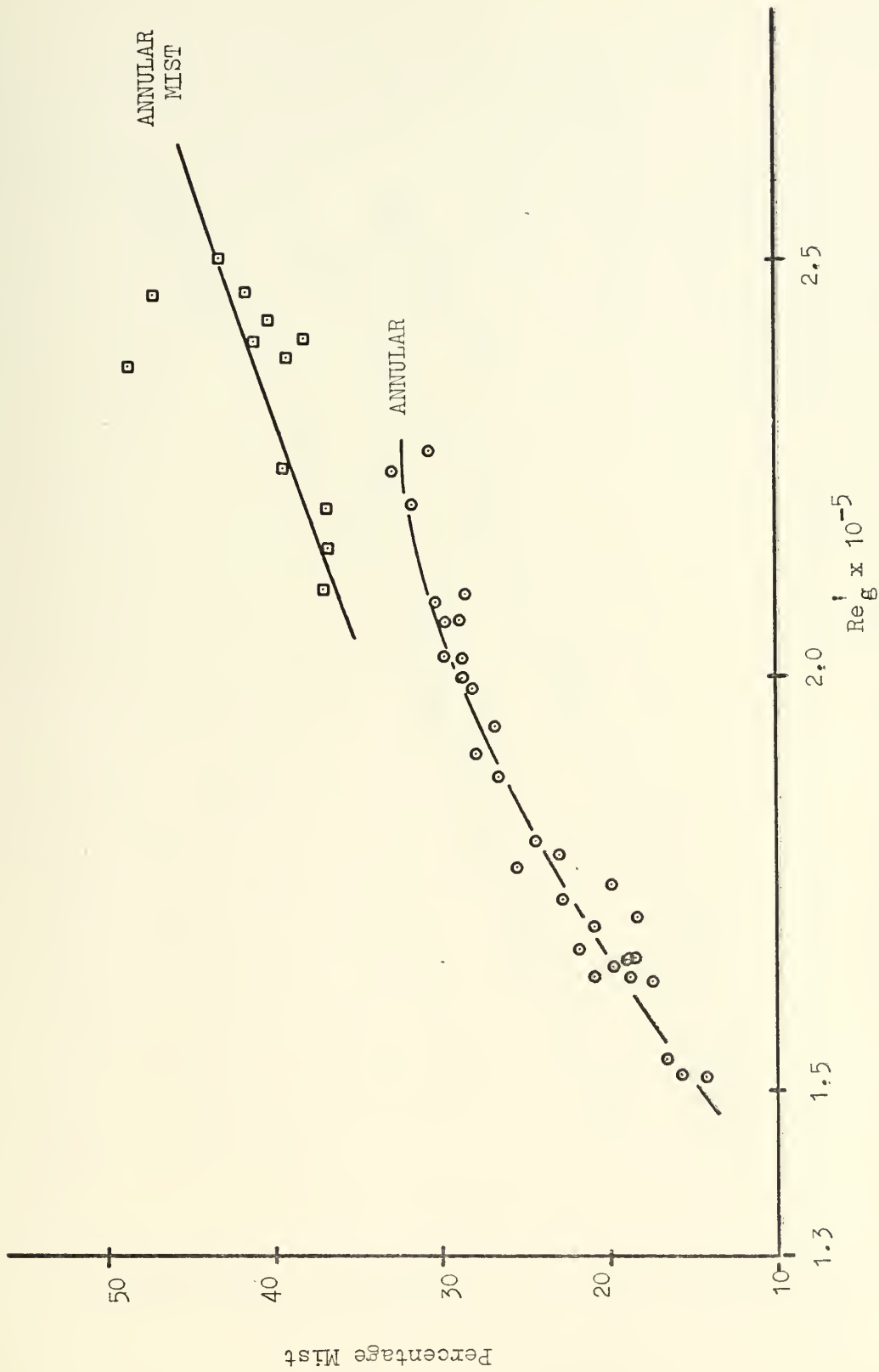


FIGURE 49 PERCENTAGE MIST INDICATING TRANSITION

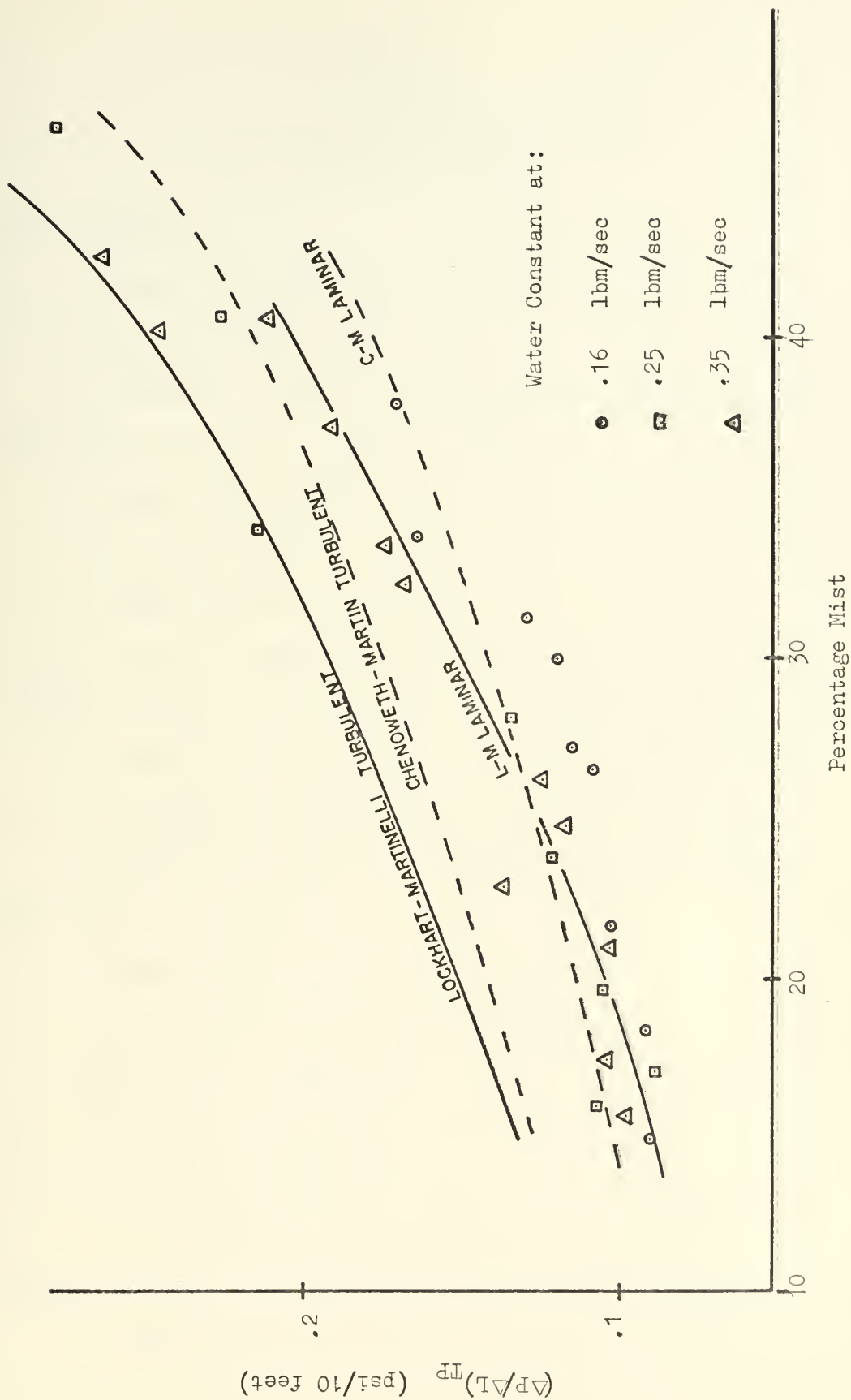


FIGURE 50 PRESSURE DROP AS A FUNCTION OF PERCENTAGE MIST

APPENDIX I

DATA REDUCTION PROGRAM NOMENCLATURE AND SAMPLE OUTPUT

INPUT PARAMETERS

M_ _ Number of interpolation pairs for subroutine SPLINI
R_ _ (I) Reynolds number values
K_ _ (I) Discharge coefficient values corresponding to R_ _ (I)

Subscripts for M_ _, R_ _ (I), K_ _ (I):

FA Flange pressure taps, air
DA D and $\frac{1}{2}$ D pressure taps, air
FW Flange pressure taps, water
DW D and $\frac{1}{2}$ D pressure taps, water

Example: RDA(I) Reynolds number for D and $\frac{1}{2}$ D taps for air flow

M_ Number of interpolation pairs for subroutine SPLINI
X_ (I) Lockhart-Martinelli two-phase flow modulus values, X
F_ _ _ (I) Lockhart-Martinelli correlation parameter values, ϕ

Subscripts for M_ , X_ (I), F_ _ _ (I):

G Lockhart-Martinelli gas correlation
L Lockhart-Martinelli liquid correlation
TT Turbulent-turbulent flow
TV Turbulent-viscous flow
VT Viscous-turbulent flow
VV Viscous-viscous flow

Example: FGTV(I) Correlation parameter, ϕ_G , for gas-phase
 turbulent-viscous flow

D1A	Inside diameter of air pipe at orifice (in)
D2A	Diameter of air orifice (in)
D1W	Inside diameter of water pipe (in)
D2W	Diameter of water orifice (in)
HMFA	Manometer fluid differential, flange taps, air (in H ₂ O)
HMDA	Manometer fluid differential, D and $\frac{1}{2}$ D taps, air (in H ₂ O)
HMFw	Manometer fluid differential, flange taps, water (in Hg)
HMDW	Manometer fluid differential, D and $\frac{1}{2}$ D taps, water (in Hg)
T1FA	Air flow temperature at orifice (deg F)
T1FW	Water flow temperature at orifice (deg. F)
TAFa	Air temperature at air orifice manometer (deg. F)
TAFw	Air temperature at water orifice manometer (deg. F)
P1	Air static pressure upstream of orifice (lb/in ²)
PT	Static pressure at test section inlet (lb/in ²)
TTFa	Air temperature at test section outlet (deg. F)
TTFw	Water temperature at test section outlet (deg. F)
DT	Inside diameter of test section (in)
LT	Length of test section (ft)

OUTPUT PARAMETERS

BETAA	Ratio of orifice-to-pipe inside diameter, air pipe
BETAW	Ratio of orifice-to-pipe inside diameter, water pipe
RFAI	Air Reynolds number based on flange taps
RDAI	Air Reynolds number based on D and $\frac{1}{2}$ D taps
RFWI	Water Reynolds number based on flange taps
RDWI	Water Reynolds number based on D and $\frac{1}{2}$ D taps
KFAI	Air discharge coefficient based on flange taps
KDAI	Air discharge coefficient based on D and $\frac{1}{2}$ D taps

KFWI	Water discharge coefficient based on flange taps
KDWI	Water discharge coefficient based on D and $\frac{1}{2}$ D taps
FRFA	Air mass flow rate based on flange taps (lbm/sec)
FRDA	Air mass flow rate based on D and $\frac{1}{2}$ D taps (lbm/sec)
FRFW	Water mass flow rate based on flange taps (lbm/sec)
FRDW	Water mass flow rate based on D and $\frac{1}{2}$ D taps (lbm/sec)
D	Inside diameter of test section (ft)
RHOWT	Water density in test section (lbm/ft ³)
RHOAT	Air density in test section (lbm/ft ³)
RLM	Liquid Reynolds number (Lockhart-Martinelli)
RGM	Gas Reynolds number (Lockhart-Martinelli)
VL	Liquid velocity (ft/sec)
VG	Gas velocity (ft/sec)
PDROPL	Fictitious liquid pressure drop (lb/ft ² /10ft)
PDROPG	Fictitious gas pressure drop (lb/ft ² /10ft)
TPPD _i	Lockhart-Martinelli two-phase pressure drop prediction. (lb/in ² /10ft) (i = 1,8)
RLC	Liquid Reynolds number (Chenoweth-Martin)
RGC	Gas Reynolds number (Chenoweth-Martin)
PDLC	Dimensionless group, Ψ_{LL} (all-liquid flow)
PDGC	Dimensionless group, Ψ_{GL} (all-gas flow)
CORPAR	Chenoweth-Martin correlation parameter
VFR	Volumetric flow ratio (liquid-to-gas)
PDRLC	Fictitious all-liquid pressure drop (lb/ft ² /10ft)
LVOLFR	Liquid volume fraction
IMO	The month (two digits)
IDAY	The day (two digits)

IYR	The year (four digits)
FWLEAK	The water labyrinth leakage (lbm/sec)
SEPWAT	The separated water collected (lbm/sec)
ATMPRS	The atmospheric pressure (psi)
FLEXR	The Red flexure reading (lbf)
FLEXB	The Black flexure reading (lbf)

DATA INPUT CARD ORDER

Card 1: MFA, MDA, MFW, MDW, MF
Card 2: RFA(I), I = 1, MFA
Card 3: KFA(I), I = 1, MFA
Card 4: RDA(I), I = 1, MDA
Card 5: KDA(I), I = 1, MDA
Card 6: RFW(I), I = 1, MFW
Card 7: KFW(I), I = 1, MFW
Card 8: RDW(I), I = 1, MDW
Card 9: KDW(I), I = 1, MDW
Card 10: MG, ML
Card 11: XG(I), I = 1, MG
Card 12: XL(I), I = 1, ML
Card 13: FGTT(I), I = 1, MG
Card 14: FGTV(I), I = 1, MG
Card 15: FGVT(I), I = 1, MG
Card 16: FGVV(I), I = 1, MG
Card 17: FLTT(I), I = 1, ML
Card 18: FLTV(I), I = 1, ML
Card 19: FLVT(I), I = 1, ML
Card 20: FLVV(I), I = 1, ML
Card 21: REYF(I), I = 1, MF
Card 22: FRIC(I), I = 1, MF
Card 23: D1A, D2A, D1W, D2W
Card 24: IMO, IDAY, IYR
Card 25: HMFA, HMDA, TLFA, TAFA, P1

Card 26: HMFw, HMDw, TLFw, TAFw

Card 27: PT, TTFw, TTFA, FWLEAK, SEPWAT

Card 28: DT, LT, ATMPRS, FLEXR, FLEXB

DATA REDUCTION PROGRAM IN FORTRAN IV LANGUAGE

```

REAL LT, LVOLFR, MIST
REAL*8 RFA(17), KFA(17), RFAI, KFAI, RDA(22), KDA(22), RDAI, KDAI,
*RFW(23), KFW(23), RFWI, KFWI, RDW(23), KDW(23), RDWI, KDWI,
*XG(17), XL(53), XI, FGIT(17), FGIV(17), FGTI(17), FGVV(17),
*FGITI, FGTVI, FGTII, FGVVI, FLTI(53), FLTV(53), FLVT(53), FLVV(53),
*FLTTI, FLTVI, FLVTI, REYF(30), FRIC(30), RGM, RLM, FG, FL
C
C VISCOSITY OF AIR AT TEMPERATURE XX (DEG F) (0<XX<500)
VISCOA(XX) = 1.089790E-05 + 1.917221E-08*XX - 7.086247E-12*XX**2
C
C VISCOSITY OF WATER AT TEMPERATURE XX (DEG F) (32<XX<120)
VISCOW(XX) = 2.546764E-03 - 6.985662E-05*XX + 1.207512E-06*XX**2 -
*1.285602E-08*XX**3 + 7.467161E-11*XX**4 - 1.788613E-13*XX**5
C
C SPECIFIC GRAVITY OF WATER AT TEMPERATURE XX (DEG F) (39.2<XX<104)
SPGRW(XX) = C.99837633 + 1.060576E-04*XX - 1.593186E-06*XX**2
C
C SPECIFIC GRAVITY OF MERCURY AT TEMPERATURE XX (DEG F) (32<XX<113)
SPGRHG(XX) = 13.63905 - .0013630303 * XX
C
C CONVERSION FACTOR -- INCHES OF WATER TO PSI AT TEMPERATURE XX (DEG
CFH2O(XX) = 62.42732 * SPGRW(XX)/1728.0
C
C CONVERSION FACTOR -- INCHES OF MERCURY TO PSI AT TEMPERATURE XX (DEG
CFHG(XX) = 0.4891585 * SPGRHG(XX)/13.54
C
C AREA EXPANSION FACTOR AT TEMPERATURE XX (DEG F)
AREAEX(XX) = 1.0 + (XX - 68.0) * 1.85185E-05
C
C KONT=0
READ (5, 100) MFA, MDA, MFW, MDW, MF
FORMAT (5I3)
100 READ (5, 21C) (RFA(I), I = 1, MFA)
READ (5, 21C) (KFA(I), I = 1, MFA)
READ (5, 21C) (RDA(I), I = 1, MDA)
READ (5, 21C) (KDA(I), I = 1, MDA)
READ (5, 21C) (RFW(I), I = 1, MFW)
READ (5, 21C) (KFW(I), I = 1, MFW)
READ (5, 21C) (RDW(I), I = 1, MDW)
READ (5, 21C) (KDW(I), I = 1, MDW)
READ (5, 150) MG, ML
150 FORMAT (2I3)
READ (5, 20C) (XG(I), I = 1, MG)
READ (5, 20C) (XL(I), I = 1, ML)
READ (5, 20C) (FGIT(I), I = 1, MG)
READ (5, 20C) (FGTV(I), I = 1, MG)
READ (5, 20C) (FGTI(I), I = 1, MG)
READ (5, 20C) (FGVV(I), I = 1, MG)

```



```

READ (5,200) (FLTT(I), I = 1, ML)
READ (5,200) (FLTV(I), I = 1, ML)
READ (5,200) (FLVT(I), I = 1, ML)
READ (5,200) (FLVV(I), I = 1, ML)
READ (5,210) (REYF(I), I=1,MF)
READ (5,210) (FRIC(I), I=1,MF)
FORMAT (10F8.0)
READ (5,210) DIA, D2A, DIW, D2W
READ (5,99) IMO, IDAY, IYR
FORMAT (2I2, I4)
READ (5,210) HMFA, HMDA, T1FA, T2FA, P1
IF (T1FA.GT.500.0) GO TO 999
READ (5,210) HMFH, HMDW, T1FW, T2FW, TAFW, SEPWAT
READ (5,210) PT, T1FW, T1FA, FWLEAK, FLEWB
READ (5,210) DT, LT, ATMPRS, FLEXR, FLEXB
P1=PT+ATMPRS
PT=PT+ATMPRS
FORMAT (8F10.0)
WRITE (6,39C)
FORMAT (1I)
FORMAT (/)
BETAA = C2A/DIA
BETAW = D2W/DIW
IF (KONT.GT.0) GO TO 910
WRITE (6,340)
KONT=KONT+1
IF (IMO.EQ.3) GO TO 33
IF (IMO.EQ.4) GO TO 44
IF (IMO.EQ.5) GO TO 55
IF (IMO.EQ.6) GO TO 66
IF (IMO.EQ.7) GO TO 77
IF (IMO.EQ.8) GO TO 88
IF (IMO.EQ.9) GO TO 97
IF (IMO.EQ.10) GO TO 110
IF (IMO.EQ.11) GO TO 120
IF (IMO.EQ.12) GO TO 130
WRITE (6,333) IDAY, IYR
GO TO 911
WRITE (6,444) IDAY, IYR
GO TO 911
WRITE (6,555) IDAY, IYR
GO TO 911
WRITE (6,666) IDAY, IYR
GO TO 911
WRITE (6,777) IDAY, IYR
GO TO 911
WRITE (6,888) IDAY, IYR
GO TO 911

```

200

909
99

210

390
391

910

33

44

55

66

77

88


```
97 WRITE(6,998) IDAY,IYR
GO TO 911
110 WRITE(6,111) IDAY,IYR
GC TO 911
120 WRITE(6,121) IDAY,IYR
GO TO 911
130 WRITE(6,131) IDAY,IYR
GO TO 911
333 FORMAT(T65,I2,MARCH,I4)
444 FORMAT(T65,I2,APRIL,I4)
555 FORMAT(T65,I2,MAY,I4)
666 FORMAT(T65,I2,JUNE,I4)
777 FORMAT(T65,I2,JULY,I4)
888 FORMAT(T65,I2,AUGUST,I4)
998 FORMAT(T65,I2,SEPTEMBER,I4)
111 FORMAT(T65,I2,OCTOBER,I4)
121 FORMAT(T65,I2,NOVEMBER,I4)
131 FORMAT(T65,I2,DECEMBER,I4)
340 FORMAT(T58,TWO-PHASE FLOW TEST RIG,/,T57,NAVAL POSTGRADUATE
* SCHOOL,/)
911 WRITE(6,341)
341 FORMAT(T25,/)
*
WRITE(6,342)
342 FORMAT(T56,MASS FLOW RATE DETERMINATION,/,T55,SQUARE-EDGE CO
*NCENTRIC ORIFICE,/,T63,ASME STANDARD,/,T80,AIR,T89,WATE
*R,/)
400 WRITE(6,400) CIA,DIW,D2A,D2W,BETAA,BETAW,T1FA,T1FW,TAFW
FORMAT(T44,PIPE DIAMETER(IN.),T75,2F10.4,/,T44,ORIFICE DIA
*METER(IN.),T75,2F10.4,/,T44,BETAA(D2/D1),T75,2F10.4,/,
*T44,TEMPERATURE IN PIPE(DEG.F.),T75,2F10.4,/,
*TURE,OF ATM.(DEG.F.),T75,2F10.4)
WRITE(6,401) PI
401 FORMAT(T44,PRESSURE IN PIPE (PSIA),T75,F10.4)
GAMMA = 1.4
R = 53.3448
T1A = T1FA + 459.69
C
C
GMU = 32.174 * MU (COEFFICIENT OF VISCOSITY)
GMUW = VISCCW(T1FW)
GMUA = VISCCA(T1FA)
C
C
SPECIFIC GRAVITY OF WATER IN PIPE
GH2O1 = SPGRW(T1FW)
C
C
DENSITY OF WATER IN PIPE
RHOW1 = 62.42732 * GH2O1
C
```



```

C SPECIFIC GRAVITY OF WATER IN AIR FLOW MEASUREMENT MANOMETER
GH20A = SPGRW(TAFA)

C SPECIFIC GRAVITY OF WATER IN WATER FLOW MEASUREMENT MANOMETER
GH20W = SPGRW(TAFW)

C SPECIFIC GRAVITY OF MERCURY IN WATER FLOW MEASUREMENT MANOMETER
GHGW = SPGRHG(TAFW)
GHGA = SPGRHG(TAFA)
RHOWA = GH2CA * 62.42732
RHOWW = GH2CW * 62.42732
RHOHGA = GHGW * RHOWW
RHOAIR = 144.0 * P1 / (R * T1A)
HWFA = HMFA * (RHOWA - RHOAIR) / 62.317
HMFA = HMFA * (RHOWA - RHOAIR) / 62.317
HMFH = HMFH * (RHOHGA - RHOHGA) / 62.317
HMDW = HMDW * (RHOHGA - RHOHGA) / 62.317
DELPF = HWFA * CFH20(68.0)
DELPD = HWCA * CFH20(68.0)
YF = EXPFAC(BETAA, DELPF, P1, GAMMA)
YD = EXPFAC(BETAA, DELPD, P1, GAMMA)
FAA = AREAEX(T1FA)
FAW = AREAEX(T1FW)
FRFA = 0.35
J = 0
250 FRAI = FRFA
    RFAI = 15.2784 * FRFA / (DIA * GMUA)
    IF (RFAI.LE.1.0E 06) GO TO 230
    KFAI = KFA(MFA)
    GO TO 260
230 IF (J.GT.0) GO TO 240
    CALL SPLIN1(RFA,KFA,MFA,RFAI,KFAI)
    GO TO 260
240 CALL SPLINN(RFA,KFA,MFA,RFAI,KFAI)
260 FRFA = 0.16384266 * KFAI * D2A**2 * FAA * YF * SQRT(P1 * HWFA/T1A)
    J = J + 1
    IF (J.GT.100) GO TO 750
    EPS2 = ABS(FRFA - FRAI)
    IF (EPS2.GT. 1.0E-06) GO TO 250
    GO TO 345
750 WRITE(6,800)
800 FORMAT(T25, 'MORE THAN 100 ITERATIONS FOR AIR FLANGE TAPS -- LATEST
    * VALUES PRINTED, /)
345 FRDA = FRFA
    K = 0
350 FRA2 = FRDA
    RDAI = 15.2784 * FRDA / (DIA * GMUA)
    IF (RDAI.LE.1.0E 06) GO TO 360

```



```

KDAI = KCA(MDA)
GO TO 380
IF(K.GT.0) GO TO 370
CALL SPLIN1(RDA,KDA,MCA,MDA,RDAI,KDAI)
GO TO 380
CALL SPLINN(RCA,KDA,MCA,MDA,RDAI,KDAI)
370 FRDA = 0.16384266 * KDAI**2 * FAA * YD * SQR(TP1 * HWFA/T1A)
380 K = K + 1
IF(K.GT.100) GO TO 850
EPS3 = ABS(FRDA - FRA2)
IF (EPS3 .GT. 1.0E-06) GO TO 350
GO TO 498
850 WRITE(6,500)
900 FORMAT(I25,'MORE THAN 100 ITERATIONS FOR AIR D TAPS -- LATEST
498 * VALUES PRINTED')
L = 0
FRFW = 35.0
FRWI = FRFW
205 RFWI = 15.2784 * FRFW/(DIW * GMUW)
IF (RFWI.LE.1.0E 06) GO TO 23
KFWI = KFW(NFW)
GO TO 26
23 IF(L.GT.0) GO TO 24
CALL SPLIN1(RFW,KFW,MFW,RFWI,KFWI)
GO TO 26
24 CALL SPLINN(RFW,KFW,MFW,RFWI,KFWI)
26 FRFW = 9.972222E-02 * KFWI * D2W**2 * FAW * SQR(T(HWFW * RHOW1)
L = L + 1
IF(L.GT.100) GO TO 75
EPS = ABS(FRFW - FRWI)
IF(EPS.GT.1.0E-06) GO TO 205
GO TO 34
75 WRITE(6,80)
80 FORMAT(I25,'MORE THAN 100 ITERATIONS FOR WATER FLANGE TAPS -- LATE
*ST VALUES PRINTED')
34 FRDW = FRFW
M = 0
300 FRW2 = FRDW
RDWI = 15.2784 * FRDW/(DIW * GMUW)
IF (RDWI.LE.1.0E 06) GO TO 36
KDWI = KDW(MDW)
GO TO 38
36 IF(M.GT.0) GO TO 37
CALL SPLIN1(RCW,KDW,MCW,MDW,RDWI,KDWI)
GO TO 38
37 CALL SPLINN(RCW,KDW,MCW,MDW,RDWI,KDWI)
38 FRDW = 9.972222E-02 * KDWI * D2W**2 * FAW * SQR(T(HWDW * RHOW1)
M = M + 1

```



```

IF(M.GT.100) GO TO 85
EPS1 = ABS(FRDW - FRW2)
IF(EPS1.GT.1.0E-06) GO TO 300
GO TO 499
85 WRITE(6,90)
90 FORMAT(T25,'MORE THAN 100 ITERATIONS FOR WATER D TAPS -- LATE
*ST VALUES PRINTED./)
499 *CALL FLLEAK(PT,FRFA,FRDA,FRFW,FRDW,AFLFLO,ADFLO,WFLFLO,WDFLO,FWLEA
*K,ATMPRS)
IF(SEPWAT.GT.(0.0)) GO TO 487
MIST=0.0
GO TO 497
487 MIST=1.0-((SEPWAT/((WFLFLO+WDFLO)/2.0))
MIST=MIST*100.0000
497 WRITE(6,402) MIST
402 FORMAT(T44,'PERCENT MIST FLOW',T75,F10.4////)
500 WRITE(6,500)
500 FORMAT(T65,'AIR',T98,'WATER',/,T51,'-----')
WRITE(6,501)
501 FORMAT(T52,'FLANGE TAPS', T71, 'D TAPS', T86, 'FLANGE TAPS',
*T105, 'D TAPS,/')
WRITE(6,600) FRFA,HMDA,HMFW,HMDW
600 FORMAT(T25,'PRESSURE DROP', T49, F9.4, T59,'IN.H2O', T66,F9.4, T7
*6, 'IN.H2O', T83, F9.4, T93, 'IN.HG', T100, F9.4, T110, 'IN.HG,')
WRITE(6,601) RFPAI,RFWI,RDWI
601 FORMAT(T25,'REYNOLDS NUMBER', T47, 1P4D17.6)
WRITE(6,602) KFAI,KDAI,KFWI,KDWI
602 FORMAT(T25,'DISCHARGE COEFFICIENT' T47, OP4D17.6)
WRITE(6,603) FRFA,FRDA,FRFW,FRDW
603 FORMAT(T25,'MASS FLOW RATE (LBM/SEC)', T50, F10.6, T66, F11.6,
*T83,F11.6, T100,F11.6)
WRITE(6,604) AFLFLO,WFLFLO,WDFLO
604 *F11.6,T100,F11.6)
FRFA=AFLFLO
FRDA=ADFLO
FRFW=WFLFLO
FRDW=WDFLO

```

C LOCKHART-MARTINELLI TWO-PHASE PRESSURE DROP PREDICTION

```

PI = 3.1415926
D = DT/12.0
A = PI * D**2/4.0
G = 32.174
FRL = (FRFW + FRDW)/2.0
FRG = (FRFA + FRDA)/2.0
GMUL = VISCCW(TTFW)

```



```

C
C
GMUG = VISCCA(TTFA)
SPECIFIC GRAVITY OF WATER IN TEST SECTION
GH2OT = SPGRW(TTFW)
RHOWT = GH2CT * 62.42732
TTA = TTFA + 459.69
RHOAT = 144.0 * PT/(R * TTA)
RLM = 4.0 * FRL/(PI * D * GMUG)
RGM = 4.0 * FRG/(PI * D * GMUG)
VL = FRL/(RHOWT * A)
VG = FRG/(RHOAT * A)

C
C
FL = FRICTION FACTOR = FG
IF(RGM.LE.2.E03) GO TO 1
CLICK=1.0
CALL SPLIN1(REYF,FRIC,MF,RGM,FG)
IF(RLM.LE.2.E03) GO TO 2
IF(CLICK.EQ.1.0) GO TO 5
CALL SPLIN1(REYF,FRIC,MF,RLM,FL)
GO TO 4
CALL SPLINN(REYF,FRIC,MF,RLM,FL)
GO TO 4
IF(RGM.EQ.0.0) GO TO 6
FG=64.0000/RGM
GO TO 3
FG=1.0
GO TO 3
IF(RLM.EQ.0.0) GO TO 7
FL=64.00000/RLM
GO TO 4
FL=1.0
CONTINUE
FLC=FL
FGC=FG

C
PDRGPL = RHCWT * FL * LT * VL**2/(G * D * 2.0)
PDRPPG = RHCAT * FG * LT * VG**2/(G * D * 2.0)
IF(PDRGPL.GT.0.0.AND.PDRPPG.GT.0.0) GO TO 255
IF(PDRGPL.GT.0.0) GO TO 235
WRITE(6,220) PDRPPG
FORMAT(/T25,'NO LIQUID FLOW - AIR PRESSURE DROP (LB/SQFT) =',
220 *T73,1PE10.4,/)
GO TO 755
WRITE(6,245) PDRGPL
FORMAT(/T25,'NO AIR FLOW - LIQUID PRESSURE DROP (LB/SQFT) =',
245 *T73,1PE10.4,/)
GO TO 755
WRITE(6,255) XI = SQRT(PDRCPPL/PDRPPG)
255 XI = SQRT(PDRCPPL/PDRPPG)

```



```

CALL SPLINI (XG,FGTT,MG,XI,FGTTI)
CALL SPLINI (XG,FGTV,MG,XI,FGTVI)
CALL SPLINI (XG,FGVV,MG,XI,FGVVI)
CALL SPLINI (XL,FLTT,ML,XI,FLTTI)
CALL SPLINI (XL,FLVT,ML,XI,FLVTI)
CALL SPLINI (XL,FLVV,ML,XI,FLVVI)
CALL SPLINI (XL,FLVV,ML,XI,FLVVI)
TPPD1 = FGTI**2 * PDROPG/144.0
TPPD2 = FGTVI**2 * PDROPG/144.0
TPPD3 = FGVVI**2 * PDROPG/144.0
TPPD4 = FLTTI**2 * PDROPL/144.0
TPPD5 = FLTTI**2 * PDROPL/144.0
TPPD6 = FLVTI**2 * PDROPL/144.0
TPPD7 = FLVTI**2 * PDROPL/144.0
TPPD8 = FLVVI**2 * PDROPL/144.0
WRITE (6,390)
WRITE (6,341) D, LT, TIFW, TIFA, PT
WRITE (6,341)
WRITE (6,341)
WRITE (6,510)
510 *N,/,/, T77, 'LOCKHART-MARTINELLI TWO-PHASE PRESSURE DROP PREDICTIO
*-----, T89, '-----
WRITE (6,511) RHOWT,RHGAT,RLM,RGM,VL,VG,PDRDPL,PDRDPLG
IF (RLM.GE.2.0E 03.AND.RGM.GE.2.0E 03) GO TO 405
IF (RLM.GE.2.0E 03.AND.RGM.LT.2.0E 03) GO TO 425
IF (RLM.LT.2.0E 03.AND.RGM.GE.2.0E 03) GO TO 450
IF (RLM.LT.2.0E 03.AND.RGM.LT.2.0E 03) GO TO 475
405 WRITE (6,512) FLTTI,FGTTI,TPPD5,TPPD1
GO TO 755
425 WRITE (6,435)
WRITE (6,512) FLTVI,FGTVI,TPPD6,TPPD2
GO TO 755
450 WRITE (6,460)
WRITE (6,512) FLVTI,FGVTI,TPPD7,TPPD3
GO TO 755
475 WRITE (6,485)
WRITE (6,512) FLVVI,FGVVI,TPPD8,TPPD4
FORMAT (T40, 'THE FLOW IS TURBULENT-TURBULENT')
FORMAT (T40, 'THE FLOW IS TURBULENT-VISCOUS')
FORMAT (T40, 'THE FLOW IS VISCOUS-TURBULENT')
FORMAT (T40, 'THE FLOW IS VISCOUS-VISCOUS')
FORMAT (T46, 'TEST SECTION DIAMETER (FT) =', E12.4,/, 'E12.4,/, T46, 'TEST SECTION PRESSURE (PSIA)
*ION WATER TEMP. =', E12.4,/, 'E12.4,/, T46, 'TEST SECTION AIR TEMP
* (DEG.F.)

```



```

*      =, E12.4,/)
511 FORMAT( T40, 'DENSITY (LBM/CU-FT) =', 1P2E14.5,/, T40,
*REYNOLDS NUMBER =', 2E14.5,/, T40, 'VELOCITY (FT/S
*EC)
*      =, 2E14.5/)
512 FORMAT( T40, 'CORRELATION PARAMETER
*PREDICTED TWO-PHASE PRESSURE',/, T53, 'DROP (PSI/10FT) =', 2E14.5/
*)

```

CCCCC

CHENOWETH-MARTIN CORRELATION COMPUTATIONS

```

755 RLC = D * (FRL + FRG)/(GMUL * A)
RGC = D * (FRL + FRG)/(GMUG * A)
PCLC = FLC * LT/D
PDGC = FGC * LT/D
CORPAR = PDGC * RHOHT/(PDLC * RHOAIR)
VLC = (FRL + FRG)/(RHOHT * A)
PDRLC = RHOHT * FLC * LT * VLC**2/(G * D * 2.0)

```

CCC

```

VOLUMETRIC FLOW RATIO -- LIQUID/GAS
VFR = (FRL * RHOAT)/(FRG * RHOHT)

```

```

LIQUID VOLUME FRACTION
LVOLFR = 1./C/(1.0 + 1.0/VFR)
CALL CHNWTN(LVOLFR, CORPAR, PDRLC, TPPDCM)
PDRPCM=TPPDCM/144.000000
WRITE (6,341)
WRITE (6,8C5)

```

```

805 FORMAT( T48, 'CHENOWETH-MARTIN TWO-PHASE FLOW CALCULATIONS',/)
WRITE (6,905) RLC, RGC, PDLC, PDGC, CORPAR, VFR, PDRLC, LVOLFR, PDRPCM
PDRPCM=TPPDCM/144.000000

```

C

```

COMPUTATION OF THE MEASURED P-DROP, DONE FOR EACH FLEXURE READING
PL=8.131488847
PLA=3.140336
PT=PT-ATMPRS
FLAB=PT*PLA
TRFLXR=FLEXR-FLAB
TRFLXB=FLEXB-FLAB
TAUR=TRFLXR/PL
TAUB=TRFLXB/PL
PT=PT+ATMPRS
WRITE(6,393) TAUR, TAUB

```

```

393 FORMAT(/, T40, 'MEASURED PRESSURE DROP (PSI/10FT)', T75, 'RED FLEXURE',
@T90, 'BLACK FLEXURE',/, T75, F11.8, T92, F11.8, //)
WRITE (6,39C)

```

```

905 FORMAT(/, T46, 'REYNOLDS NUMBER (LIQUID) =', 1PE15.6,/,

```



```

*T46,'REYNOLDS NUMBER (GAS)
*OUP (ALL LIQUID) =, E15.6/, T46,'DIM.--LESS GROUP (ALL GAS)
*E15.6/,T46,'CORRELATION' PARAMETER =, E15.6/,T46,'FICT. ALL-LIQ. P
*VOLUMETRIC FLOW RATIO (LQ/GS) =, E15.6/, T46,'LIQUID VOLUME FRACTION
*RESS.DROP(PSP) =, E15.6/,T46,'PREDICTED TWO PHASE PRESSURE',/T60,'DROP(PSP)/10
*FT) =, E14.6//)
GO TO 909
STOP
END

```

999

C
C
C

MAS02060
MAS02070
MAS02080

```

SUBROUTINE SPLIN1(X,Y,M,XINT,YINT)
IMPLICIT REAL*8 (A-H),REAL*8 (O-Z)
DIMENSION X(M),Y(M),C(4,300)
CALL SPLICG(X,Y,M,C)
K=1
ENTRY SPLINN(X,Y,M,XINT,YINT)
IF(XINT-X(1)) 70,1,2

```

MAS02090
MAS02100
MAS02110
MAS02120
MAS02130
MAS02140
MAS02150
MAS02160
MAS02170
MAS02180
MAS02190
MAS02200
MAS02210
MAS02220
MAS02230
MAS02240
MAS02250
MAS02260
MAS02270
MAS02280
MAS02290
MAS02300
MAS02310
MAS02320
MAS02330
MAS02340
MAS02350
MAS02360
MAS02370

```

3 70 K=1
1 GO TO 7
1 YINT=Y(1)
2 RETURN
2 IF(XINT-X(K+1))6,4,5
4 YINT=Y(K+1)
5 RETURN
5 K=K+1
71 IF(M-K) 71,71,3
71 K=M-1
6 GO TO 7
12 IF(XINT-X(K))13,12,11
12 YINT=Y(K)
13 RETURN
13 K=K-1
7 GO TO 6
101 PRINT 101,XINT = D18.9,32H, OUT OF RANGE FOR INTERPOLATION)
7 FORMAT(8H0XINT)
101 YINT=(X(K+1)-XINT)*C(1,K)+(X(K+1)-XINT)**2+C(3,K))
11 YINT=YINT+(XINT-X(K))*C(2,K)*(XINT-X(K))**2+C(4,K))
11 RETURN
END

```



```

SUBROUTINE SPLICO(X,Y,M,C)
IMPLICIT REAL*8 (A-H),REAL*8 (O-Z)
DIMENSION X(M),Y(M),C(4,300),D(300),P(300),E(300),A(300,3),B(300),
1Z(300)
MM=M-1
DO 2 K=1,MM
D(K)=X(K+1)-X(K)
P(K)=D(K)/6
2 E(K)=(Y(K+1)-Y(K))/D(K)
DO 3 K=2,MM
B(K)=E(K)-E(K-1)
A(1,2)=-1-C(1)/D(2)
A(1,3)=D(1)/D(2)
A(2,3)=P(2)-P(1)*A(1,3)
A(2,2)=2*(P(1)+P(2))-P(1)*A(1,2)
A(2,3)=A(2,3)/A(2,2)
B(2)=B(2)/A(2,2)
DO 4 K=3,MM
A(K,2)=2*(P(K-1)+P(K))-P(K-1)*A(K-1,3)
B(K)=B(K)-P(K-1)*B(K-1)
A(K,3)=P(K)/A(K,2)
B(K)=B(K)/A(K,2)
Q=D(M-2)/D(M-1)
A(M,1)=1+Q+A(M-2,3)
A(M,2)=-Q-A(M,1)*A(M-1,3)
B(M)=B(M-2)-A(M,1)*B(M-1)
Z(M)=B(M)/A(M,2)
MN=M-2
DO 6 I=1,MN
K=M-I
Z(1)=B(K)-A(K,3)*Z(K+1)
6 Z(1)=-A(1,2)*Z(2)-A(1,3)*Z(3)
DO 7 K=1,MN
Q=1/(6*D(K))
C(1,K)=Z(K)*Q
C(2,K)=Z(K+1)*Q
C(3,K)=Y(K)/D(K)-Z(K)*P(K)
7 C(4,K)=Y(K+1)/D(K)-Z(K+1)*P(K)
RETURN
END

```

```

FUNCTION EXPFAC(B,DP,P,G)
EXPFAC = 1.0 - (0.41 + 0.35 * B**4) * DP/(P * G)
RETURN
END

```



```

SUBROUTINE FLLEAK(PT,FRFA,FRDA,FRFW,FRDW,AFLFLO,ADFLO,WFLFLO,WDFLO
*,FWLEAK,ATMPRS)
PT=PT-ATMPRS
PT=PT*100.0
FALEAK=1.5098023+(0.43360737)*PT-(0.00439747)*(PT*PT)+0.0000333847
@*(PT*PT*PT)
FALEAK=FALEAK/10000.0
CALEAK=1.2219926+0.40631258*PT-0.0021436015*(PT*PT)
DALEAK=DALEAK/10000.0
PT=PT/100.0
IF(PT.NE.(0.0)) GO TO 1
FALEAK=0.0
CALEAK=0.0
ADFLO=FRFA-FALEAK
ADFLO=FRDA-CALEAK
WFLFLO=FRFW-FWLEAK
WDFLO=FRDW-FWLEAK
PT=PT+ATMPRS
RETURN
END

```

1

```

SUBROUTINE CHAWTH(LVOLFR,CORPAR,PORLC,TPPDCM)
IMPLICIT REAL*8(A-H),REAL*8(O-Z)
REAL*8 LX,LVOLFR
DIMENSION VECOR(5),VECPAR(5)
CORPAR=CORPAR/100.00
IF(LVOLFR.LE.1.E-07) GO TO 16
IF(LVOLFR.LE.1.E-06) GO TO 15
IF(LVOLFR.LE.1.E-05) GO TO 14
IF(LVOLFR.LE.1.E-04) GO TO 13
IF(LVOLFR.LE.1.E-03) GO TO 12
IF(LVOLFR.LE.1.E-02) GO TO 11
IF(LVOLFR.LE.1.E-01) GO TO 10
GO TO 9
LX=0.0001
GO TO 100
TX=LVOLFR*1000000.0000
IF(TX.GT.(10.5)) GO TO 51
LX=DLOG10(TX)*2.75
GO TO 100
TX=LVOLFR*1000000.0000
IF(TX.GT.(10.5)) GO TO 51
LX=DLOG10(TX)*2.75+2.75
GO TO 100
TX=LVOLFR*100000.0000
IF(TX.GT.(10.5)) GO TO 51
LX=DLOG10(TX)*2.75+5.5

```

16

15

14

13


```

12 GO TO 100
TX=LVOLFR*1000.00000
IF(TX.GT.(10.5)) GO TO 51
LX=DLOG10(TX)*2.75+8.25
GO TO 100
11 TX=LVOLFR*100.0000
IF(TX.GT.(10.5)) GO TO 51
LX=DLOG10(TX)*2.75+11.0
GO TO 100
10 TX=LVOLFR*100.0000
IF(TX.GT.(10.5)) GO TO 51
LX=DLOG10(TX)*2.75+13.75
GO TO 100
9 TX=LVOLFR*10.00000
LX=DLOG10(TX)*2.75+16.50
VECPAR(1)=0.5
VECPAR(2)=1.00
VECPAR(3)=2.00
VECPAR(4)=5.0
VECPAR(5)=10.00
a3-0.0013618*(LX)**4+0.00026593084*(LX)**5
LY=6.535581+0.17478593*(LX)-0.088343004*(LX)**2+0.018834985*(LX)**3
a3-0.0028135885*(LX)**4+0.000063668*(LX)**5
LY=8.2758206+0.3598576*(LX)-0.1850545*(LX)**2+0.037487725*(LX)**3-
VECCOR(2)=LY
a3-0.0039945371*(LX)**4+0.0000984666*(LX)**5
LY=10.119765+0.40142316*(LX)-0.23065599*(LX)**2+0.049665197*(LX)**3
VECCOR(3)=LY
a3-0.00571398+0.12305994*(LX)-0.11015919*(LX)**2+0.034598867*(LX)**
VECCOR(4)=LY
a3-0.0034766087*(LX)**4+0.00009721735*(LX)**5
LY=14.489644-37225766*(LX)+.14650342*(LX)**2-.008375957*(LX)**3-0
a.0007929*(LX)**4+0.000040414*(LX)**5
VECCOR(5)=LY
IF(LX.GT.(16.499)) AND. CORPAR.LT.(0.50)) GO TO 300
CALL SPLIN1(VECPAR,VECCOR,5,CORPAR,YLOG)
CONTINUE
IF(YLOG.LE.(2.369)) GO TO 20
IF(YLOG.LE.(8.369)) GO TO 21
Y=(YLOG-8.369)*(10.0/60.)
TY=10.0**Y
TY=TY*100.0
RY=TY
GO TO 77
20 Y=(YLOG+3.61)*(10.0/59.79)
TY=10.0**Y
RY=TY

```



```

21      GO TO 77
      Y=(YLOG-2.369)*(10.0/60.)
      TY=10.0**Y
      TY=TY*10.0
      RY=TY
      TPPDCM=PDRLC*RY
      CCRPAR=CCRP*100.D0
      RETURN
51      WRITE(6,111)
      RY=0.0
      GO TO 77
111     FORMAT('1 LVOLFR CONVERTED OUT OF SCALE FOR EQUATION. NO GO.')
```

```

      CCRPAR=CCRP*100.D0
      RETURN
300     YLOG=LY
      GO TO 30
      END
```


26 AUGUST 1970

MASS FLOW RATE DETERMINATION
SQUARE-EDGE CONCENTRIC ORIFICE
ASME STANDARD

	AIR	WATER
PIPE DIAMETER (IN.)	2.0872	1.0000
ORIFICE DIAMETER (IN.)	1.4602	0.2500
BETA (D2/D1)	0.6996	0.2500
TEMPERATURE IN PIPE (DEG.F.)	58.2000	65.0000
TEMPERATURE OF ATM. (DEG.F.)	59.0000	59.0000
PRESSURE IN PIPE (PSIA)	22.0406	
PERCENT MIST FLOW	40.1158	

	AIR		WATER	
	FLANGE TAPS	D TAPS	FLANGE TAPS	D TAPS
PRESSURE DROP	160.8918 IN.H2O	171.6179 IN.H2O	5.9500 IN.HG	5.9500 IN.HG
REYNOLDS NUMBER	3.521124D 05	3.718165D 05	5.755102D 03	5.742324D 03
DISCHARGE COEFFICIENT	0.695889D 00	0.739875D 00	0.621977D 00	0.620596D 00
MASS FLOW RATE (LBM/SEC)	0.576735	0.609009	0.264672	0.264084
CORR. FLOW RATE (LBM/SEC)	0.575828	0.608119	0.256338	0.255750

TEST SECTION DIAMETER (FT)	=	2.5883E-01
TEST SECTION LENGTH (FT)	=	1.0000E 01
TEST SECTION WATER TEMP. (DEG.F.)	=	5.7800E 01
TEST SECTION AIR TEMP. (DEG.F.)	=	5.7800E 01
TEST SECTION PRESSURE (PSIA)	=	1.4868E 01

LOCKHART-MARTINELLI TWO-PHASE PRESSURE DROP PREDICTION

DENSITY (LBM/CU-FT)	=	6.23763E 01	WATER	7.75579E-02	AIR
REYNOLDS NUMBER	=	1.61748D 03		2.43024D 05	
VELOCITY (FT/SEC)	=	7.80126E-02		1.45060E 02	
FICT. PRESS. DROP (PSF/10FT)	=	9.01851E-03		1.75556E 01	

THE FLOW IS VISCOUS-TURBULENT

CORRELATION PARAMETER	=	0.56532D 02	0.12952D 01
PREDICTED TWO-PHASE PRESSURE DROP (PSI/10FT)	=	0.20015E 00	0.20450E 00

CHENOWETH-MARTIN TWO-PHASE FLOW CALCULATIONS

REYNOLDS NUMBER (LIQUID)	=	5.357102E 03
REYNOLDS NUMBER (GAS)	=	3.481384E 05
DIM.-LESS GROUP (ALL LIQUID)	=	1.528691E 00
DIM.-LESS GROUP (ALL GAS)	=	6.921986E-01
CORRELATION PARAMETER	=	2.458523E 02
VOLUMETRIC FLOW RATIO (LQ/GS)	=	5.377976E-04
FICT. ALL-LIQ. PRESS. DROP (PSF)	=	9.892690E-02
LIQUID VOLUME FRACTION	=	5.375084E-04
PREDICTED TWO PHASE PRESSURE DROP (PSI/10FT)	=	1.818377E-01

MEASURED PRESSURE DROP (PSI/10FT)	RED FLEXURE	BLACK FLEXURE
	0.22520298	0.22151357

LIST OF REFERENCES

1. Department of Mechanical Engineering, Engineering Projects Laboratory, Massachusetts Institute of Technology. Report No. DSR 8734-3, An Introduction To Two-Phase Gas-Liquid Flow, by S. W. Gouse, Jr., p. 50-55, June 1964.
2. Dukler, A. E., Wicks, W. III, and Cleveland, R. G., "Frictional Pressure Drop in Two-Phase Flow: A. A Comparison of Existing Correlations for Pressure Loss and Holdup," A.I.Ch.E. Journal, v. 10, no. 1, p. 38-43, January 1964.
3. Lockhart, R. W., and Martinelli, R. C., "Proposed Correlation of Data for Isothermal Two-Phase, Two-Component Flow in Pipes," Chemical Engineering Progress, v. 45, no. 1, p. 39-48, January 1949.
4. Chenoweth, J. M. and Martin, M. W., "Turbulent Two-Phase Flow," Petroleum Refiner, v. 34, no. 10, p. 151-155, October 1955.
5. Reid, R. C., and others, "Two-Phase Pressure Drops in Large Diameter Pipes," A.I.Ch.E. Journal, v. 3, no. 3, p. 321-324, December 1957.
6. Chien, Sze-Foo., Ibele, W., "Pressure Drop and Liquid Film Thickness of Two-Phase Annular and Annular-Mist Flows," Journal of Heat Transfer, ASME Trans., v. 86, series C, no. 1, p. 89-96, February 1964.
7. Watson, W. G., Computer Optimization of Water-Augmented Turbo-fan Concept and Development of a Test Facility for Two-Phase Flow, Engineer's Thesis, Naval Postgraduate School, Monterey, California, 1969.
8. Power Test Codes Supplement, Chapter 4, "Flow Measurement-Instruments and Apparatus," PTC 19.5, v. 4, part 5, American Society of Mechanical Engineers, 1959.
9. Wallis, G. B., One-Dimensional Two-Phase Flow, 1 st ed., p. 375-393, McGraw-Hill, 1969.

INITIAL DISTRIBUTION LIST

	No. Copies
1. Defense Documentation Center Cameron Station Alexandria, Virginia 22314	2
2. Library, Code 0212 Naval Postgraduate School Monterey, California 93940	2
3. Chairman, Department of Aeronautics Naval Postgraduate School Monterey, California 93940	1
4. Associate Professor R. D. Zucker Department of Aeronautics Naval Postgraduate School Monterey, California 93940	1
5. LTJG John M. Bonds, USN c/o Pawlowski 4334 Lee Street Holt, Michigan 48842	1

DOCUMENT CONTROL DATA - R & D

(Security classification of title, body of abstract and indexing annotation must be entered when the overall report is classified)

1. ORIGINATING ACTIVITY (Corporate author) Naval Postgraduate School Monterey, California 93940		2a. REPORT SECURITY CLASSIFICATION Unclassified	
		2b. GROUP	
3. REPORT TITLE Measured and Predicted Pressure Drops in Two-Phase Air Water Flows			
4. DESCRIPTIVE NOTES (Type of report and, inclusive dates) Master's Thesis; September 1970			
5. AUTHOR(S) (First name, middle initial, last name) John Meredith Bonds			
6. REPORT DATE September 1970		7a. TOTAL NO. OF PAGES 112	7b. NO. OF REFS 9
8a. CONTRACT OR GRANT NO.		9a. ORIGINATOR'S REPORT NUMBER(S)	
b. PROJECT NO.			
c.		9b. OTHER REPORT NO(S) (Any other numbers that may be assigned this report)	
d.			
10. DISTRIBUTION STATEMENT This document has been approved for public release and sale; its distribution is unlimited.			
11. SUPPLEMENTARY NOTES		12. SPONSORING MILITARY ACTIVITY Naval Postgraduate School Monterey, California 93940	
13. ABSTRACT			

Two-phase, air-water flow is studied in a horizontal pipe. Water injection methods are compared to determine an efficient means of attaining fully developed homogeneous flow. Wall shear forces are measured directly through flexures attached to a "floating" test section. The pressure drops are compared to those predicted by the Lockhart-Martinelli and Chenoweth-Martin correlation schemes. A computer program is presented for data reduction. For the flow rates investigated it is concluded that the Lockhart-Martinelli correlation gives better results than does the Chenoweth-Martin scheme providing one knows the existing flow pattern. A new method is suggested for predicting the transition between the Annular and Mist flow regimes.

KEY WORDS

LINK A

LINK B

LINK C

ROLE

WT

ROLE

WT

ROLE

WT

Two-Phase Flow

Pressure Drop Prediction

Air-Water Flow



Thesis
B6793
c.1

Bonds

124423

Measured and predicted
pressure drops in
two-phase air water
flows.

Thesis
B6793
c.1

Bonds

124423

Measured and predicted
pressure drops in
two-phase air water
flows.

thesB6793

Measured and predicted pressure drops in



3 2768 002 07489 0

DUDLEY KNOX LIBRARY